



TECHNICAL REPORT

**Smart Body Area Network (SmartBAN);
Measurements and modelling of SmartBAN
Radio Frequency (RF) environment**

Reference

DTR/SmartBAN-006

Keywords

MAC, measurement, network

ETSI

650 Route des Lucioles
F-06921 Sophia Antipolis Cedex - FRANCE

Tel.: +33 4 92 94 42 00 Fax: +33 4 93 65 47 16

Siret N° 348 623 562 00017 - NAF 742 C
Association à but non lucratif enregistrée à la
Sous-Préfecture de Grasse (06) N° 7803/88

Important notice

The present document can be downloaded from:
<http://www.etsi.org/standards-search>

The present document may be made available in electronic versions and/or in print. The content of any electronic and/or print versions of the present document shall not be modified without the prior written authorization of ETSI. In case of any existing or perceived difference in contents between such versions and/or in print, the only prevailing document is the print of the Portable Document Format (PDF) version kept on a specific network drive within ETSI Secretariat.

Users of the present document should be aware that the document may be subject to revision or change of status. Information on the current status of this and other ETSI documents is available at
<https://portal.etsi.org/TB/ETSIDeliverableStatus.aspx>

If you find errors in the present document, please send your comment to one of the following services:
<https://portal.etsi.org/People/CommiteeSupportStaff.aspx>

Copyright Notification

No part may be reproduced or utilized in any form or by any means, electronic or mechanical, including photocopying and microfilm except as authorized by written permission of ETSI.

The content of the PDF version shall not be modified without the written authorization of ETSI.
The copyright and the foregoing restriction extend to reproduction in all media.

© European Telecommunications Standards Institute 2016.
All rights reserved.

DECT™, **PLUGTESTS™**, **UMTS™** and the ETSI logo are Trade Marks of ETSI registered for the benefit of its Members.
3GPP™ and **LTE™** are Trade Marks of ETSI registered for the benefit of its Members and of the 3GPP Organizational Partners.
GSM® and the GSM logo are Trade Marks registered and owned by the GSM Association.

Contents

| | |
|---|----|
| Intellectual Property Rights | 5 |
| Foreword..... | 5 |
| Modal verbs terminology..... | 5 |
| 1 Scope | 6 |
| 2 References | 6 |
| 2.1 Normative references | 6 |
| 2.2 Informative references..... | 6 |
| 3 Symbols and abbreviations..... | 7 |
| 3.1 Symbols..... | 7 |
| 3.2 Abbreviations | 8 |
| 4 Introduction and Background..... | 10 |
| 5 Coexistence | 10 |
| 5.0 Introduction | 10 |
| 5.1 Bands..... | 11 |
| 6 Measurements..... | 11 |
| 6.1 Background & Motivation..... | 11 |
| 6.2 Spectrum Occupancy Evaluations (SOEs) | 11 |
| 6.3 Measurement Campaigns | 13 |
| 6.3.0 Introduction..... | 13 |
| 6.3.1 Measurement campaigns in Oulu, Finland | 13 |
| 6.3.1.0 Introduction..... | 13 |
| 6.3.1.1 Daily Surgery SOEs (Campaign 1) | 14 |
| 6.3.1.2 Accident & Emergency Ward SOEs (Campaign 2) | 24 |
| 6.3.1.3 X-Ray & Radiology Ward SOEs (Campaign 3)..... | 29 |
| 6.3.2 Analytical Stochastic Model for Spectrum Occupancy | 31 |
| 6.3.3 Extracting Mathematical Interference model..... | 34 |
| 6.3.4 Measurement Campaigns in Florence, Italy | 37 |
| 6.3.4.0 Introduction..... | 37 |
| 6.3.4.1 Occupancy..... | 38 |
| 6.3.4.1.0 Introduction | 38 |
| 6.3.4.1.1 Percentiles | 39 |
| 6.3.4.2 PDF | 40 |
| 6.3.4.3 Interference as a function of time and frequency | 41 |
| 6.3.4.4 Parameters characterizing the distribution | 42 |
| 6.3.4.5 Home and office environments | 42 |
| 6.3.4.6 Extract the mathematical model..... | 45 |
| 6.3.4.6.0 Introduction | 45 |
| 6.3.4.6.1 First results of CNIT-UNIFI..... | 45 |
| 6.4 Statistical model of the interference | 53 |
| 6.4.0 Introduction..... | 53 |
| 6.4.1 Cluster dimension | 54 |
| 6.4.2 Inter-arrival time..... | 55 |
| 6.4.3 Interfering cluster amplitude..... | 57 |
| 6.4.4 Conclusions..... | 60 |
| 6.5 Extracting the mathematical model of the interference | 60 |
| 7 SmartBAN communication system simulator | 69 |
| 7.0 Introduction | 69 |
| 7.1 Getting started | 69 |
| 7.2 Simulator model | 72 |
| 7.2.0 Introduction..... | 72 |
| 7.2.1 Node..... | 72 |
| 7.3 Hub..... | 73 |

| | | |
|-----------------|--|-----------|
| 7.3.0 | Introduction..... | 73 |
| 7.3.1 | Simulation parameters | 74 |
| 7.4 | PHY layer | 75 |
| 7.4.0 | Introduction..... | 75 |
| 7.4.1 | PHY transmitter | 75 |
| 7.4.2 | Channel, interference and noise..... | 75 |
| 7.4.2.0 | Introduction..... | 75 |
| 7.4.2.1 | Interference | 76 |
| 7.4.3 | PHY receiver | 77 |
| 7.5 | MAC - Frame retransmission | 77 |
| 7.6 | Verification results | 79 |
| 8 | Simulation results | 80 |
| 8.0 | Introduction | 80 |
| 8.1 | Simulation parameters | 80 |
| 8.2 | AWGN channel | 81 |
| 8.3 | Fading channel | 83 |
| 8.4 | Fading channel and interference..... | 85 |
| 8.5 | Discussion | 87 |
| Annex A: | Spatial Sample Clustering Algorithm | 88 |
| History | | 91 |

Intellectual Property Rights

IPRs essential or potentially essential to the present document may have been declared to ETSI. The information pertaining to these essential IPRs, if any, is publicly available for **ETSI members and non-members**, and can be found in ETSI SR 000 314: *"Intellectual Property Rights (IPRs); Essential, or potentially Essential, IPRs notified to ETSI in respect of ETSI standards"*, which is available from the ETSI Secretariat. Latest updates are available on the ETSI Web server (<https://ipr.etsi.org/>).

Pursuant to the ETSI IPR Policy, no investigation, including IPR searches, has been carried out by ETSI. No guarantee can be given as to the existence of other IPRs not referenced in ETSI SR 000 314 (or the updates on the ETSI Web server) which are, or may be, or may become, essential to the present document.

Foreword

This Technical Report (TR) has been produced by ETSI Technical Committee Smart Body Area Network (SmartBAN).

Modal verbs terminology

In the present document "**should**", "**should not**", "**may**", "**need not**", "**will**", "**will not**", "**can**" and "**cannot**" are to be interpreted as described in clause 3.2 of the [ETSI Drafting Rules](#) (Verbal forms for the expression of provisions).

"**must**" and "**must not**" are **NOT** allowed in ETSI deliverables except when used in direct citation.

1 Scope

The present document specifies the state-of-the-art and the future investigations on coexistence for allowing smart body area network (SmartBAN) devices to properly work and co-operate in the Industrial, Scientific and Medical (ISM) band. Interference appears to be one of the major threats as well as coexistence with other existing systems radiating in the same portion of the frequency spectrum. The present document describes the coexistence measurements and analysis that need to be considered in order to specify the requirements for the SmartBAN compatible devices.

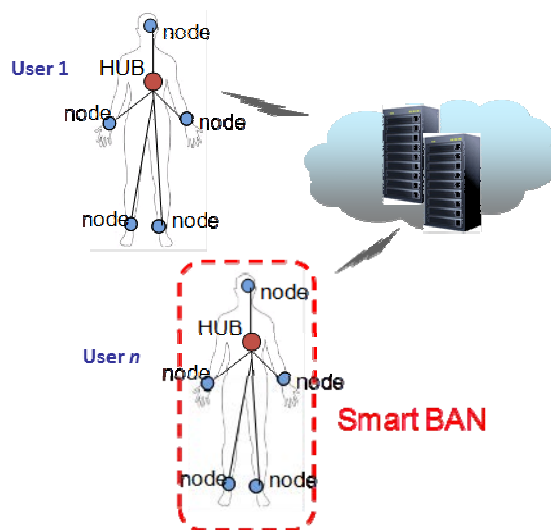


Figure 0: Scope of a SmartBAN

2 References

2.1 Normative references

Normative references are not applicable in the present document.

2.2 Informative references

References are either specific (identified by date of publication and/or edition number or version number) or nonspecific. For specific references, only the cited version applies. For non-specific references, the latest version of the referenced document (including any amendments) applies.

NOTE: While any hyperlinks included in this clause were valid at the time of publication, ETSI cannot guarantee their long term validity.

The following referenced documents are not necessary for the application of the present document but they assist the user with regard to a particular subject area.

- [i.1] ETSI TS 103 326 (V1.1.1) (04-2015): "Smart Body Area Network (SmartBAN); Enhanced Ultra-Low Power Physical Layer".
- [i.2] Void.
- [i.3] IEEE 802.11TM: "IEEE Standard for Information technology--Telecommunications and information exchange between systems Local and metropolitan area networks--Specific requirements Part 11: Wireless LAN Medium Access Control (MAC) and Physical Layer (PHY) Specifications".

- [i.4] Valenta, V. (2010): "Survey on spectrum utilization in Europe: Measurements, analyses and observations", 5th International Conference on Cognitive Radio Oriented Wireless Networks Communications.
- [i.5] ITU-R (2011): "ITU-R handbook for spectrum monitoring".
- [i.6] Report Recommendation ITU-R SM.2256: "Spectrum occupancy measurements and evaluation".
- [i.7] Report Recommendation ITU-R SM.2180 (2010): "Impact of ISM equipment on radio communication services".
- [i.8] Virk, M. H., Vuohtoniemi, R., Hämäläinen, M., Iinatti, J., & Mäkela, J.-P. (2015): "Stochastic Spectral Occupancy Modeling: A Body Area Network Perspective in ISM Band", 9th International Symposium on Medical Information & Communication Technology (ISMICT). Kamakura, Japan.
- [i.9] J. J. Lehtomäki, e. a. (2012): "Energy detection based estimation of channel occupancy rate with adaptive noise estimation", IEICE Transactions on Communications.
- [i.10] Virk, M. H., Vuohtoniemi, R., Hämäläinen, M., Iinatti, J., & Mäkela, J.-P. (2014): "Spectrum Occupancy Evaluations at 2.35-2.50 GHz ISM Band in a Hospital Environment", International Conference on Body Area Networks (BodyNets'14). London, UK.
- [i.11] ETSI TS 103 325 (2014): "Smart Body Area Network (SmartBAN); Low Complexity Medium Access Control (MAC) for SmartBAN".
- [i.12] Matlab, Product help, R2011b.
- [i.13] Yazdandoost, K.Y. and Sayrafian-Pour, K.: "Channel Model for Body Area Network (BAN)," IEEE P802.15-08-0780-09-0006, 2009.
- [i.14] Proakis, J.G.: "Digital Communications", McGraw-Hill, 2001.
- [i.15] Griffin, A.: "Coding CPFSK for Differential Demodulation." University of Canterbury Christchurch, New Zealand, 2000.
- [i.16] IEEE 802.15.6™ (2012): "IEEE Standard for Local and metropolitan area networks - Part 15.6: Wireless Body Area Networks".
- [i.17] Rahman M., Elbadry, M and Harjani R.: "An IEEE 802.15.6 Standard Compliant 2.5 nJ/Bit Multiband WBAN Transmitter Using Phase Multiplexing and Injection Locking" IEEE Journal of Solid-State Circuits, Vol. 50, No. 5, May 2015, pp. 1126 -1136.

3 Symbols and abbreviations

3.1 Symbols

For the purposes of the present document, the following symbols apply:

| | |
|-------------|--|
| C | Channel Number |
| $E_i, E()$ | Expected Value |
| f_c | Centre Frequency |
| H_0 | Null hypothesis |
| H_1 | Alternative Hypothesis |
| i | Channel Identifier |
| K | Number of Samples Collected from the Band in One Sweep |
| k | Shape Parameter |
| \hat{L} | Maximized Value Of Likelihood Function |
| n | Number of Samples Collected in the Channel |
| O_i | Observed Value |
| PFA_{DES} | Probability of False Alarm |
| $P(X_i(j))$ | Sample Power j at Channel i |
| T | Number of Sweeps |

| | |
|--------------|---|
| T_{CME} | Threshold for Consecutive Mean Excision |
| t | Time |
| X | Sample Space |
| α | Significance Level |
| $\Gamma()$ | Gamma Function |
| λ | Arrival Rate |
| μ | Location Parameter |
| σ | Scale Parameter |
| γ | Noise Threshold |
| ν | shape parameter |
| σ_k | The log-normal variance of the measured data between path loss and K-factor |
| σ_p | The log-normal variance in dB around the mean, representing the variations measured at different body and room locations. This parameter will depend on variations in the body curvature, tissue properties and antenna radiation properties at different body locations. |
| E_b/N_0 | Energy per bit to noise power spectral density ratio |
| h | Modulation index |
| I_{dB} | Implementation losses in dB |
| K_0 | The fit with measurement data for the K-factor for low path loss |
| K_{dB} | K factor of Ricean distribution in dB |
| L | Pulse length |
| L_{slot} | Length of slot |
| m | Numerator of modulation index |
| m_0 | The average decay rate in dB/cm for the surface wave traveling around the perimeter of the body |
| m_k | The slope of the linear correlation between path loss and K-factor |
| M | M-ary number |
| NF_{dB} | Noise figure in dB |
| n_k | Zero mean and unit variance Gaussian random variable |
| n_p | Zero mean and unit variance Gaussian random variable |
| p | Denominator of modulation index |
| P_0 | The average loss close to the antenna |
| P_1 | The average attenuation of components in an indoor environment radiated away from the body and reflected back towards the receiving antenna |
| P_b | Bit error probability |
| PL_{dB} | Path loss in dB |
| $PPDU_{rep}$ | Times of PPDU repetition |
| $Q()$ | Q function |
| R | Data rate |
| S_{dBm} | Receiver sensitivity |
| T_{min} | T_s/L_{slot} |

3.2 Abbreviations

For the purposes of the present document, the following abbreviations apply:

| | |
|--------|--|
| ACK | Acknowledgement |
| AIC | Akaike Information Criterion |
| ANL | Average Noise Level |
| ARA | Antenna Research Associate |
| AWGN | Additive White Gaussian Noise |
| BAN | Body Area Network |
| BCH | Bose, Chaudhuri, and Hocquenghem |
| BER | Bit Error Rate |
| BIC | Bayesian Information Criterion |
| BLE | Bluetooth Low Energy |
| BPF | Bandpass Filter |
| BT | BlueTooth |
| CCA | Clear Channel Assessment |
| CCA-ED | Clear Channel Assessment Based On Energy Detection |
| CDF | Cumulative Distribution Function |
| CM | Channel Model |
| CO | Channel Occupancy |

| | |
|--------|--|
| CSRR | Clean Sample Rejection Rate |
| DSSS | Direct Sequence Spread Spectrum |
| ED | Energy Detection |
| EGC | Equal Gain Combining |
| FBO | Frequency Band Occupancy |
| FCME | Forward Consecutive Mean Excision |
| FER | Frame Error Rate |
| FH | Frequency Hopping |
| GEV | Generalized Extreme Value |
| GEVD | Generalized Extreme Value Distribution |
| GFSK | Gaussian Frequency Shift Keying |
| HI | High Interference |
| ICT | Information and Communication Technology |
| ISM | Industrial, Scientific and Medical |
| ITU-R | Telecommunication Union - Radio Communication Sector |
| JPG | Joint Photographic Experts Group |
| KS | Kolmogorov-Smirnov |
| LI | Low Interference |
| LNA | Low Noise Amplifier |
| MAC | Medium ACcess |
| MATLAB | Matrix Laboratory |

NOTE: A multi-paradigm numerical computing environment and fourth-generation programming language. A proprietary programming language developed by MathWorks™.

| | |
|----------|---|
| MC | Measurement Campaign |
| Med-FCME | Median Forward Consecutive Mean Excision |
| MLE | Maximum Likelihood Estimate |
| MLSD | Maximum-Likelihood Sequence Detector |
| MPDU | MAC Protocol Data Unit |
| MRI | Magnetic Resonance Imaging |
| OBW | Occupied BandWidth |
| OFDM | Orthogonal Frequency Division Multiplexing |
| OYS | Oulun Yliopistollinen Sairaala (Oulu University Hospital) |
| PDF | Probability Distribution Function |
| PHY | PHYSical layer |
| PLCP | Physical Layer Convergence Procedure |
| PPDU | Physical-Layer Protocol Data Unit |
| PSDU | Physical-layer Service Data Unit |
| RBW | Resolution BandWidth |
| RF | Radio Frequency |
| SA | Spectrum Analyser |
| SNR | Signal-to-Noise Ratio |
| SOE | Spectrum Occupancy Evaluation |
| SRO | Spectrum Resource Occupancy |
| SSC | Spatial Sample Clustering |
| TC | Technical Committee |
| TCME | Threshold for Consecutive Mean Excision |
| TLSD | t Location-Scale Distribution |
| TS | Technical Specification |
| UHF | Ultra High Frequency |
| UWB | Ultra WideBand |
| WBAN | Wireless Body Area Network |
| WI | Work Item |
| WLAN | Wireless Local Area Network |
| WPAN | Wireless Personal Area Networks |

4 Introduction and Background

Modern medical and health monitoring equipment is moving towards the trend of wireless connectivity between the data collection or control centre and the medical devices or sensors. Therefore, the need for standardized communication interfaces and protocols between the actors is required. This network of actors performing some medical monitoring or functions in this context is called a Smart Body Area Network (Smart BAN).

Most emerging radio technologies for Wireless Personal Area Networks (WPAN) are designed to operate around the 2,4 GHz ISM band. Since both standardized (such as Bluetooth and IEEE 802.11™ [i.3]) and non-standardized (proprietary) devices use the same frequency band, interference may lead to significant performance degradation of medical (and other) devices operating in the band. The main goal of this work item (WI) is to describe the interference problem, and to highlight a coexistence framework for the medical information and communication technologies (ICT) to operate in a proximal environment. In the present document a synthesis of the problem of interference and coexistence around the 2,4 GHz ISM band is given. Measurements carried out in hospital and campus will be described in order to have a better insight on the problem. Then, the measurement campaigns exhaustively accumulated data in order to formulate a mathematical model of the interference at the channel in the 2,36 - 2,5 GHz band will be described.

5 Coexistence

5.0 Introduction

A number of use cases have been identified as potential scenarios for SmartBAN. These use cases serve as scenarios where the real channel occupancy measurements are needed. The environments to be considered for investigating the coexistence issues are such as:

- Hospital
- Home
- Office
- Outdoor

These cases include the typical environments where a patient wearing a SmartBAN system lives and stays. However, the present document is focusing on indoor environments only.

Moreover, existing interferers are classified into two classes based on their usage of the spectrum. Devices implementing the direct sequence spread spectrum (DSSS) technique constitute one class of interferers that utilize a fixed channel in the band. Typically this channel is 22 MHz wide, although the width of the signal depends on the transmitter's implementation. The second class of interferers is represented by devices implementing a type of frequency hopping (FH) mechanism. Note that the IEEE 802.11 [i.3] specifications include a frequency hopping technique that uses a deterministic frequency pattern. On the other hand, the Bluetooth specifications define a pseudo-random frequency sequence based on the Bluetooth device's address and its internal clock. While interference among systems from the same type, such as Bluetooth on Bluetooth, or IEEE 802.11 [i.3] on IEEE 802.11 [i.3], interference can be significant, it is usually considered early on in the design stages of the protocol (phenomena is called as multiuser interference.) A third class can be included, which comprehend the devices using orthogonal frequency division multiplexing (OFDM) technique. Therefore, the worst realistic interference scenario consists of a mix of heterogeneous devices, i.e. devices belonging to different classes.

In evaluating the performance with respect to coexistence issues, variations in the operational environment need to be considered, including both the characteristics of the interfering wireless services and the radio frequency (RF) propagation characteristics. This ensures that the evaluation takes into account the uncertainty in an installation's location and in the interfering traffic. Evaluating the performance requirements in terms of coexistence issues provides a method for quantifying the applications interference susceptibility and assists in establishing usage policies.

The analytical model for evaluating the coexistence in terms of the operational environment is developed based on the following process:

- Characterize the interference under static conditions, i.e. when both interfering and desired signals remain stationary. Empirical test results are used to estimate model parameters and to substantiate the model.

- Extract a mathematical model of the aggregate interference in all operational environments.

5.1 Bands

For coexistence purposes the typical interference levels are evaluated in the following bands:

- ISM band
- 30 MHz before the ISM band
- 30 MHz after the ISM band
- Option for UWB lower band

6 Measurements

6.1 Background & Motivation

Radio frequency is a finite resource coordinated by regulatory bodies all over the globe. For medical usage, varying regulations are imposed in different countries involving allocation of various chunks of both licensed and unlicensed frequency resource [i.4]. Some of the license-free solutions include, e.g. sub-gigahertz ISM band, 2,4 GHz ISM band and 3 GHz to 10 GHz ultrawide band etc. [i.4]. 2,4 GHz ISM band is an unregulated, license free frequency band where many communication technologies share the frequency resources, e.g. wireless local area networks (WLAN), Bluetooth (BT), wireless sensor networks, cordless phones, etc. In a hospital environment if a wireless body area network (WBAN) is planned to be deployed in the 2,4 GHz ISM band, it will require certain measures in order to co-exist with other wireless communication technologies.

ETSI SmartBAN physical layer (PHY) defines 40 channels in 2,4 GHz ISM band, including 37 data channels and 3 control channels. Each channel is 2 MHz wide and no guard bands between two adjacent channels are defined [i.1]. There had been other considerations as well for PHY solutions, e.g. channels in 2,36 GHz to 2,40 GHz band, which has already been allocated for medical use in USA. However, in Europe this particular band has been allocated for LTE special purpose use.

Increasing deployments of wireless technologies inside hospital premises will significantly increase the electromagnetic clutter in hospital environments and hence interference will be the limiting factor. Spectrum occupancy evaluations (SOEs) provide statistical quantification of spectrum utilization patterns and highlight temporal characteristics of the band under consideration. In essence, SOEs can also be used as a probe to reflect upon the degree a victim network would suffer under the influence of an aggressor. In other words, SOE can provide an insight regarding the opportunities a wireless network will have, causing presumably no interference to already existing networks. Yet another way to look at SOE is to study the suitability a particular frequency band is for deployment of a new kind of network. In a nut-shell, it is highly motivating to perform SOEs in 2,36 GHz to 2,4 GHz band and 2,4 GHz ISM band in order to characterize aggregate interference which would potentially be harmful to ETSI SmartBAN compliant devices.

6.2 Spectrum Occupancy Evaluations (SOEs)

Generally, spectrum occupancy measurements involve collection of measurement data, processing the measured data for occupancy assessment and development of models to characterize the spectrum utilization. The key factors influencing the measurements are measurement bandwidth span, channel bandwidths, number of channels, observation time per channel, revisit time to a specific channel, total duration of monitoring and statistical integration time if monitoring is sufficiently long. The International Telecommunication Union - Radio Communication Sector (ITU-R) guidelines for spectrum occupancy measurements are elaborated in a special handbook [i.5] and also in two short reports [i.7] and [i.6]. Stochastic parameters regarding spectrum occupancy evaluations include channel occupancy (CO), frequency band occupancy (FBO) and spectrum resource occupancy (SRO). Spectrum occupancy measurements usually involve:

- Spectrum sensing, utilizing an antenna coupled with a band pass filter and a spectrum analyser.
- Sample collection and saving the records in hard disk drive.

- Processing and analysis of recorded data in order to calculate occupancies of interest.

Spectrum occupancy measurement handbook published by ITU-R [i.5] suggests to divide the sample space, i.e. one full record of the band (one sweep) into channels of the expected system, which is utilizing the spectrum resource. Then, each channel is searched for number of samples above a predefined noise threshold. If more than 50 % of the samples in the channel are above a noise threshold, channel is marked as occupied. In this way, individual channel occupancies (CO) are calculated for all the channels.

There are two more metrics which can also be calculated, frequency band occupancy and spectrum resource occupancy. FBO provides statistical information about how much the whole frequency band is used, independently of a particular system. SRO is a system specific metric, which gives information about the utilization of resources available to a specific system [i.5]. After intensive review of literature, it was found that there were propositions which lacked the objectivity in relation to fully unregulated band, like ISM, with so diverse access technologies. Even those studies which were performed especially for ISM band could not grasp the whole picture. For example:

- Many of the studies considered revisit time of more than a second for a span of more or less 100 MHz, which is impractical for bursty transmissions, and a large portion of the band might appear empty during observation. If a too fast revisit time is used, one might not get enough samples above noise threshold in a certain channel to declare it occupied with enough confidence.
- Another example of ambiguity is the channelization of the band under observation. A number of studies talked about ISM band but end up finding occupancies for WLAN only. Although ITU-R suggests a method which involved at first division of the sample space into channels of the wideband system, calculation of occupancies and then modifying the sample space by deleting the samples identified inside a wideband channel. Secondly, the modified sample space was supposed to be divided in channels of the narrowband system (or next wideband system with narrower bandwidth as compared to the previous one) and then following the same procedure as before. But in real scenarios, sometimes it can lead to misclassification or even no detection, depending on the quality of samples acquired, which in turn depends on the radio channel conditions.
- Overestimation or underestimation of occupancies due to less careful noise threshold setting, insufficient number of samples in order to obtain statistical confidence, and inability to dig the signal out in case of very low signal-to-noise ratio (SNR). 50 % premise, used by ITU-R handbook, results in underestimation of true occupancies, because channel nulls or under-sampling can vanquish formidable part of channel, which would then appear to be as noise.
- A comprehensive study of occupancies in ISM band considering possible coexisting systems had been lacking.
- Efficient and robust bandwidth and centre frequency estimation algorithms are missing.

In order to dig legitimate signals very close to noise levels, especially in case of low signal-to-noise ratio (SNR) or spread spectrum scenarios, one cannot rely upon static noise thresholds. From previous research works, a dynamic noise thresholding algorithm known as median forward consecutive mean excision (Med-FCME) [i.9] is adopted. Contrary to previous implementations, the algorithm is applied per each sweep. The idea was to establish a noise threshold for every sweep because after a single sweep, a blind period is encountered, when measurement equipment was saving the sweep data, and supposedly the noise floor is also fluctuating. Clean sample rejection rate (CSRR) is a measure to quantify the number of noise-only samples wrongly classified as outliers having signal components by FCME. The concept of CSRR is presented in [i.9]. CSRR can be preset as a probabilistic limit so that only a given amount of misclassification is tolerated, i.e. a false alarm. This metric is termed as desired probability of false alarm, PFA_{DES} . The desired probability of false alarm value is given as a parameter to the FCME algorithm which calculates a threshold for consecutive mean excision T_{CME} as:

$$T_{CME} = -\ln(PFA_{DES}), \quad (1)$$

and then performs the iterative algorithm to find out the noise thresholds. In our measurement campaign, a target CSRR is set to be 5 %, i.e. $PFA_{DES} = 0,05$. Hence, $T_{CME} = 2,99$.

The most important goals achieved through this undertaking can be listed as:

- CO, FBO and SRO evaluation for the 2,35 - 2,50 GHz band in a hospital environment to characterize potential interferers in two different countries (in our case Finland and Italy).
- A novel centre frequency and bandwidth estimation algorithm named as Spatial Sample Clustering (SSC).
- An overhauled, robust and much more objective mechanism for SOE evaluations with a sufficiently low desired probability of false alarm.

- d) Mathematical models for quantification of interference.

For various equations including CO, FBO, SRO calculation and the complete analytical approach towards the problem, please refer to [i.8].

The spectrum sensing approach used was Energy Detection (ED) because of its simplicity of implementation. Other methods like cyclostationarity or wavelet decomposition cannot be used as any information about the signals being encountered is known. This makes the process blind, i.e. any electromagnetic energy being radiated into the channel has to be taken into account and no decisions about the nature or any feature of the already existing systems is taken. This is exactly the same as Clear Channels Assessment (CCA) based on ED as defined in the recently accepted ETSI SmartBAN PHY document [i.1].

A Neyman-Pearson type of energy detector chain is used and a decision statistics based on the dynamically calculated noise threshold is formulated. This problem can be written mathematically as a hypothesis test, i.e. a null hypothesis that a channel contains only noise, and an alternative hypothesis that a channel contains noise along with a legitimate signal.

H_0 : The channel contains only noise (Null Hypothesis)

H_1 : The channel contains noise and signal (Alternative Hypothesis)

$$D(X_i) = \frac{1}{n} \sum_{j=1}^n P(X_i(j)) \underset{H_1}{\overset{H_0}{\leq}} \gamma. \quad (2)$$

where i is the channel identifier, n is the number of samples collected from the channel, $P(X_i(j))$ is the sample power j at channel I , and γ is the noise threshold. So, if the average power in the channel exceeds a certain threshold, there is a signal plus noise in a channel (alternative hypothesis), otherwise the null hypothesis stands.

6.3 Measurement Campaigns

6.3.0 Introduction

Various measurement campaigns were undertaken in Oulu (Finland) and Florence (Italy) to analyze the channel usage patterns in essentially at the 2,35 GHz to 2,50 GHz band. Different analysis techniques have been applied in order to dig out maximum information regarding varying spectrum usage mainly in modern hospital environments. Office and home environments were studied in Florence only. The process had been evolutionary and the campaigns differ slightly in parameter settings as well as in implementation perspective. More light will be shed on it in the following clauses. After evaluations of spectrum occupancy, mathematical models for channel occupancy description were extracted.

The measurement results, in both Finland and Italy, had been in accord in general. However, there had been slight variations due to the differing radio environments, different measurement equipment and different analysis strategies. The measurement campaigns carried out in Oulu University Hospital, Oulu, Finland is first presented. Later the corresponding measurement campaigns carried out in San Giuseppe Hospital in Empoli, Florence, Italy is described.

6.3.1 Measurement campaigns in Oulu, Finland

6.3.1.0 Introduction

Oulun yliopistollinen sairaala (OYS, or Oulu University Hospital), situated in the city of Oulu is the north most of the five university hospitals in Finland. The hospital is affiliated to the University of Oulu, Faculty of Medicine and operates with more than a 1 000 beds. The hospital is also equipped with state-of-the-art medical equipment, several ambulatory bays and a helipad.

Three measurement campaigns were carried out in OYS premises between December 2013 to June 2014. The following list describes the locations used in the campaigns:

- Daily Surgery (10th - 16th December 2013)
- Accident & Emergency Ward (10th - 17th June 2014)

- X-ray & Radiology (18th - 25th June 2014)

6.3.1.1 Daily Surgery SOEs (Campaign 1)

Figure 2 shows the map of the ground floor of Daily surgery ward where the measurements were carried out. A red dot shows the location where the measurement equipment was placed. Green circles show the locations of the active Wi-Fi access points installed in the premises. Such channel occupancy measurements are always highly dependent upon the location or placement of the equipment because the measurement equipment itself does not emit any probing signal in the air and the measurements rely only on the energy detection perceived from the radio channel. It should be noted here that in this kind of measurement no assumptions on radio signal propagation characteristics (i.e. channel model) are needed, as only electromagnetic radiations' level in the air is of interest. In other words, no signal decoding is done here, it is just simple old school blind energy detection that was done.

However, sometimes it becomes important to identify the interfering radiation or signal. That is why in the data analysis phase a blind detect and identify method (SSC) is implemented in order to characterize the specific systems occupying the frequency band of interest. For more details about SSC, please refer to [i.8].

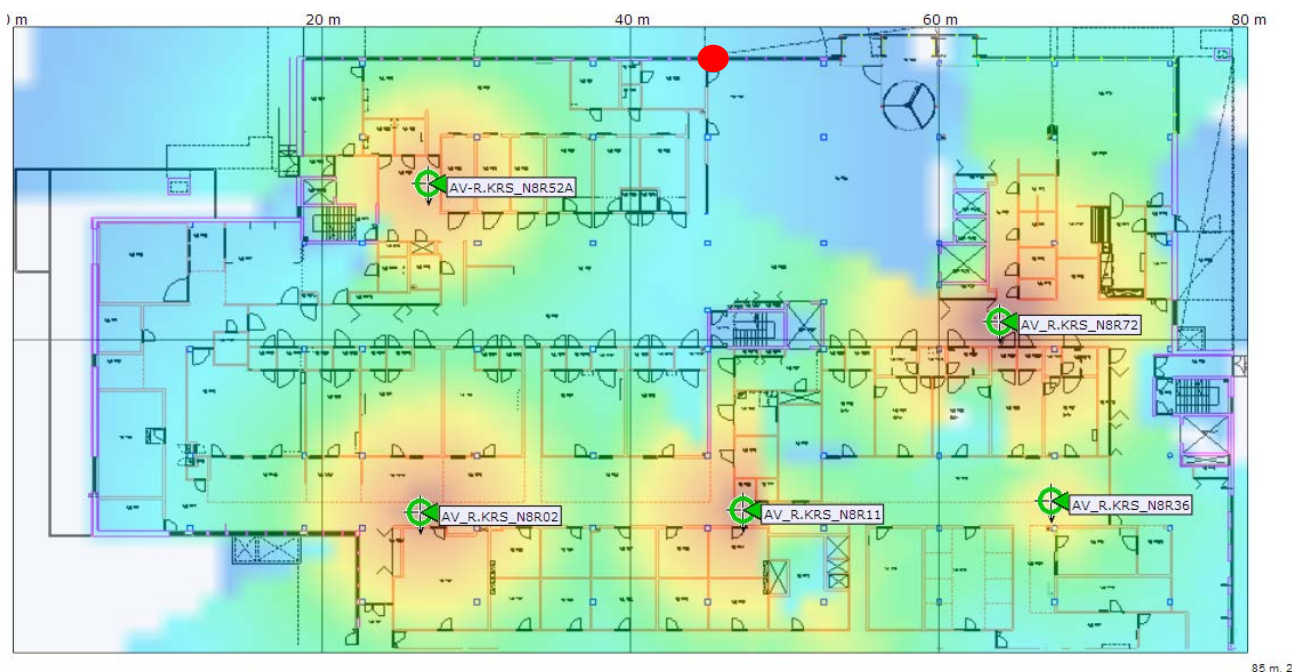


Figure 1: Map of ground floor (Daily Surgery Ward)

Measurements were carried out using high performance spectrum analyser (SA) Agilent™ E4446A connected to a computer. Instrument Control Toolbox was used to connect MATLAB directly to the spectrum analyser enabling control over SA and direct measurement results' analysis. The spectrum analyser was connected with a 1 m length cable to an omnidirectional, wideband antenna ARA CMA-118/A. Measurement setup is displayed in Figures 3 and 4. Before the measurement campaign signal levels were measured and dynamic range of the spectrum analyser was optimized for the specific environment. Measurement campaigns are affected by certain key parameters which are set before the start of the campaign. Such parameters set for the campaign in Daily Surgery are listed in the Table 1.

NOTE: SA Agilent™ E4446A is (are) an example(s) of a suitable product(s) available commercially. This information is given for the convenience of users of the present document and does not constitute an endorsement by ETSI of this (these) product(s).

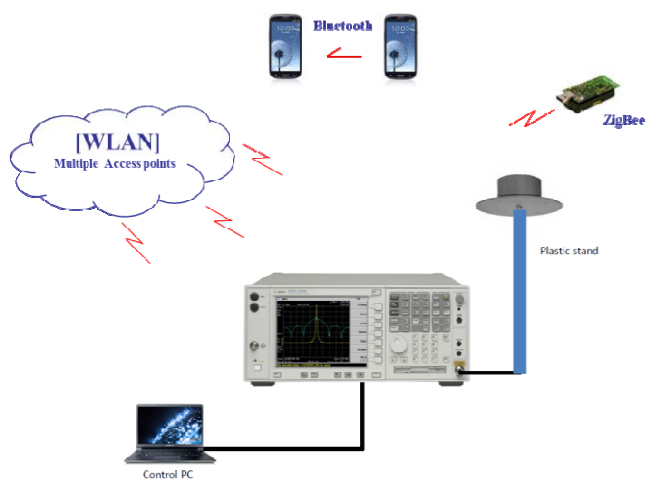


Figure 2: Logical Measurement Setup



Figure 3: Actual cabinet keeping the SA, omnidirectional antenna and control PC

Table 1: Parameter setting for Daily Surgery Campaign

| Parameter Name | Value |
|-----------------------------------|---------------------------------|
| Frequency band | 2,35 to 2,50 GHz |
| Bandwidth | 150 MHz |
| Number of recorded frequency bins | 1 601 |
| Resolution bandwidth | 300 kHz |
| Bin-width | 93,7 kHz |
| No. of sweeps | 10 000 |
| Sweep time | 2 ms approx. |
| Processing time | 22 ms |
| Integration time | 4 minutes |
| Measurement duration | 7 days (6 x *24 hrs + 1*10 hrs) |

The campaign in Daily Surgery section of Oulu University Hospital lasted for a week, and 564 gigabytes (GB) of data divided into 4 minute long blocks were collected. Figure 4 shows a plot regarding one such block. This is unprocessed, raw data plot displaying all the detected signal energy (traffic) in the band of interest. Also the corresponding noise floor can be seen. In order to be processed, in the analysis phase data was passed through dynamic noise thresholding, SSC and occupancy evaluation blocks.

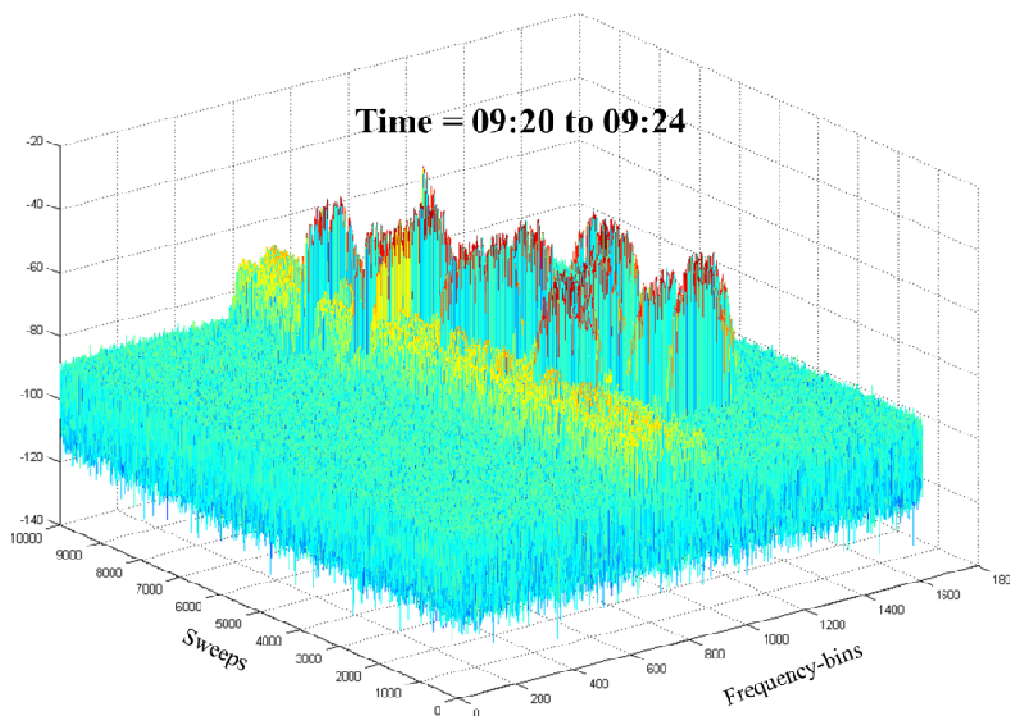


Figure 4: Raw Interference Plot

Some of the interesting plots and figures from the week long campaign are presented next. Figures 5 to 8 show occupancy evaluations for a single day, Friday 13th of December, 2013 and then few plots shed light upon one week long SOE. The processed data plots reveal the systems working in our band of interest.

It should be noted that the colour schemes used in temperature plots, i.e. Figures 5 to 7 are locally significant. For example, the red colour in Figure 5 marks near about 10 % occupancy whereas in Figure 6, it marks about 0,6 % occupancy. The band from 2,35 GHz to 2,40 GHz is found to be completely empty, which means that the newly allocated band 2 360 MHz to 2 400 MHz for medical purposes in US seems to be open for exploitation in OYS. However, in Europe, this particular band is allocated for LTE, which might cause interference for the Medical BANs in the future if it is taken into use. SSC was unable to distinguish among different narrowband systems. There had been 2 MHz wide signals as well as 1 MHz wide signals. Bluetooth Smart or Bluetooth Low Energy (BLE) use 2 MHz wide signals with frequency hopping and some proprietary protocols, like the one used in Logitech Mice/Keyboards, utilize 2 MHz bandwidth with time division multiplexing. SSC cannot infer a hopping pattern so it was not possible to discriminate with confidence among 2 MHz wide signals. Enough doubt is left to distinguish a ZigBee® system from a 2 MHz wide Bluetooth system, as both use the same channel allocation scheme and bandwidths. That is why all narrowband systems are shown in one single plot without any further processing in Figure 7. It also means that SRO for narrowband systems cannot be calculated as distinguishing among different systems is not possible.

Interesting finding is that the system independent metric FBO seems almost to follow the pattern of a system dependent metric, which is the highest, i.e. the most significant SRO of a system as shown in Figure 8. In our case, IEEE 802.11b and g had been the most impactful systems with highest SRO among all, and FBO nearly follows its distribution. Of course, it is quite legit and logical, as occupancies for IEEE 802.11n were found to be very close to zero.

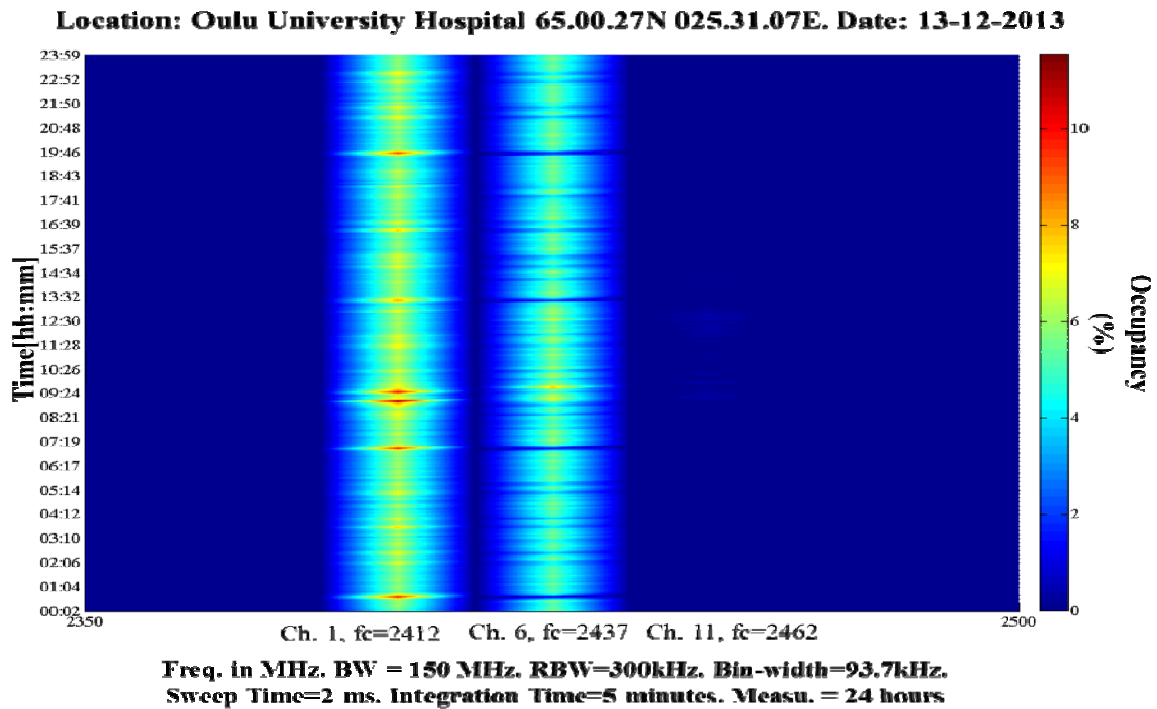


Figure 5: CO, IEEE 802.11 b/g (13-12-2013)

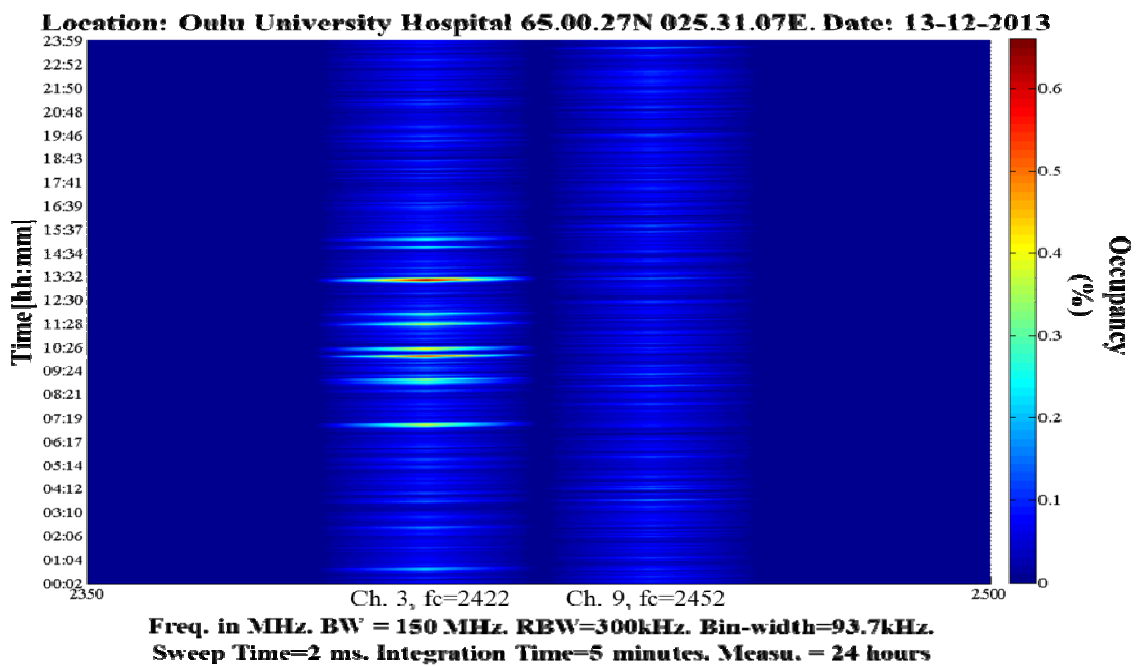


Figure 6: CO, IEEE 802.11 n (13-12-2013)

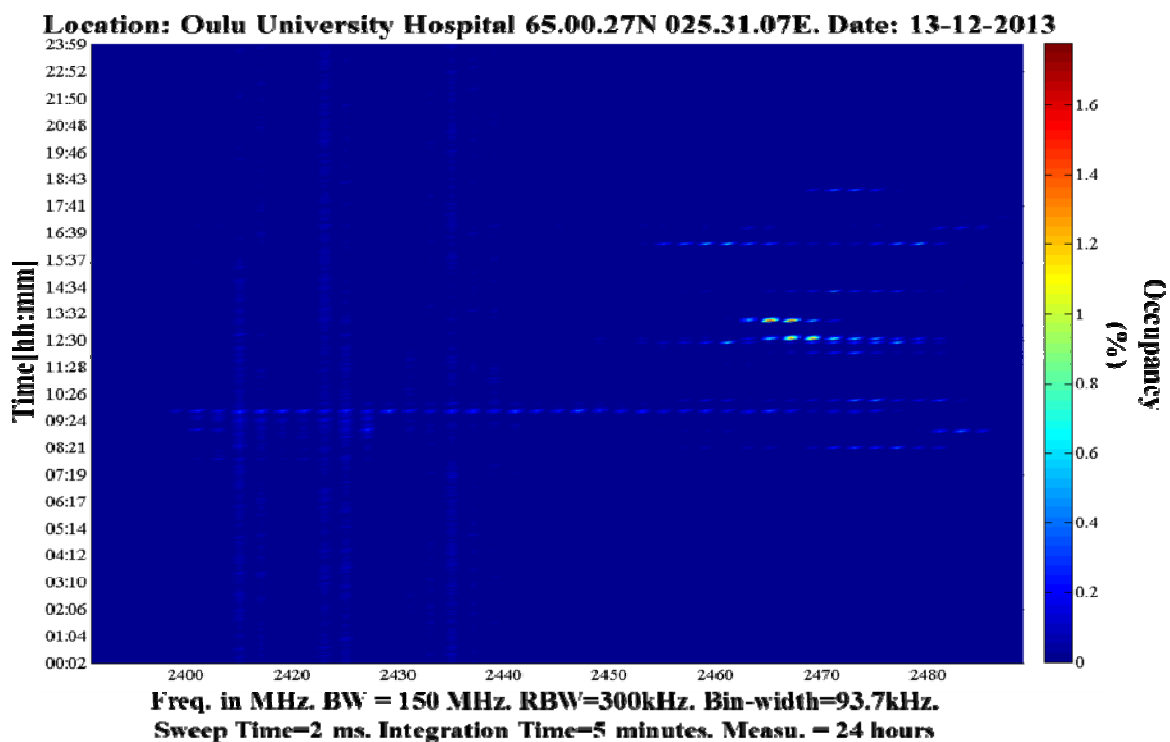


Figure 7: Occupancy of Narrowband systems (13-12-2013)

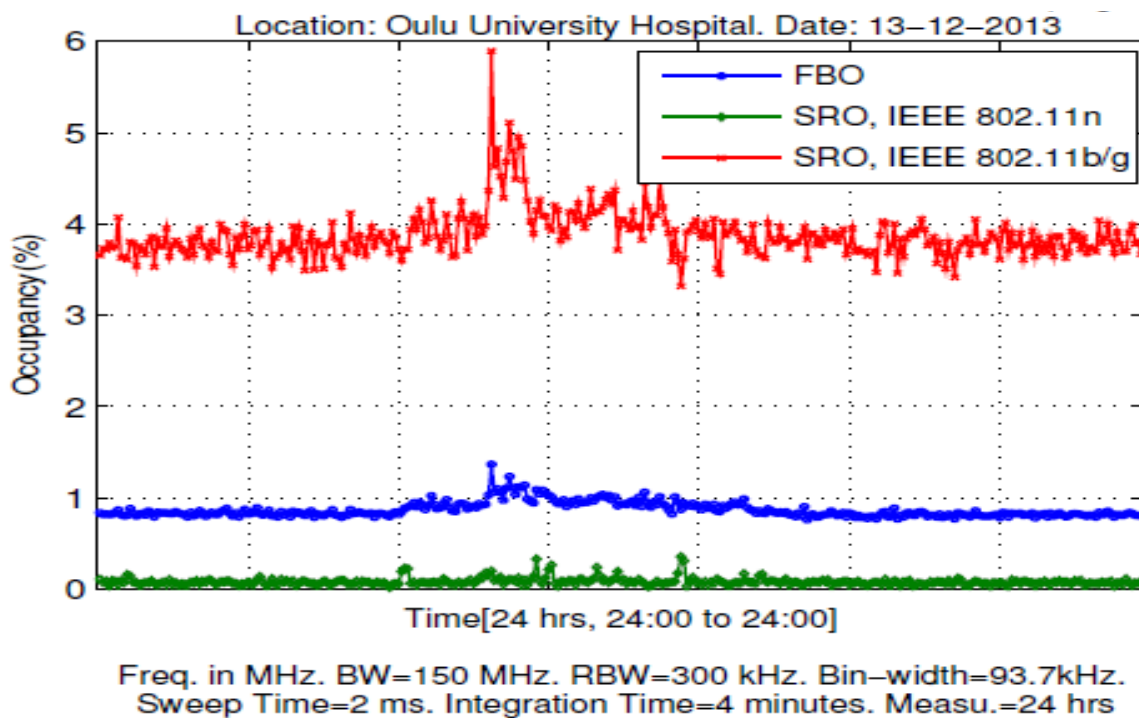


Figure 8: FBO and SRO for the identified systems (13-12-2013)

Figure 9 shows variations of FBO and Figure 10 shows variations of SRO for IEEE 802.11 [i.3] type systems over the period of a week.

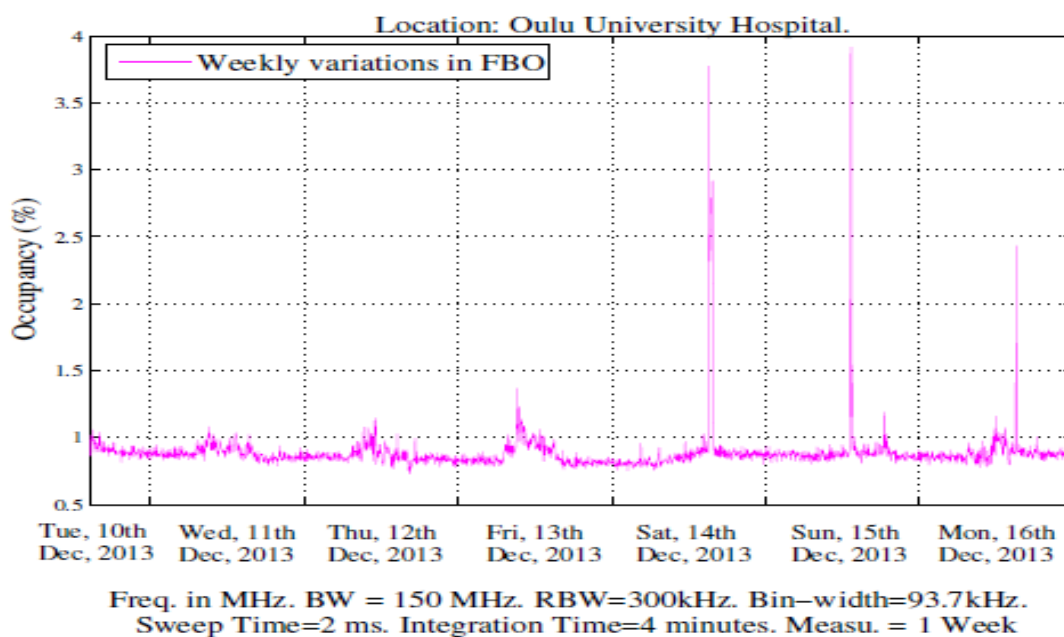


Figure 9: FBO weekly variations

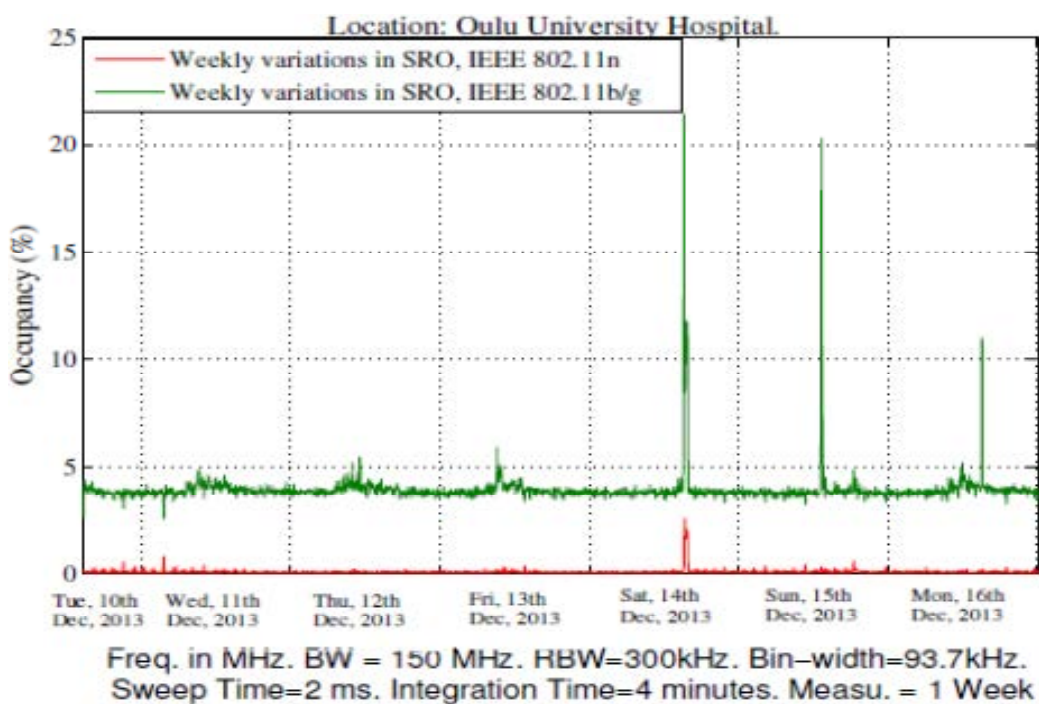


Figure 10: Weekly variations of SRO for two IEEE 802.11 systems

Previous literature had shown that channel occupancies had been between 10 to 15 percent even at some of the busiest hotspots. Literature often views it as a problem inherent to measurement equipment, which underestimates the true, legitimate occupancy values in comparison to measured ones. Our method has been robust enough to fight against channel nulls, variable noise floor and to identify various systems working in parallel.

Figures 9 and 10 depict whole week FBO and SRO analyses starting from 10th of December and ending at 16th of December. During our campaign, on Saturday and Sunday, some maintenance and updates were scheduled at the hospital premises. There had been significant amount of wireless traffic being generated. Our system detected 50 % to 60 % occupancies in the time window of 2 hours. Plots of Saturday are presented here only as an example, i.e. from Figure 11 to Figure 14. During maintenance, all channels were occupied, as shown in Figure 11, even the channel no. 11, which had shown least activity during the other days. There had been no narrowband activity in the whole day except when there was maintenance and update processes going on, and the plot in Figure 13 seems to suggest the existence of a Bluetooth based device as a frequency hopping pattern can be seen. Figure 14 shows that while SRO metric for IEEE 802.11b/g was touching 22 % mark, FBO was still at 4 %. This is a very interesting result, which tells us that there are still 96 % of the band resources free, when there was a certain channel occupied more than 50 % of the time. The region from 2,35 GHz to 2,4 GHz had always been found empty and can be utilized for medical applications. Figures 15 and 16 show comparisons among channel occupancies of the IEEE 802.11b/g and IEEE 802.11n systems over a period of one week.

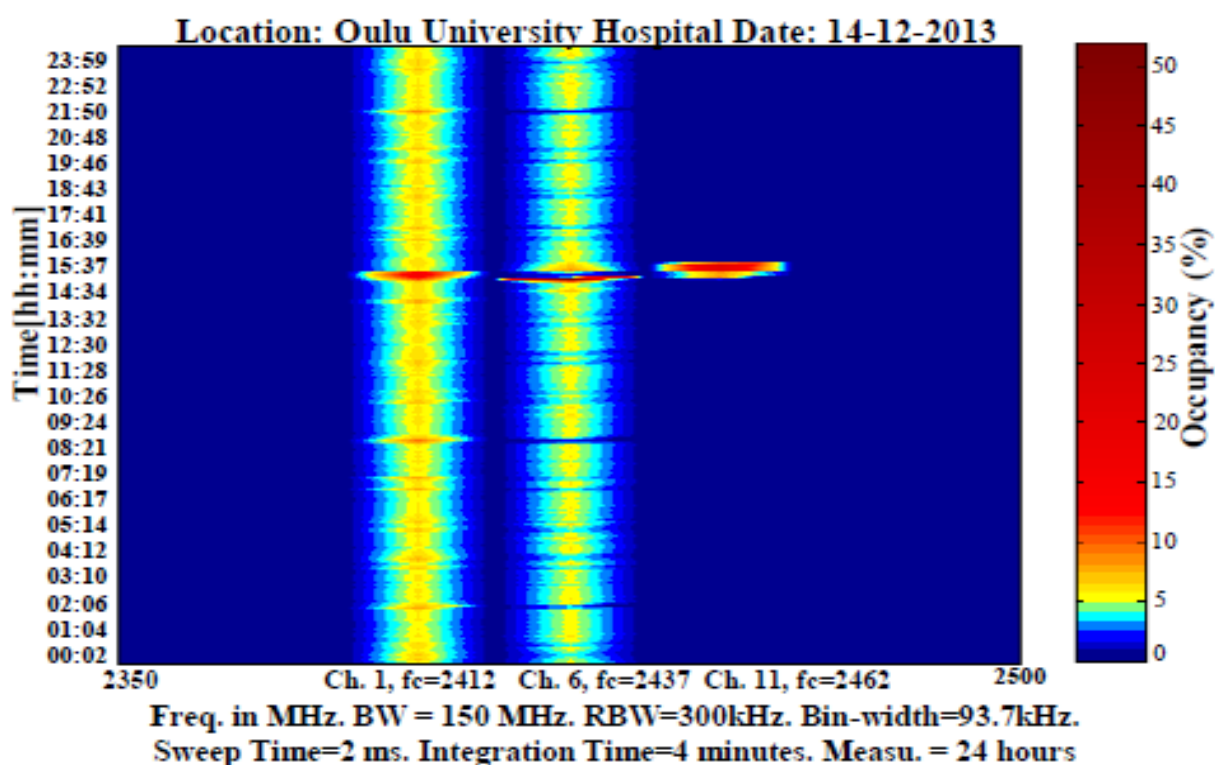


Figure 11: CO, IEEE 802.11 b/g (14-12-2013)

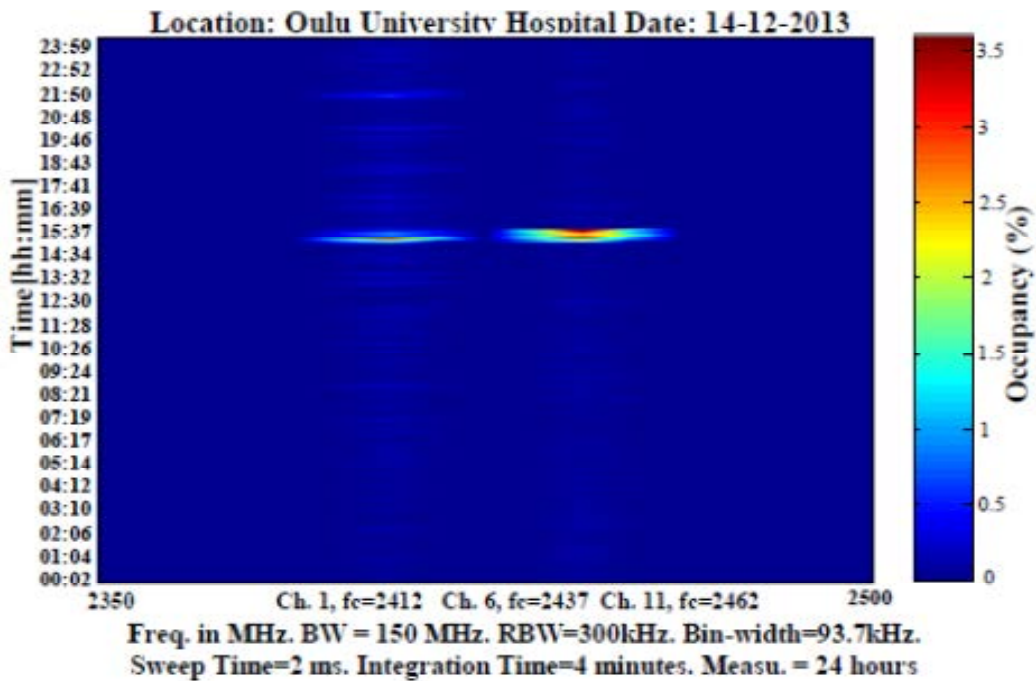


Figure 12: CO, IEEE 802.11 [i.3] n (14-12-2013)

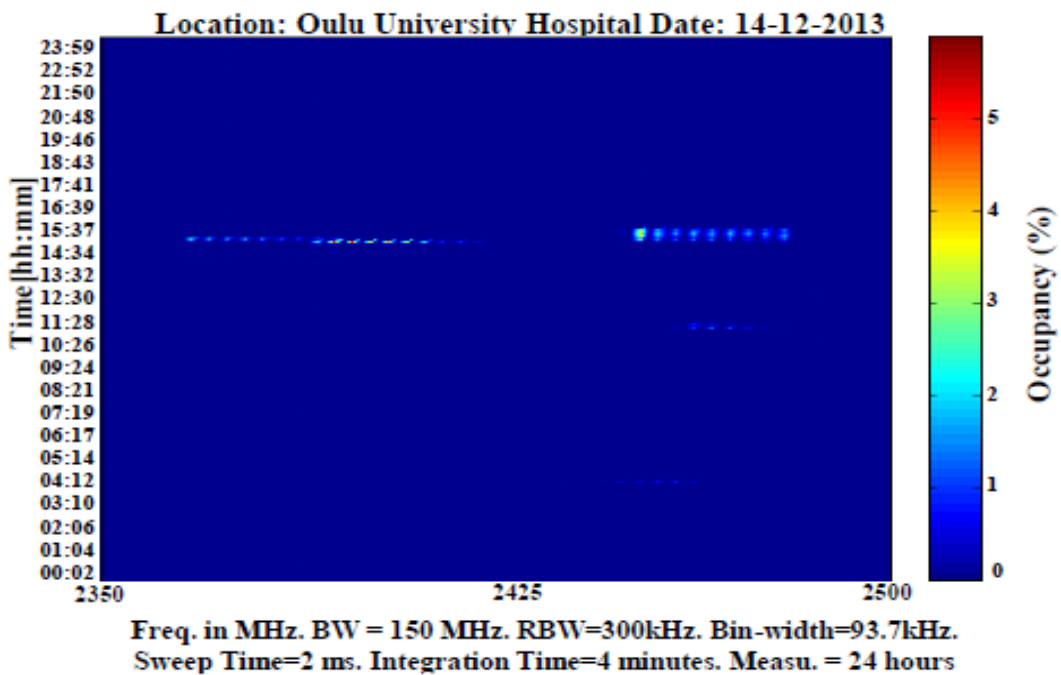


Figure 13: Occupancy, Narrowband Systems (14-12-2013)

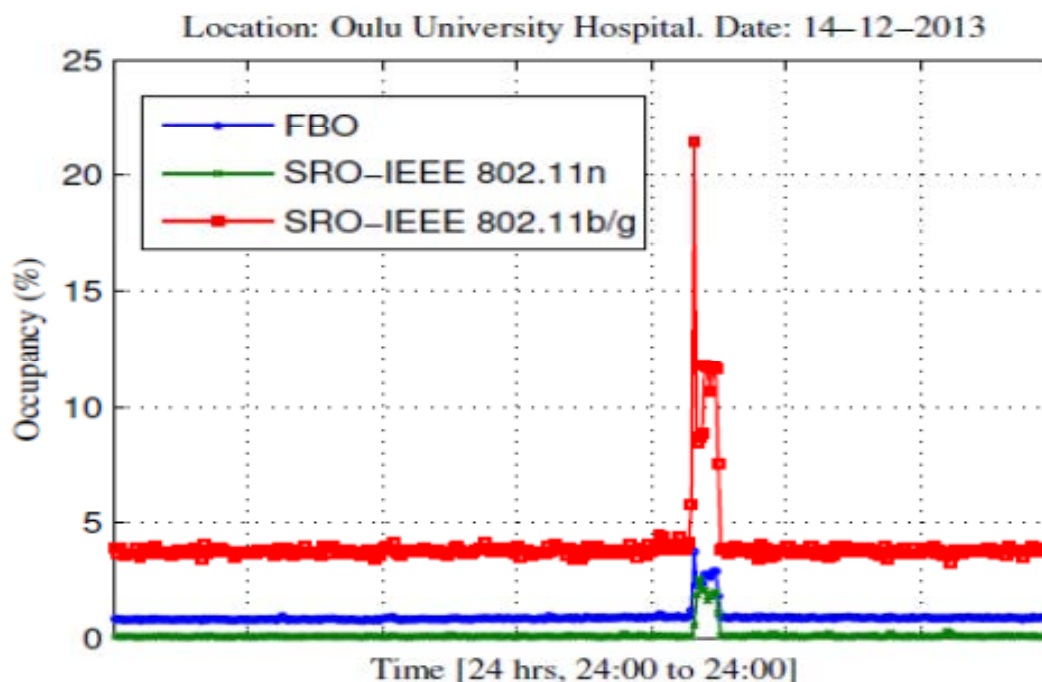


Figure 14: FBO, SRO for the identified systems (14-12-2013)

Figure 15 presents channel occupancy comparison among 20 MHz wide IEEE 802.11b/g channels throughout the week long campaign. Out of the 14 legitimate channels of this system, three channels (1, 6 and 11) were found to be occupied, which is the, so called, safest configuration of the system, i.e. three non-overlapping channels are operating in the same environment. One strange observation was that whenever the Channel 1 was highly occupied, occupancy level of Channel 6 fell down. This behaviour had been consistent the whole span of measurement.

However, there exists an explanation for such a behaviour. IEEE 802.11b/g only specifies centre frequencies and a spectral mask. IEEE 802.11b spectral mask requires that the signal power should be at least 30 dB less than its peak power at ± 11 MHz and at least 50 dB less at ± 22 MHz from the centre frequency. If there is a very powerful transmitter, signal can be quite strong even beyond ± 22 MHz point, which means all channels will actually overlap, even the non-overlapping ones. This phenomenon gives rise to a problem known as near-far problem where two communication systems encounter interference when a foreign station that transmits on an adjacent channel is in much closer proximity than the intended one. Figure 15 shows actually the near-far problem, where the access point which is assigned Channel 11 is much closer to our measurement equipment as compared to the access point which is assigned Channel 6. In the case of IEEE 802.11n systems, the comparison of channel occupancies in Figure 16 clearly shows that near-far problem is non-evident.

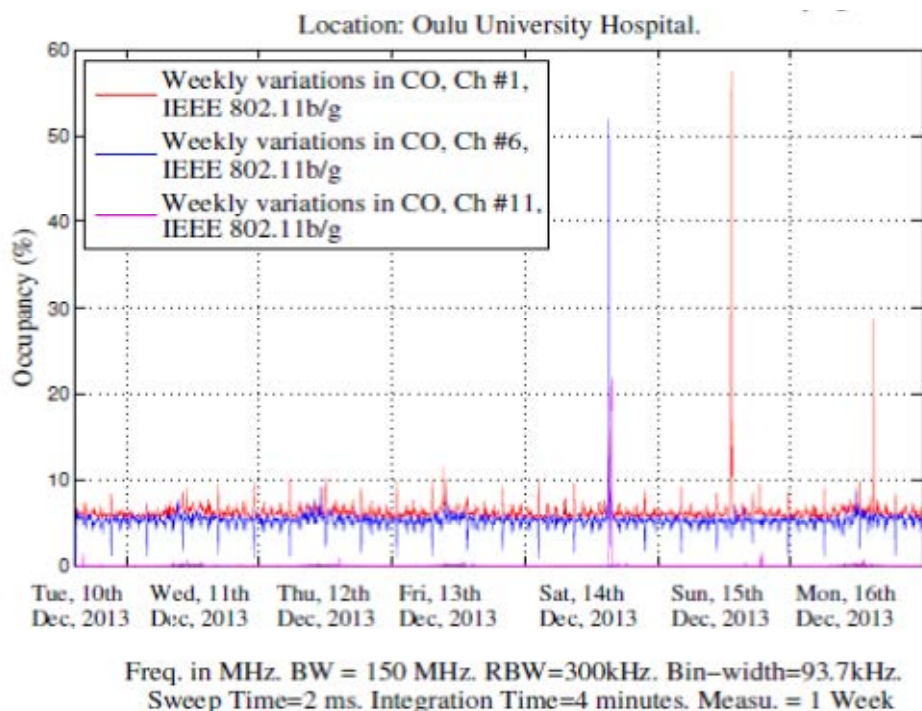


Figure 15: CO comparison among IEEE 802.11 b/g channels over the period of a week

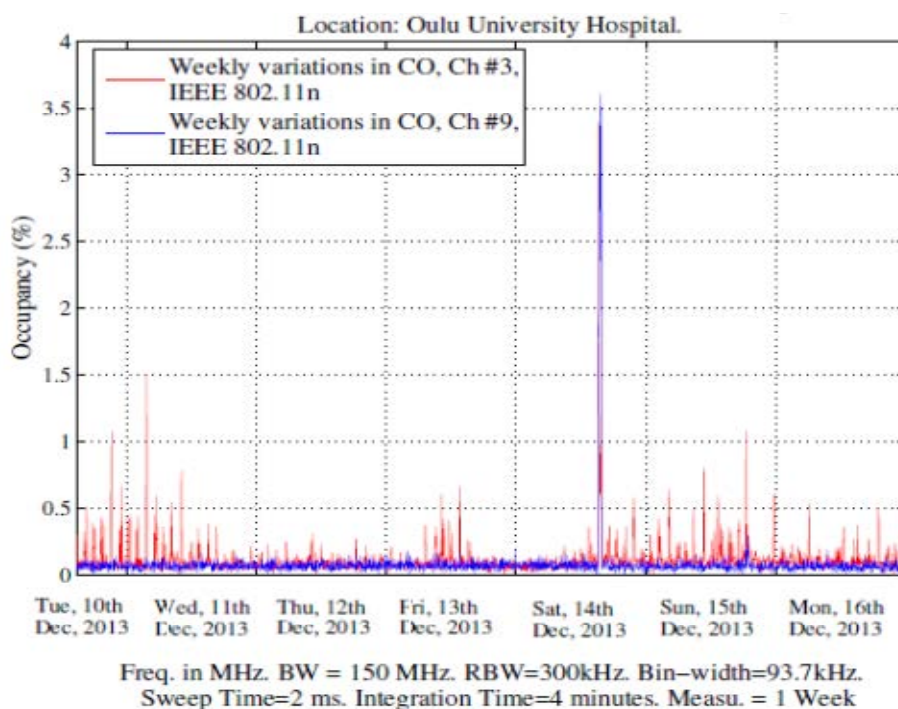


Figure 16: CO comparison among IEEE 802.11 n channels over the period of a week

The analysis suggests that 2,4 GHz ISM band still provides enough opportunities to be considered for medical BANs. Even in the case of high occupancies there were free resources, and especially, there were white spaces available in between the bursty transmissions, which suggests that the cognitive solution might save the day. Also radio network planning in hospitals should be done with due care. Inappropriate network planning can lead to intra-network interference. However, it is always a question of required quality-of-service (QoS) level, what occupancy level is acceptable in the case of medical related communication.

6.3.1.2 Accident & Emergency Ward SOEs (Campaign 2)

In the second measurement campaign, which was carried out at accident & emergency ward at OYS, the measurement strategy was updated. Due to the location of the SA and the connected antenna, an extended ISM band low noise amplifier (LNA) had to be added, as well as a specially designed bandpass filter (BPF) to increase the level of received energy. LNA had almost 20 dB gain in the extended ISM band and a significantly low noise figure. A logical representation of a measurement equipment after addition of LNA is shown in Figure 17.

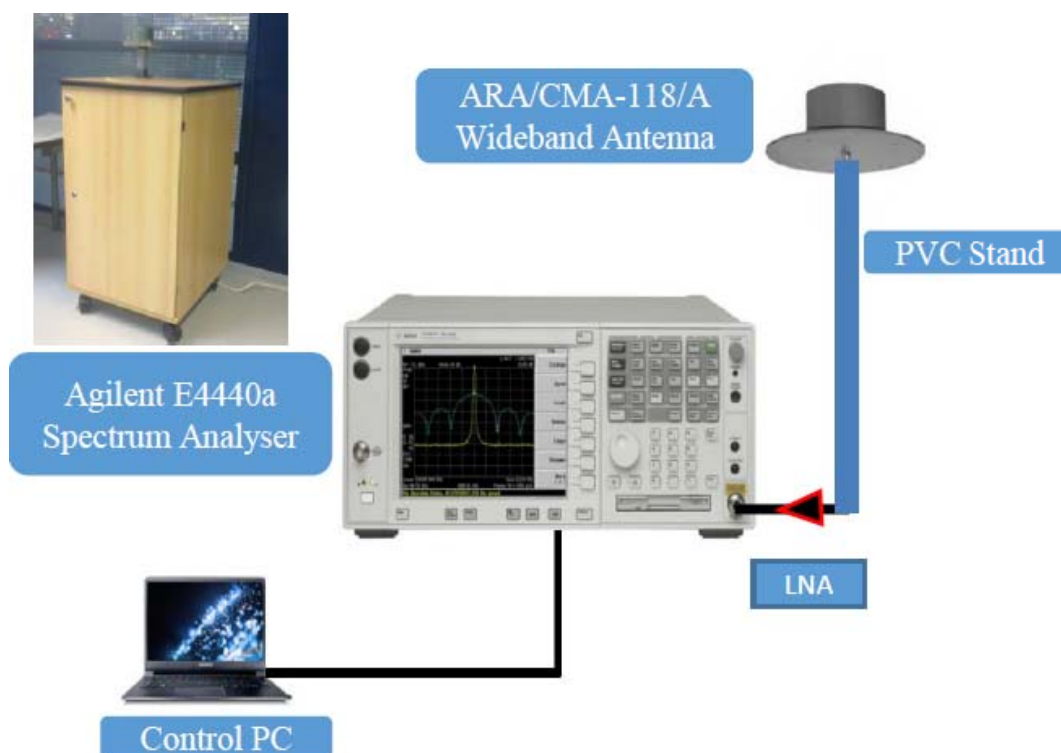


Figure 17: Measurement Equipment with extended ISM band LNA

The frequency band of interest is based again on the requirements given by the ETSI TC SmartBAN [i.1]. During the data post-processing phase, the frequency band was divided into 150 hypothetical WBAN channels, each with 1 MHz bandwidth. SOE metrics evaluated include channel occupancy (CO) and spectrum resource occupancy (SRO). Channel statistics were obtained using a Neyman-Pearson type of detector along-with a dynamic noise threshold algorithm (Med-FCME) at a false alarm probability of 0,05. The measurement parameters used in this particular campaign are given in Table 2.

Table 2: Measurement Parameters for Accident & Emergency Ward

| Parameter Name | Value |
|----------------------|----------------------|
| Frequency band | 2,35 GHz to 2,50 GHz |
| Bandwidth | 150 MHz |
| Frequency bins | 1 200 |
| Resolution bandwidth | 250 kHz |
| Bin-width | 125 kHz |
| No. of sweeps | 1 250 per minute |
| Sweep time | 3 ms approx. |
| Processing time | 45 ms |
| Integration time | 1 minute |
| Measurement duration | 1 week |

$T \times K$ data samples were collected from the band into one minute long blocks. $T = 1\,250$ represents the number of sweeps, i.e. sensing iterations over the band per minute, whereas K represents the number of samples collected from the band in one sweep. Bin-separation, i.e. the distance between any two adjacent samples was 125 kHz. In this way, $K = 1\,200$ frequency bins (or frequency points) represent 150 MHz wide frequency band. The resolution bandwidth (RBW) for the SA was chosen to be 250 kHz, which is exactly $\frac{1}{4}$ of the minimum channel bandwidth (1 MHz) of ISM band users, as proposed by ITU-R in [i.5].

To give our analysis a proper perspective, a hypothetical scenario is considered. The band 2,35 GHz to 2,50 GHz is divided into 150 channels, where each channel is 1 MHz wide. If a WBAN device would work in any of these channels, it might perform a clear channel assessment before transmission and back-off if channel is sensed busy. The main idea here is to get statistics, which would describe how many times or how long the channel was found to be occupied or idle over a period of time. In order to establish that in a certain sweep a channel X_i ; $i = 1, 2, 3, \dots, 150$ was occupied or not, a hypothesis test is performed. The problem is formulated as either observing only noise N or observing a signal with noise. Mathematically,

$$\begin{aligned} H_0 : X_i &= N, i = 1, 2, 3, \dots, 150 \\ \text{and} \\ H_1 : X_i &= S|N, i = 1, 2, 3, \dots, 150 \end{aligned} \quad (3)$$

where H_0 is the null hypothesis that there is only noise in the channel and H_1 is the alternative hypothesis that there is signal plus noise in the channel. A detection decision problem takes the form given by:

$$D(X_i) = \frac{1}{n} \sum_{j=1}^n P(X_i(j)) \underset{H_1}{\overset{H_0}{\gtrless}} \gamma \quad (4)$$

where $\sum P(X_i(j))$ is the sum of $j = 1, 2, 3, \dots, n$ sample powers in linear units for a channel X_i , $D(X_i)$ is the decision statistic and γ is the decision threshold.

Mean power in the channel X_i is then compared to the threshold, which is obtained using a dynamic noise threshold algorithm called as median forward consecutive mean excision. If the power is found to be less than the threshold, the channel is defined not to be occupied, and vice versa. The method is pretty similar to the real implementations of clear channel assessment based on energy detection (CCA-ED). In other words, if the signal energy in the channel crosses a certain threshold set for CCA, the channel is marked busy until the medium energy is below the threshold. The decision statistic for a specific channel X_i can simply be marked either 0 if unoccupied or 1 if occupied. Hence, a binary $T \times K$ matrix, which provides occupancy matrix over the period of 1 minute, was produced. Using this strategy, 183 GB of data recorded during the measurement campaign was processed into a minute long binary blocks. For example, a binary matrix O_{MAT} with elements $O_{MAT}(T, C)$ is produced by calculating mean powers for every channel X_i using decision statistic as

$$O_{MAT}(\mathbf{T}, \mathbf{C}) = \begin{cases} 1, & \text{if } \frac{1}{n} \sum_{j=1}^n P(X_i(j)) > \gamma \\ 0, & \text{if } \frac{1}{n} \sum_{j=1}^n P(X_i(j)) < \gamma, \end{cases} \quad (5)$$

where $T = 1, 2, 3, \dots, 1250$ is the sweep number and $C = 1, 2, 3, \dots, 150$ is the channel number.

Spectrum occupancy evaluations were then performed just as in the previous campaign. Figure 18 shows a plot regarding channel occupancies for all 150 channels over the period of 1 week. Similarly, a channel occupancy plot can be presented for each day as shown in Figure 19. Maximum and mean occupancies over a period of the whole week are shown in Figure 20. Maximum curve points show the maximum level of occupancy observed in a specific channel, and the mean points represent the average occupancy observed in that particular channel over the week. Moreover, mean occupancies provide us with an interesting insight that occupancy levels fluctuate greatly but, on the average, a large part of the studied frequency band is free. It can be observed in the plots that there are WLAN users within a band from 2 400 MHz to 2 470 MHz. Some low-powered narrowband signals with occupied bandwidth (OBW) varying from 2 to 3 MHz, which might belong to some system utilizing audio/video wireless transceivers, were also observed. Most of the narrowband activity was observed around the centre frequencies $f_c = 2\ 406\ \text{MHz}$, $2\ 427\ \text{MHz}$ and $2\ 490\ \text{MHz}$. The frequency band from 2 350 MHz to 2 400 MHz was used the least. However, occasionally some very low power signals were found with OBW close to 10 MHz. Those signals may belong to 13 cm ultra-high frequency (UHF) amateur radio users who can use the frequency band from 2 300 MHz to 2 400 MHz on secondary basis internationally. An evidence of such stray signals can be seen in Figure 21. However, because of their seldom appearing during longer analyses, they were averaged out from the final results.

SRO is a measure reflecting how much of the band resources are being utilized simultaneously at a given time. Figure 22 shows the SRO observed over the whole week for the full band under observation, i.e. 2 350 MHz to 2 500 MHz. Maximum SRO was observed on day 6, when it reached about 16 %. The mean SRO calculated was about 4,5 %, which implies that 95,5 % of the channel resources out of 150 were unoccupied, on the average, over the whole campaign.

However, Figure 22 might be taken as a little biased, because the band from 2 350 MHz to 2 400 MHz is mostly empty. That is why the SRO for 2 360 MHz to 2 400 MHz band and 2 401 MHz to 2 480 MHz band were calculated separately, as shown in Figure 23. It can be observed that the 40 channels from 2 360 MHz to 2 400 MHz are scarcely occupied. Maximum SRO, 6,49 % was observed on day 6 and the mean SRO was observed to be 0,1 %. Whereas, while observing 80 channels from 2 401 MHz to 2 480 MHz, which is actually the 2,4 GHz ISM band, the maximum SRO was observed to be 26,38 % and the mean SRO was 8,01 %. Hence, still 91,99 % of the channel resources are available in the 2,4 GHz ISM band.

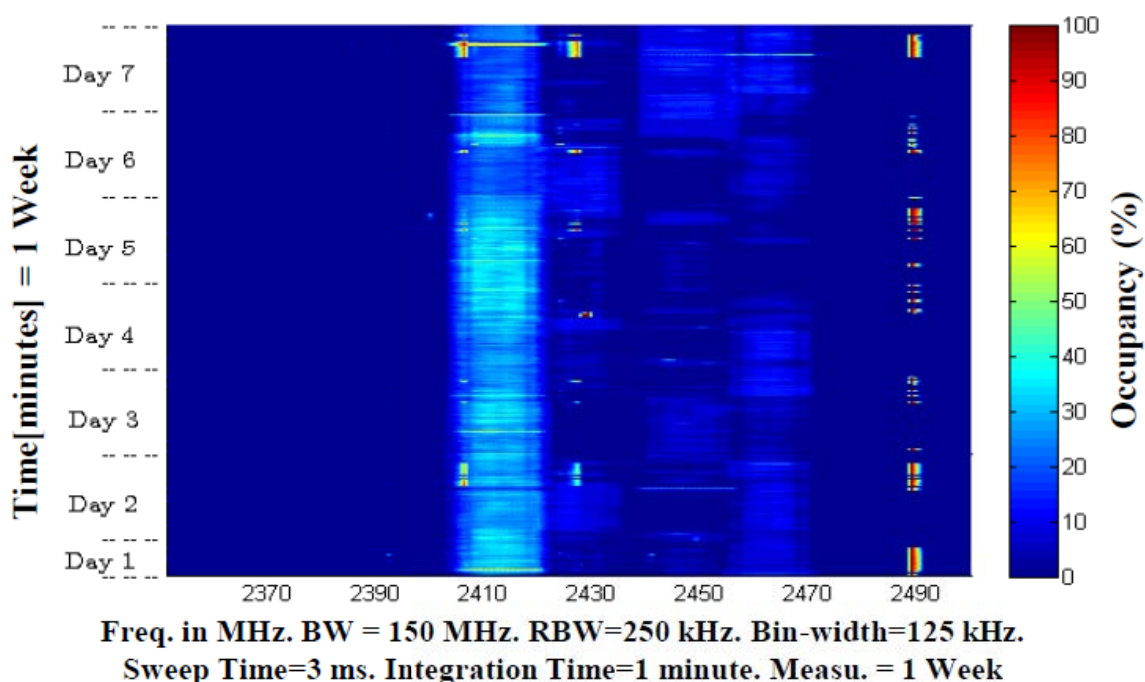
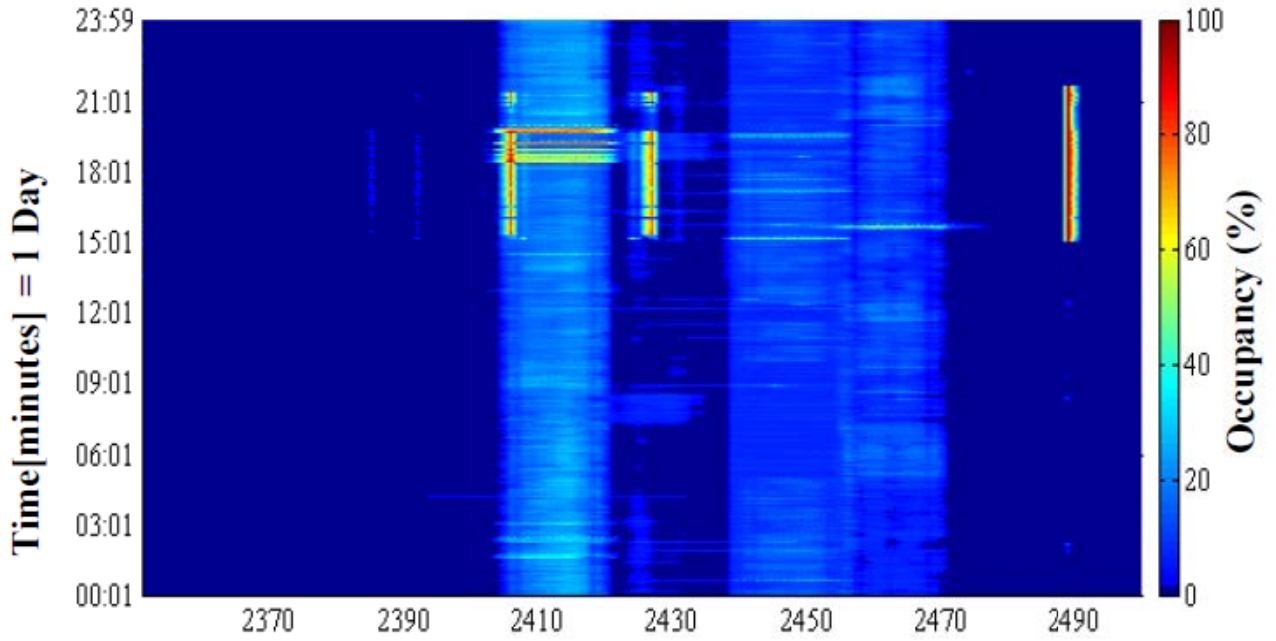


Figure 18: Weekly Occupancy in Accident & Emergency Ward



Freq. in MHz. BW = 150 MHz. RBW=250 kHz. Bin-width=125 kHz. Sweep Time=3 ms. Integration Time=1 minute. Measu. = 1 Day

Figure 19: A Single day occupancy for Accident & Emergency Ward

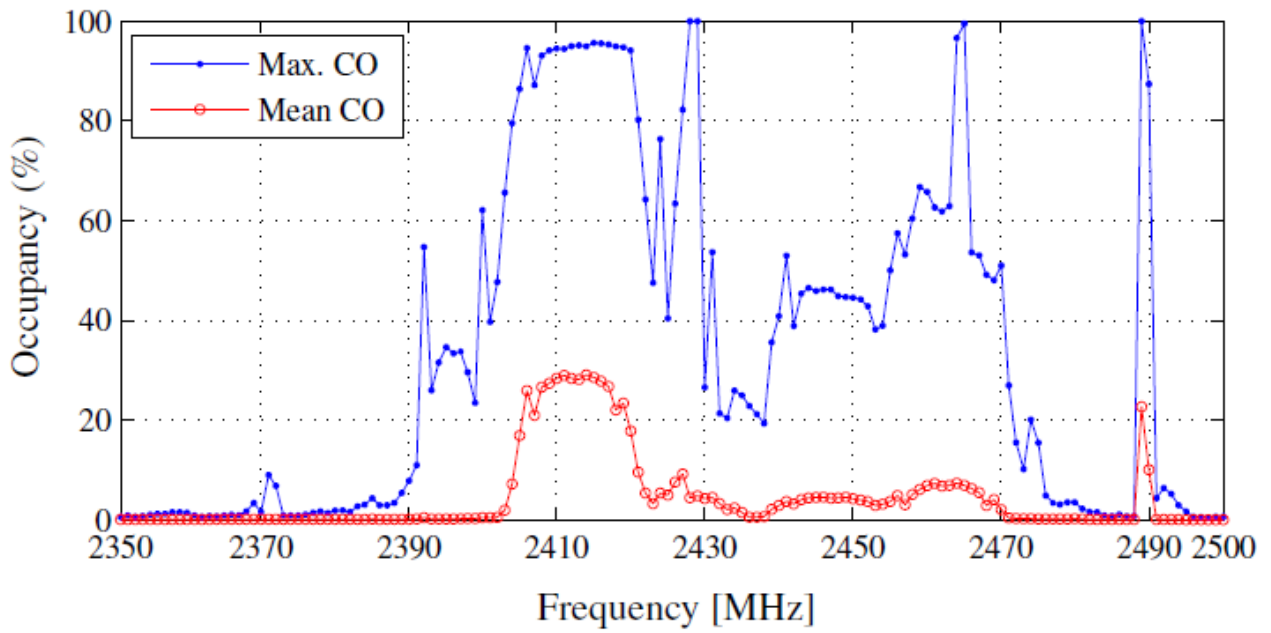


Figure 20: CO, Mean & Max curves at Accident & Emergency Ward

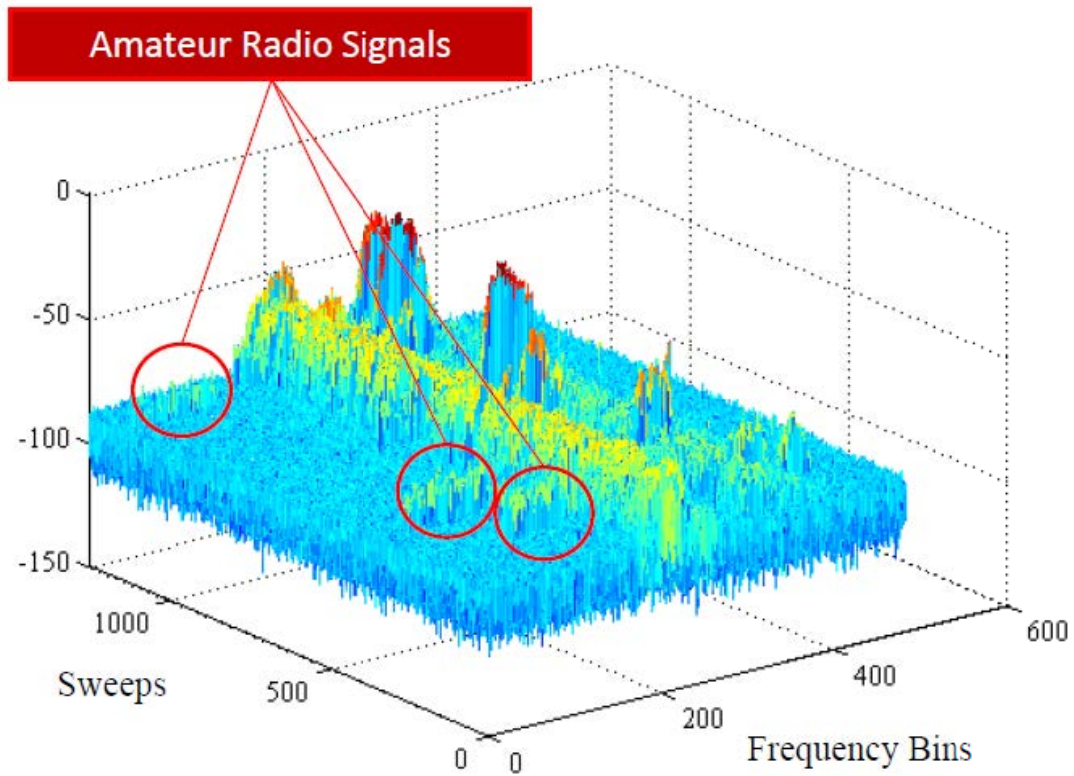


Figure 21: Existence of possible Amateur Radio Signals

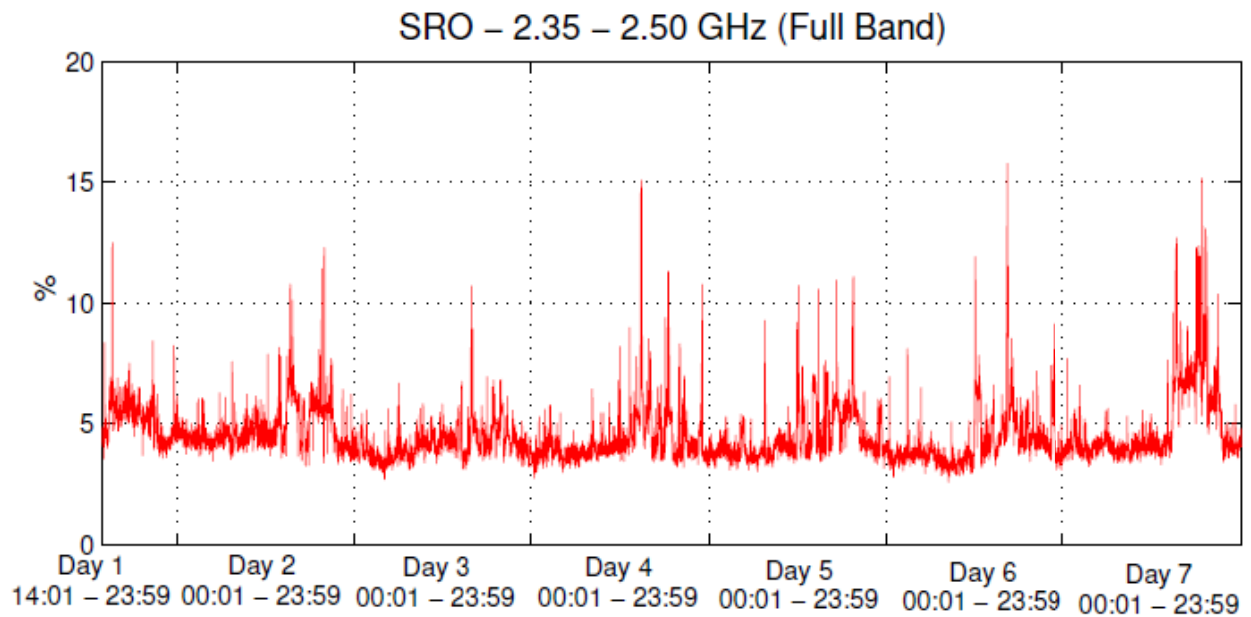


Figure 22: SRO (Full Band) at Accident & Emergency Ward

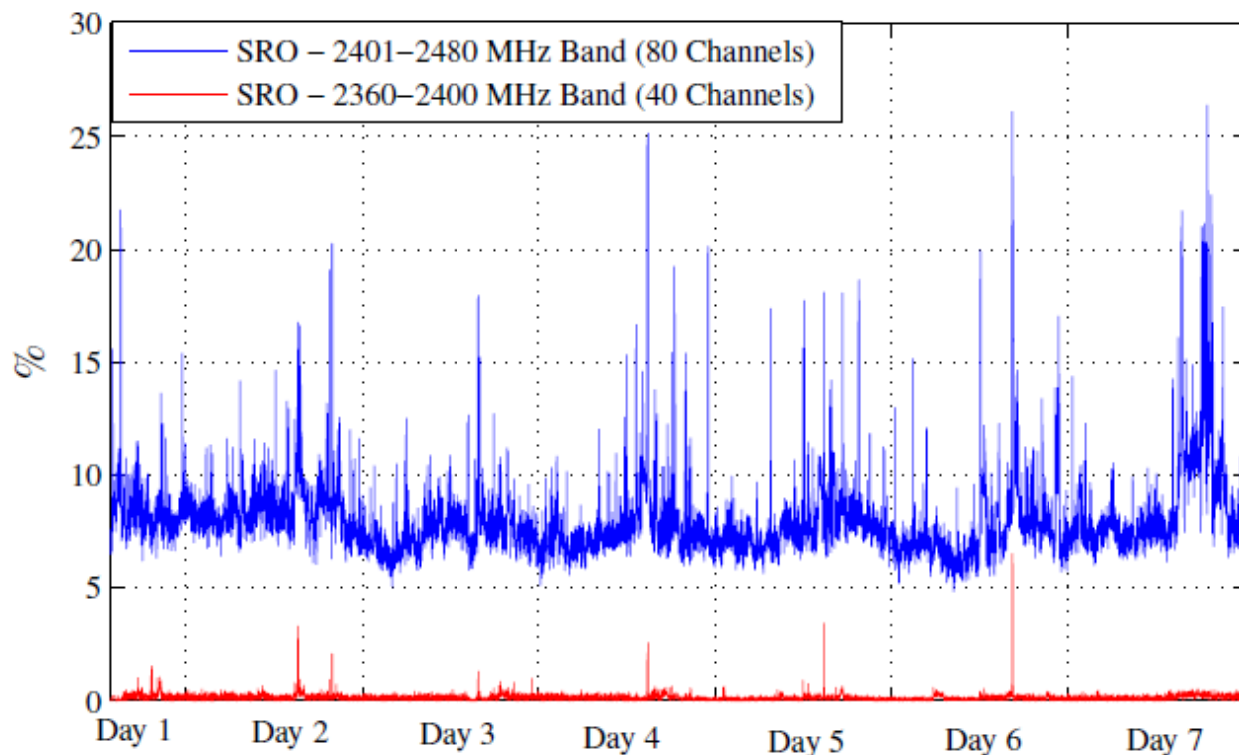


Figure 23: SRO for 2 360 MHz to 2 400 MHz and 2 401 MHz to 2 480 MHz bands

Various channels in the band were observed to be highly occupied, i.e. CO reached 90 % to 100 %. On the other hand, some channels were not occupied at all. However, mean occupancies over the week in channels ranging from 2 401 to 2 426 reached 30 %. SRO for the whole band from 2 350 MHz to 2 500 MHz band was observed to be 4,5 %, on the average, and the maximum was seen to be 16 %. SRO for the band from 2 360 MHz to 2 400 MHz was observed to be 0,1 % on the average, which implies that this portion of the band is open for further exploitation. Finally, SRO for 2 401 MHz to 2 480 MHz was calculated, and it showed that there were 91,99 % channel resources free, on average.

6.3.1.3 X-Ray & Radiology Ward SOEs (Campaign 3)

A similar campaign as described in the previous clause was undertaken at X-ray & radiology ward of Oulu University Hospital. The campaign lasted for a week and the measurements were analysed exactly in the same way as in the accident & emergency ward's case. The X-ray & radiology ward contained state-of-the-art computer aided tomography machines, X-ray machines, microwave and radio ablation & diathermy machines. Some sweeping radiations have been witnessed throughout the band that might have arose due to the use of microwave and radio ablation & diathermy devices because the radiation leakage of other devices does not fall in ISM band or pre-ISM band. The detected radiation powers have usually been close to -85 dBm and occasionally stronger powers were detected. The first six days of the campaign showed this kind of behaviour. An example of such behaviour is shown in Figure 24. However, on the 7th day, there had been a narrowband emission near 2 390 MHz which was present in last campaign as well. Figure 25 displays the occupancy on the last day of the campaign, 25th June 2014. Figure 26 shows the occupancy for the whole week.

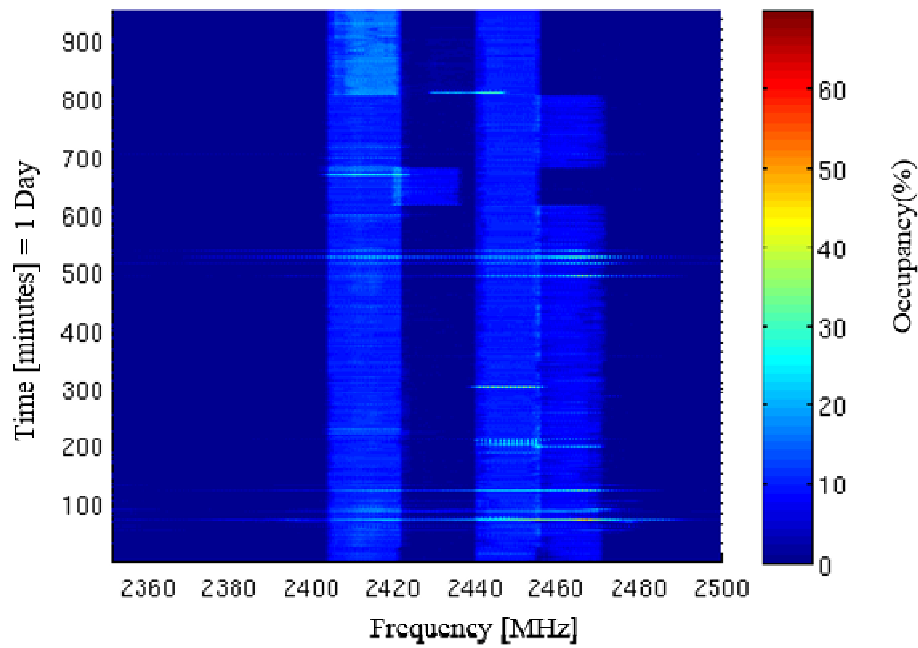


Figure 24: Occupancy for first day (18th June 2014) at X-Ray & Radiology Ward

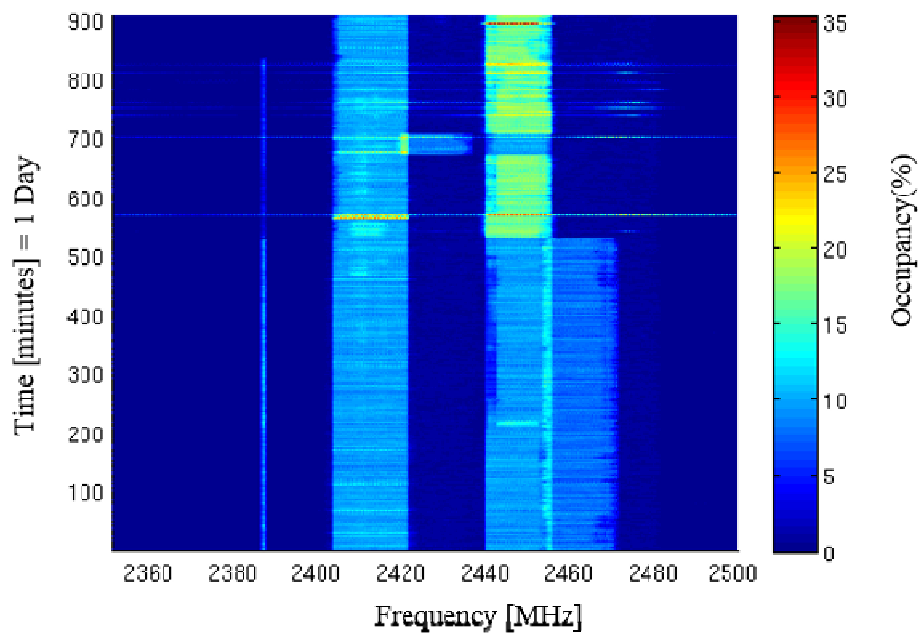


Figure 25: Occupancy on the last day (25th June 2014) at X-Ray & Radiology Ward

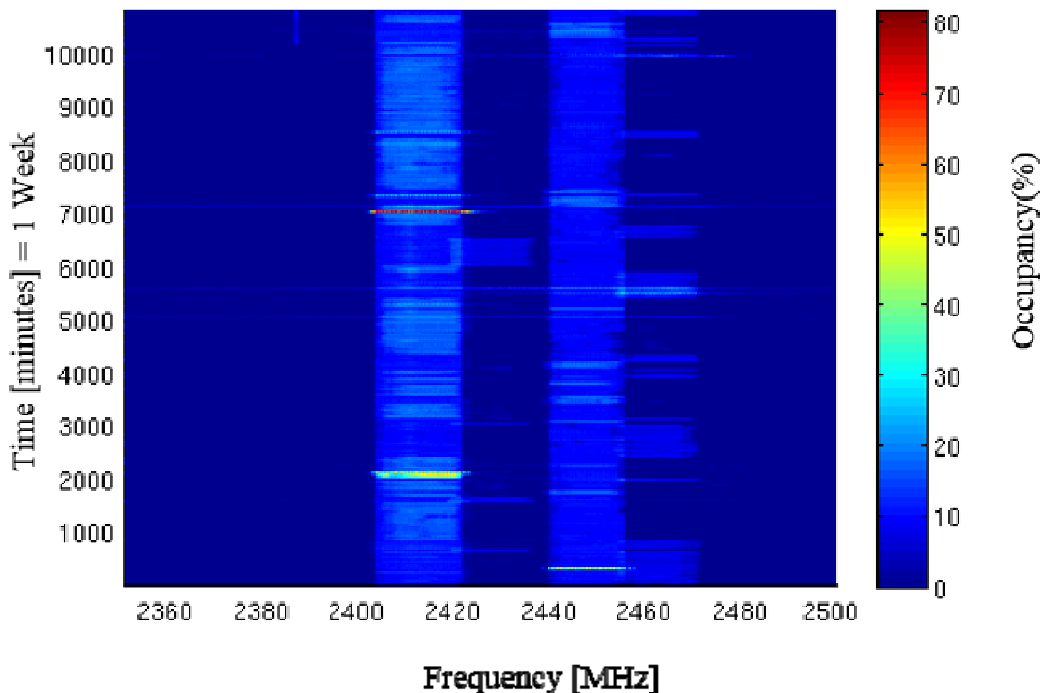


Figure 26: Weekly occupancy at X-Ray & Emergency Ward

6.3.2 Analytical Stochastic Model for Spectrum Occupancy

In order to mathematically characterize the potential interference to WBANs in a hospital environment, stochastic mathematical models for channel and spectrum resource occupancy in 2,35 GHz to 2,50 GHz band are proposed. The models present spectrum occupancy framework from the view point of WBANs. The probability density functions proposed by the model are then validated by statistical hypothesis tests utilizing real measurement data. Measurement data from Oulu University Hospital was used to validate the models. The idea behind this work was to formulate a statistical perspective regarding frequency resource utilization in a hospital environment, which would provide industry and academia with tools to regenerate similar utilization patterns in the laboratory and simulation environment. The model can be used in simulations for WBANs considering interference management, network design, and testing coexistence scenarios, etc. Detection and channel decision statistics were calculated just as mentioned in the previous clauses.

Without going into the details regarding formulation of the models, here the most important results obtained are presented. For more details about the model formulation and theory behind the idea, please refer to [i.10]. The stochastic modelling process for an individual channel can be viewed logically as a coin-flip experiment with two possible outcomes. Relating to the fact that a binary matrix representing occupied (1) and unoccupied (0) channels is created, previous presumption makes sense. A binomial process models the signal arrival times within a 1 minute long block. A Poisson process models the arrival times of signals in an arbitrarily long train of 1 minute long blocks. Markovian chains are defined for the models, and then Chi-square test statistic is used to validate the model against the real measured data. Arrival rates were estimated using maximum likelihood estimate (MLE) from the data acquired from hospital.

1 440 minutes (24 hours) long data are considered as a statistical population for a single channel. Random samples with replacement worth of 432 minutes are recorded, which accounts for 35 % of the actual population. Arrival rates were estimated from the data, so one degree of freedom is lost. A Monte-Carlo type of simulation was done for 10 000 iterations and Chi-square test statistic χ^2 was evaluated as

$$\chi^2 = \frac{\sum_{i=1}^n (O_i - E_i)^2}{E_i}, \quad (6)$$

where O_i is the observed value and E_i is the expected value. Degree of freedom is calculated as $n-1-1$ because the arrival rate λ was estimated, whereas n is the cumulative frequency of the observation set $\{O\}$. After obtaining Chi-square statistics, the p-value (probability) can be evaluated by calculating cumulative distribution function (CDF) of Chi-square distribution. P-value is then compared against a significance level $\alpha = 0,05$, i.e. 95 % certain about our results is wanted. Figure 27 shows the results for Channel no. 62, which was one of the most occupied channels.

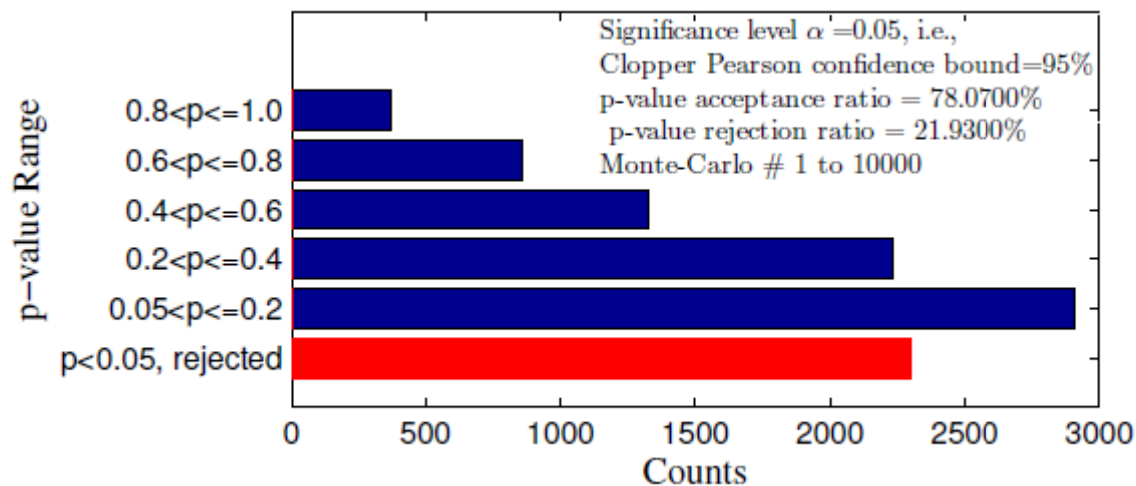


Figure 27: P-value ranges against Monte-Carlo iterations

The results show that 78 % of the time our null hypothesis was accepted, i.e. the model was consistent with the actual data. After analysing all the channels, an interesting phenomenon was observed. Channels with low occupancy levels were fitted to the model better as compared to the highly occupied ones. For example, the same hypothesis testing for channel no. 50, $f_c = 2\,400$ MHz results in 94,79 % acceptance ratio. The reason for deviation is the fact that the highly occupied channels result in very large mean arrival rate λt of the order of hundreds, e.g. λt for Ch. 62 = 393,32. An example, mean arrival rate for a low occupancy channel Ch. 50 is $\lambda t = 4,76$. Rate λt can be thought of as an average rate over t in the whole day, for all local arrival rates λ per minute. This makes our process doubly Poisson, i.e. arrival rates themselves are random variables. Theory suggests that Poisson process with very large λ tends towards Normal distribution and the process can be approximated by applying Yate's continuity correction and undergoing Normal approximation to Poisson. By applying Normal approximation to the highly occupied channels, the null hypothesis acceptance ratio was found out deteriorated further to approximately 71 %. As an example, probability distribution function (PDF) and CDF fitting plots for Channel 62 are presented in Figures 28 and 29.

For SRO, when the spectrum is divided into 150 channels, an analogy of 150 coins being flipped simultaneously can be conceived. If the outcomes of all coin flips are independent, the process can be defined as discrete multi-state Markov process with Poisson distribution depending upon the number of trials n , just as explained in the previous clause. Only difference here is that the model can choose any state from 0 to 150. At least one state has to be chosen. For example, if 10 channels out of 150 are found occupied simultaneously, then the state selected is 10. If none is occupied, state is 0, representing SRO = 0 %. Every state can be reached from any other state. Complete transition matrix for such a model is of course quite complicated to calculate. However, thanks to Markov property, the last state has to be known and the probabilities can be calculated directly from the probability distribution functions. Hypothesis testing was performed with the null hypothesis that the SRO at any sweep n follows a Poisson distribution. A Monte-Carlo type of simulation was performed for 10 000 iterations and χ^2 statistic was evaluated. In every iteration, a single sweep data was randomly selected from the pool of whole day, i.e. 150 points were selected. Every point represented a channel and a number K was counted, which represented the number of total channels being occupied at that particular time. The hypothesis acceptance ratio was found to be 99,96 %. PDF and CDF fitting plots are shown in Figures 30 and 31. Table 3 provides a short summary of acceptance ratios for both CO and SRO models. Poisson process converges to normality in case of higher occupancies but hypothesis tests' results become more deteriorated. This suggests that the channel should be characterized by a continuous distribution other than Normal or Gaussian. In the case of spectrum resource occupancy model, the results showed remarkable consistency.

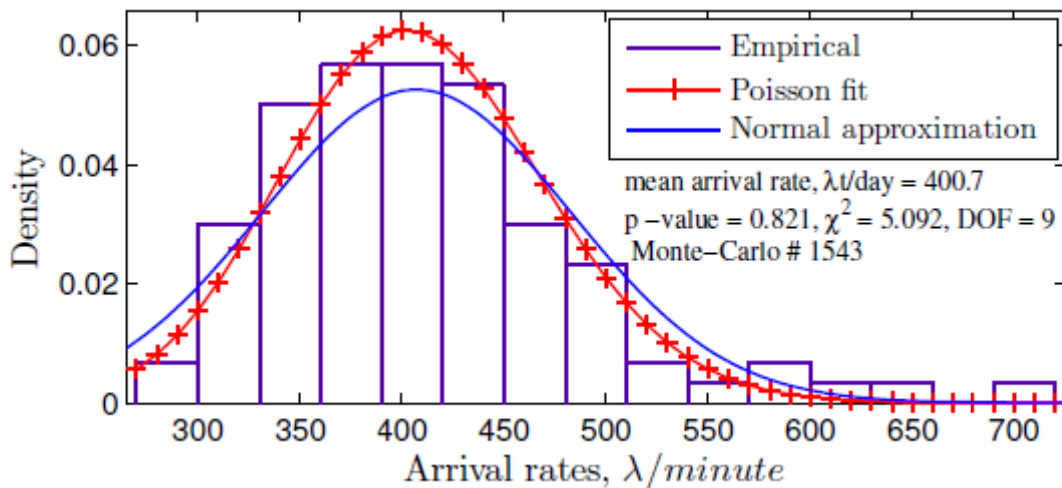


Figure 28: PDF Fitting to Channel 6, fc=2412

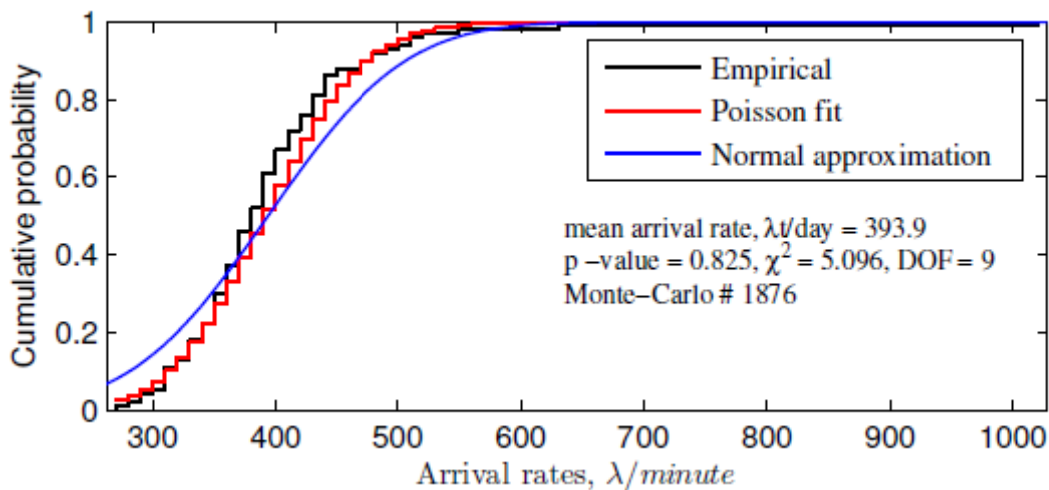


Figure 29: CDF fitting to Channel 62, fc=2412

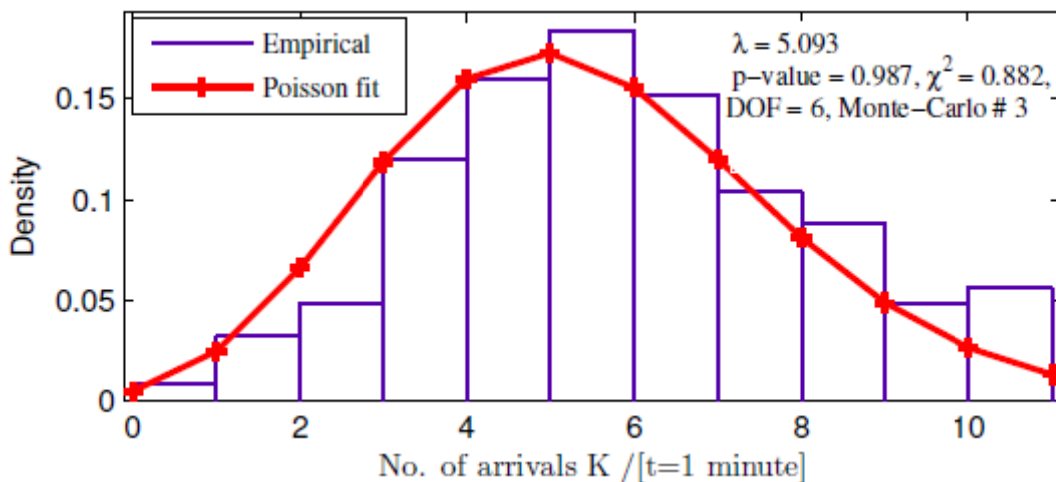


Figure 30: PDF fit for SRO an arbitrary sweep

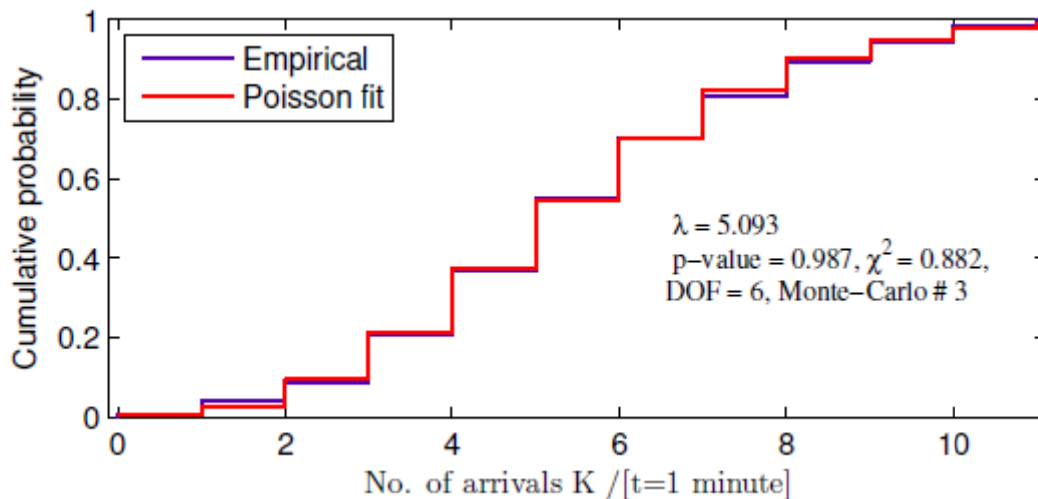


Figure 31: CDF fit for SRO at an arbitrary sweep

Table 3: Summary of Acceptance ratios

| | Binary, 1 minute long Binomial Process Statistic = Binomial Exact | Concatenated, N minutes long Poisson Process Statistic = χ^2 |
|-----------|---|---|
| CO Model | 100% | 78.07% |
| SRO Model | 100% | 99.96% |

6.3.3 Extracting Mathematical Interference model

The analytical models were not very efficient in describing the behaviour of highly occupied channels and the original data. The Normal approximation to Poisson resulted in deteriorated model acceptance ratios. This observation leads us to believe that a better model would be continuous, perhaps long-tailed and heavily skewed. For the extraction of mathematical model, our largest data set which was acquired from daily surgery ward is selected. The total amount of recorded data was 564 GB. Mathematical distribution modelling for the data of such a large scale is a tough nut to crack for a single machine. A distributed computer architecture could have been an option, but it is opted, for simplicity, a optimality based on an observation that most of the elements in the sample space were the noise-only samples. So, if those noise-only samples were declared to be zero, a sparse matrix of 4 minutes long data block is got. Then nonzero elements from the sparse were collected and queued. In the end, when all the data blocks and their corresponding vectors were processed, they can be concatenated to make a single large vector. Finally, this vector is passed through a script which applies various distributions on it and decides the best fit. The decision is based on Bayesian information criterion, as:

$$BIC = -2 \cdot \ln \hat{L} + k \cdot \ln(n), \quad (7)$$

where n is the number of data points in the vector, i.e. number of observations, \hat{L} is the maximized value of likelihood function for the model as:

$$\hat{L} = p(x|\hat{\theta}, M). \quad (8)$$

Here x is the vector, $\hat{\theta}$ are the parameters values that maximize the likelihood function and M is the corresponding model under evaluation. In case of whole day spectrum variations, Normal, Extreme-value, Generalized Extreme-value, Generalized Pareto, Logistic and t-location scale distributions were applied and evaluated, as it was decided to use the vector samples in logarithmic units rather than linear. To model the variations in the spectrum over the time period of a week and a day individually as well, the best fitting mathematical distribution models were evaluated. It was observed that spectrum was varying in a fashion that could be best described by Generalized extreme-value (GEV) and the next most likely model was t-location scale. Interestingly, week long variations and all individual day long variations were following the same distribution. Probability distribution function for GEV can be written as:

$$y = f(x|k, \mu, \sigma) = \left(\frac{1}{\sigma}\right) \exp \left[- \left[1 + k \frac{(x-\mu)}{\sigma} \right]^{\frac{1}{k}} \right] \left[1 + k \frac{(x-\mu)}{\sigma} \right]^{-1-\frac{1}{k}}, \quad (9)$$

for $1 + k \frac{(x-\mu)}{\sigma} > 0$. Here k is the shape parameter, μ is the location parameter, and σ is the scale parameter. The distribution was Type II Frechet distribution as k was greater than zero in every case. Hence, the expected value of x from a sample space X can be given as:

$$E(X) = \mu - \frac{\sigma}{k} + \frac{\sigma}{k} g_1, \quad (10)$$

where $g_n = \Gamma(1 - nk) \forall n \in N = \{1, 2, 3, 4, \dots\}$ and $\Gamma(t)$ is the gamma function.

In addition to that, models for week long variations in FBO, SRO and certain channel occupancies were evaluated. The models under deeper study in this case were Beta, Birnbaum-Saunders, Burr, Exponential, Extreme-value, Gamma, Generalized extreme-value, Generalized Pareto, Inverse Gaussian, Logistic, Log-Logistic, Lognormal, Nakagami, Normal, Rayleigh, Rician, t location-scale and Weibull.

Weekly variations in IEEE 802.11b/g Channel 1 occupancies were observed to follow Burr Type XII distribution whereas the next most likely model was GEV. The PDF for Burr is given as:

$$Y = \frac{kc}{\alpha} \left(\frac{x}{\alpha}\right)^{c-1} \quad (11)$$

and

$$\Phi = \left(1 + \left(\frac{x}{\alpha}\right)^c\right)^{k+1} \quad (12)$$

then

$$y = f(x|\alpha, c, k) = \frac{Y}{\Phi} \quad \forall x, \alpha, c, k > 0. \quad (13)$$

The distribution has been observed to be heavily skewed and long-tailed, which suggests a large number of unique higher occupancy values that essentially make up the tail far away from the distribution head or mean. Long tailed behaviour was seen from 8 % to 60 % of occupancies with low probability density, whereas higher density values comprising the head were seen from 4 % to 7 %.

Week long variations in IEEE 802.11b/g Channel 6 occupancies are following t location-scale model. The PDF for t-location scale is given as:

$$f(x|\mu, \sigma, v) = \frac{\Gamma\left(\frac{v+1}{2}\right)}{\sigma\sqrt{\pi v}\Gamma\left(\frac{v}{2}\right)} \left(\frac{v + \left(\frac{x-\mu}{\sigma}\right)^2}{v}\right)^{-\frac{v+1}{2}}, \quad (14)$$

where μ is a location parameter, σ is a scale parameter and v is a shape parameter. If all the distribution parameters for x are greater than zero, just as in our case, then $\frac{x-\mu}{\sigma}$ have a Student's t distribution with v degrees of freedom. It was observed that the degree of freedom $v = 1.99 \cong 2$, which implies a special case and the distribution is reduced to fairly simple form as:

$$f(x) = \frac{1}{2} + \frac{x}{2\sqrt{2+x^2}}. \quad (15)$$

It is a heavy two-tailed distribution, and in our case, it was made up of one left short tail and another right long tail. Left tail was comprised of occupancy values ranging from 0,6 % to 3 % with very low probability density, head ranged from 4 % to 7 % with sufficiently higher probability density values, and the right tail wagged from 8 % to 53 %, again with very low density.

Variations in IEEE 802.11b/g Channel 11 had been observed to follow Logistic model. PDF of the Logistic distribution is given as:

$$f(x|\mu, \sigma) = \frac{\exp\left(-\frac{x-\mu}{\sigma}\right)}{\sigma\left(1+\exp\left(-\frac{x-\mu}{\sigma}\right)\right)^2}, \quad (16)$$

where μ is the location parameter and $\sigma > 0$ is the scale parameter. This model also belongs to the family of heavy tailed distributions, and in our case, it was lacking shoulder with large kurtosis. The reason was that the channel was found to be completely unoccupied at some occasion. It should be noted that the occupancies are a measure of average usage over the integration time of 4 minutes. It means that at certain occasions Channel 11 was unoccupied for equal to or more than 4 minutes. The tail was observed to be wagged from 1 % to 21 % with very low density, and the head was comprised of 0,01 % to 0,9 % with higher probability density. IEEE 802.11n Channel 3 and Channel 9 were also observed to be following Logistic model. Both of these channels had low occupancy levels ranging from 0 % to 4 %, approximately. Moreover, weekly variations in FBO and SRO (for WLAN systems) were following t-location scale distribution. Table 4 provides a summary of best fit models and Table 5 provides the parameters for the models. Following assumptions can be inferred from the results:

- 1) Extremely low occupancies, model is Logistic.
- 2) Moderately low occupancies, model is t-location scale or GEV.
- 3) Higher occupancies, model is Burr Type XII.

Table 4: Summary of Models with BIC values

| Observation | Best fit model with BIC value | Next best fit model & BIC value |
|---------------------------------|-------------------------------|---------------------------------|
| Day 1 spectrum variations | GEV, 1.7017e+06 | t-location scale, 1.8271e+06 |
| Day 2 spectrum variations | GEV, 1.5874e+06 | t-location scale, 1.6852e+06 |
| Day 3 spectrum variations | GEV, 1.5854e+06 | t-location scale, 1.6940e+06 |
| Day 4 spectrum variations | GEV, 1.5681e+06 | t-location scale, 1.6946e+06 |
| Day 5 spectrum variations | GEV, 1.6713e+06 | t-location scale, 1.7990e+06 |
| Day 6 spectrum variations | GEV, 1.7507e+06 | t-location scale, 1.8707e+06 |
| Day 7 spectrum variations | GEV, 1.6795e+06 | t-location scale, 1.7988e+06 |
| Whole week spectrum variations | GEV 1.7843e+06 | t-location scale, 1.8975e+06 |
| Whole week IEEE 802.11b/g Ch.1 | Burr Type XII, 3.4712e+03 | GEV 3.4808+03 |
| Whole week IEEE 802.11b/g Ch.6 | t-location scale, 4.2516e+03 | Logistic, 4.8131e+03 |
| Whole week IEEE 802.11b/g Ch.11 | Logistic, -1.7821e+04 | Generalized Pareto, -8.6108e+03 |
| Whole week IEEE 802.11n Ch.3 | GEV, -6.7644e+03 | t-location scale, -6.3864+03 |
| Whole week IEEE 802.11n Ch.9 | Logistic, -9.4174e+03 | t-location scale, -9.2838e+03 |
| Whole week FBO variations | t-location scale, -6.5017e+03 | GEV, -6.4239e+03 |
| Whole week SRO (IEEE 802.11b/g) | GEV, -1.8972e+04 | t-location scale, -1.8916e+04 |
| Whole week SRO (IEEE 802.11n) | t-location scale, -387.73 | Log-logistic, 264.27 |

Table 5: Models with parameter description

| Observation | Distribution Model | Parameter Description |
|---------------------------------|--------------------|---|
| Day 1 spectrum variations | GEV | $k = 0.6676, \sigma = 2.9557, \mu = -85.9427$ |
| Day 2 spectrum variations | GEV | $k = 0.6370, \sigma = 2.8504, \mu = -85.5746$ |
| Day 3 spectrum variations | GEV | $k = 0.7941, \sigma = 2.8023, \mu = -85.7233$ |
| Day 4 spectrum variations | GEV | $k = 0.8568, \sigma = 2.6080, \mu = -85.9357$ |
| Day 5 spectrum variations | GEV | $k = 0.7900, \sigma = 2.7385, \mu = -85.8011$ |
| Day 6 spectrum variations | GEV | $k = 0.8520, \sigma = 3.0775, \mu = -85.6074$ |
| Day 7 spectrum variations | GEV | $k = 0.7739, \sigma = 2.9172, \mu = -85.6607$ |
| Whole week spectrum variations | GEV | $k = 0.7812, \sigma = 2.8348, \mu = -85.9843$ |
| Whole week IEEE 802.11b/g Ch.1 | Burr Type XII | $\alpha = 5.7691, c = 43.5808, k = 0.2567$ |
| Whole week IEEE 802.11b/g Ch.6 | t-location scale | $\mu = 5.3937, \sigma = 0.3650, \nu = 1.9946$ |
| Whole week IEEE 802.11b/g Ch.11 | Logistic | $\mu = -0.0094, \sigma = 0.0290$ |
| Whole week IEEE 802.11n Ch.3 | GEV | $k = 0.2759, \sigma = 0.0380, \mu = 0.0711$ |
| Whole week IEEE 802.11n Ch.9 | Logistic | $\mu = 0.0563, \sigma = 0.0047$ |
| Whole week FBO variations | t-location scale | $\mu = 0.8664, \sigma = 0.0360, \nu = 2.4698$ |
| Whole week SRO (IEEE 802.11b/g) | GEV | $k = 0.4101, \sigma = 0.0022, \mu = 0.0055$ |
| Whole week SRO (IEEE 802.11n) | t-location scale | $\mu = 3.8262, \sigma = 0.1370, \nu = 2.2628$ |

6.3.4 Measurement Campaigns in Florence, Italy

6.3.4.0 Introduction

The experiment consist of several measurements of the interference levels sensed in the emergency ward of the Hospital "San Giuseppe" in Empoli, a medium-size town 20 km west of Florence, Italy. Figure 32 shows the planimetry of the emergency ward of the hospital where the experiment was conducted. The red points are the locations of the interfering sources in the ward (Wi-Fi access points), the blue, green and yellow points are the locations where the interference plus noise has been measured. For each location, the received power samples have been collected for 5 hours. The scanned frequency interval was set to $B_s = [2,399; 2,4835]$ GHz. The frequency band B_s was scanned with a step of 0,5 MHz.

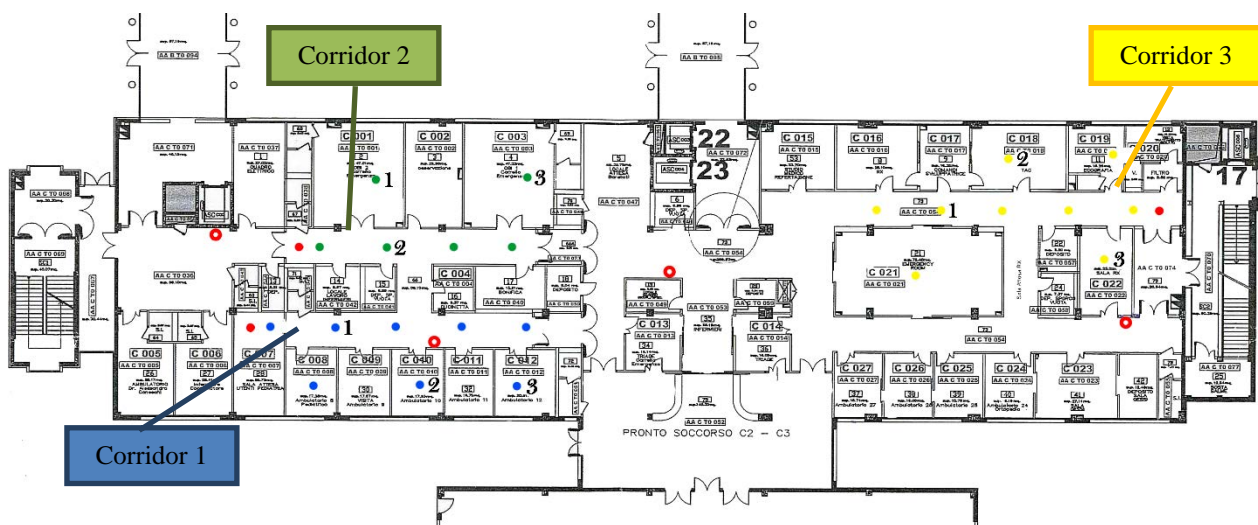


Figure 32: Map of the emergency ward of the hospital

The emergency ward can be seen as a "worst case" of the hospital environments, since typically it includes many medical devices radiating in the ISM band. For modelling the interference, the receiving samples are collected by using a spectrum analyser held in different rooms of the emergency ward of the hospital. No probing signal was sent during the measurements of the interference levels.

The interference is evaluated by putting the spectrum analyser (Agilent™ E4446A) in the corridors, as described above, and into the rooms of each corresponding corridor. In corridor 1, different kinds of ambulatories are present. The corridor 2 is used for bedridden patients, from acute health problems to low-risk health issues. Corridor 3 is dedicated to any kind of radiological analysis: X-ray, tomography, magnetic resonance imaging (MRI), ultrasound, etc. In corridor 3 there is also the "red room", for the extreme urgent operations (intensive care and surgeries). All the measurements were taken during the busiest time of the day; personnel and patients were moving around in the building.

NOTE: Measurements were carried out using high performance spectrum analyzer (SA) Agilent™ E4446A connected to a computer.

The spectrum analyser Agilent™ E4446A used has the following main parameters:

Range: 2 350 MHz to 2 550 MHz

Resolution: 1 kHz

Sweep time: 140 ms

Average noise level: -115 dBm

Amplitude resolution: 0,5 dBm

The parameters extracted from the measurements are:

- Percentage of occupancy of the each band, i.e. the amount of time that the received amplitude keeps over the noise level plus 20 dB.
- Probability distribution function of the received samples.
- The best PDF that approximates the real samples' distribution.
- The waterfall graph of the interference levels as a function of both the time and frequencies.

6.3.4.1 Occupancy

6.3.4.1.0 Introduction

The occupancy for several points are reported in the following figures.

The occupancy of the frequencies of the ISM band over time is the percentage of time that the received amplitude keeps 20 dB over the noise level. Figures 33 and 34 show how different the traffic, and thus, the mutual interference, can be in different locations of a ward.

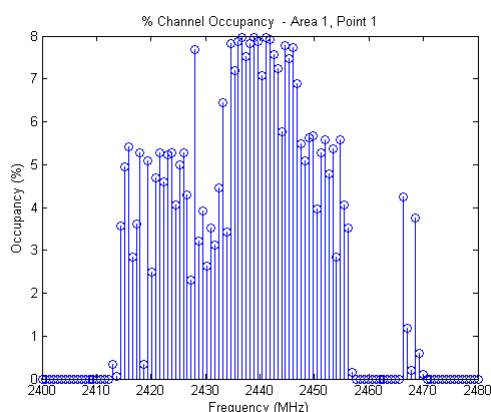


Figure 33: % occupancy for the blue point n. 1

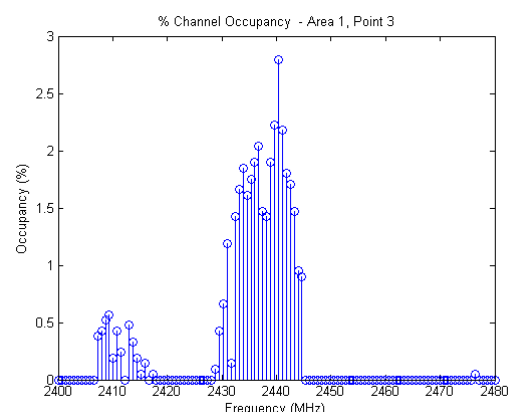


Figure 34: % occupancy for the blue point n. 3

6.3.4.1.1 Percentiles

Figures 35 and 36 show the percentiles of the interference plus noise power in the measured ISM band over time for two locations at zone 1. A percentile is a measure used in statistics indicating the value below which a given percentage of observations in a group of observations fall. For example, the 20th percentile is the value below which 20 percent of the observations are found. Focusing on Figure 36, it is evident that the 90 % of the interference plus noise power samples (over the entire samples collected for 5 hours) fall below -87 dBm. Consequently, only 10 % of the total interference samples were higher than -87 dBm. The average noise level (ANL) was measured to be -100 dBm.

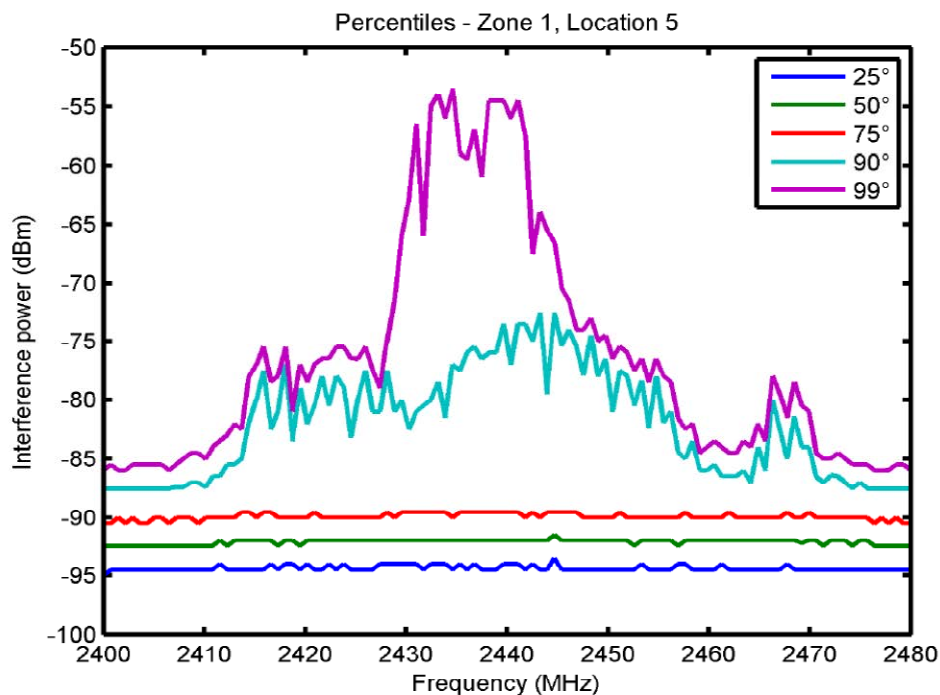


Figure 35: Percentiles - Corridor 1, Point 1

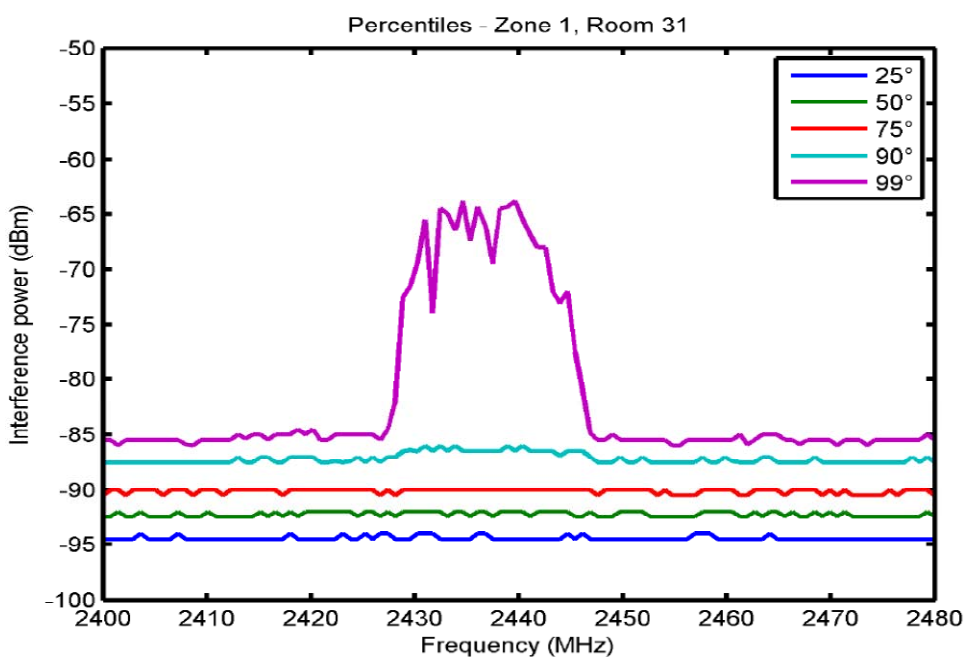


Figure 36: Percentiles - Corridor 1, Point 3

6.3.4.2 PDF

For the same locations the fitting PDF for each frequency in the ISM band have been calculated.

How to read the following figures: the numbers on the y-axis of the graphics indicate the index associated to the best fitting PDF for the specific frequency observed. The PDFs considered have been enumerated from 1 to 16 and they are listed in Table 6.

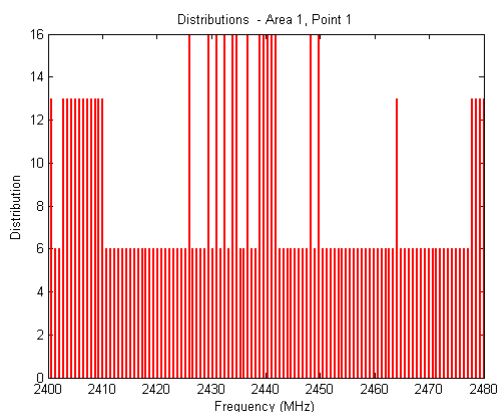


Figure 37: Best fitting PDF for each frequency; location: blue point n. 1

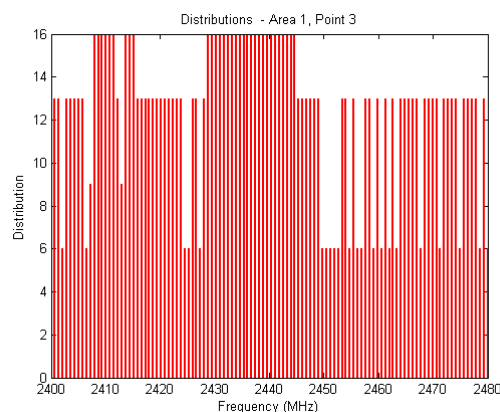


Figure 38: Best fitting PDF for each frequency; location: blue point n. 3

Table 6: Index of the probability distribution functions considered for finding the best fitting ones for each scanned frequency

| Distribution | Index |
|---------------------------|-------|
| Beta | 1 |
| Birnbaum-Saunders | 2 |
| Exponential | 3 |
| Extreme value | 4 |
| Gamma | 5 |
| Generalized extreme value | 6 |
| Generalized Pareto | 7 |
| Inverse Gaussian | 8 |
| Logistic | 9 |
| Log-logistic | 10 |
| Lognormal | 11 |
| Nakagami | 12 |
| Normal | 13 |
| Rayleigh | 14 |
| Rician | 15 |
| t location-scale | 16 |
| Weibull | 17 |

As seen from Figures 37 and 38, if there's enough interference in a frequency, the distribution of the received samples is t location-scale, while if in a frequency there is only noise, then the distribution changes to generalized extreme value. Also the Normal distribution is frequent, but not as often as the GEVD.

The t location-scale distribution (TLSD) has the density function:

$$f(x|\mu, \sigma, \nu) = \frac{\Gamma(\frac{\nu+1}{2})}{\sigma\sqrt{\pi\nu}\Gamma(\nu/2)} \cdot \left(\frac{\nu + \frac{(x-\mu)^2}{\sigma^2}}{\nu} \right)^{-\frac{\nu+1}{2}} \quad (17)$$

with location parameter μ , scale parameter $\sigma > 0$, and shape parameter $\nu > 0$. If x has a t location-scale distribution, with parameters μ , σ , and ν , then:

$$f(x|\mu, \sigma) = \frac{x-\mu}{\sigma} \quad (18)$$

has a Student's t distribution with ν degrees of freedom.

The t location-scale distribution is useful for modelling data distributions with heavier tails (more prone to outliers) than the normal distribution. It approaches the normal distribution as ν approaches infinity, and smaller values of ν yield heavier tails.

The probability density function for the **generalized extreme value distribution (GEVD)** with location parameter μ , scale parameter σ , and shape parameter $k \neq 0$ is:

$$y = f(x | k, \mu, \sigma) = \left(\frac{1}{\sigma}\right) \exp\left[-\left(1 + k \frac{(x-\mu)}{\sigma}\right)^{-\frac{1}{k}}\right] \left(1 + k \frac{(x-\mu)}{\sigma}\right)^{-1-\frac{1}{k}} \quad (19)$$

for

$$1 + k \frac{(x-\mu)}{\sigma} > 0, \quad (20)$$

$k > 0$ corresponds to the Type II case, while $k < 0$ corresponds to the Type III case. For $k = 0$, corresponding to the Type I case, the density is:

$$y = f(x | 0, \mu, \sigma) = \left(\frac{1}{\sigma}\right) \exp\left(-\exp\left(-\frac{(x-\mu)}{\sigma}\right) - \frac{(x-\mu)}{\sigma}\right) \quad (21)$$

Like the extreme value distribution, the generalized extreme value distribution is often used to model the smallest or largest value among a large set of independent, identically distributed random values representing measurements or observations. The generalized extreme value combines three simpler distributions into a single form, allowing a continuous range of possible shapes that includes all three of the simpler distributions. Any one of those distributions can be used to model a particular dataset of block maxima. The generalized extreme value distribution allows to "let the data decide" which distribution is appropriate. The three cases covered by the generalized extreme value distribution are often referred to as the Types I, II, and III. Each type corresponds to the limiting distribution of block maxima from a different class of underlying distributions. Distributions whose tails decrease exponentially, such as the normal, lead to the Type I. Distributions whose tails decrease as a polynomial, such as Student's t , lead to the Type II. Distributions whose tails are finite, such as the beta, lead to the Type III.

6.3.4.3 Interference as a function of time and frequency

In this clause waterfall graphs are shown, i.e. the received amplitude levels as a function of time and frequency. As an example, Figures 37 and 38 show the waterfall graphs for the measurement points 1 and 3 at Corridor 1.

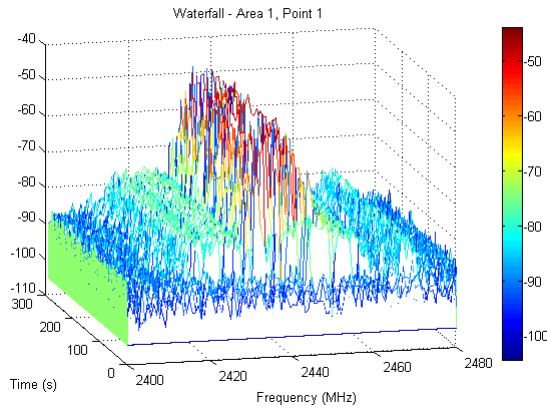


Figure 37a: Interference plus noise as a function of time and frequency; location: blue point n. 1

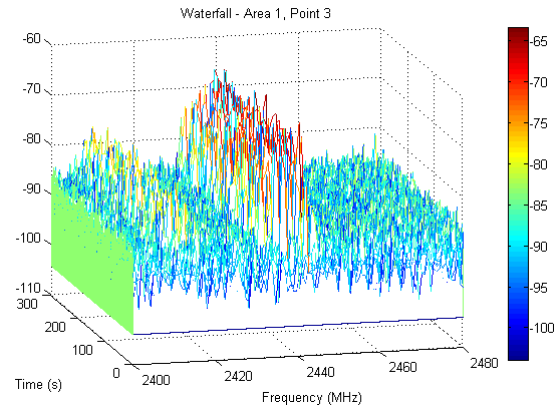


Figure 38a: Interference plus noise as a function of time and frequency; location: blue point n. 3

6.3.4.4 Parameters characterizing the distribution

The parameters of the distribution that best fit the received samples in each location of the hospital ward are reported. An example for location blue point n. 1 (corridor 1) is Table 7.

Table 7: Parameters defining the distribution of the received samples for the location 1 of corridor 1

| Frequency | Distribution | Parameters | | | | | | | | |
|-----------|---------------------------|------------|-------------|---------|-------|-------------|-------|------|----------------------|---------|
| | | Name | Description | Value | Name | Description | Value | Name | Description | Value |
| 2412 | generalized extreme value | k | (shape) | -0.205 | sigma | (scale) | 3.197 | mu | (location) | -93.297 |
| 2417 | generalized extreme value | k | (shape) | -0.050 | sigma | (scale) | 3.359 | mu | (location) | -93.310 |
| 2422 | generalized extreme value | k | (shape) | 0.006 | sigma | (scale) | 3.371 | mu | (location) | -93.472 |
| 2427 | generalized extreme value | k | (shape) | -0.033 | sigma | (scale) | 3.405 | mu | (location) | -93.507 |
| 2432 | generalized extreme value | k | (shape) | 0.071 | sigma | (scale) | 3.515 | mu | (location) | -93.478 |
| 2437 | tllocationscale | mu | (location) | -92.302 | sigma | (scale) | 2.600 | nu | (degrees of freedom) | 1.796 |
| 2442 | tllocationscale | mu | (location) | -92.303 | sigma | (scale) | 2.501 | nu | (degrees of freedom) | 1.727 |
| 2447 | generalized extreme value | k | (shape) | 0.071 | sigma | (scale) | 3.590 | mu | (location) | -93.484 |
| 2452 | generalized extreme value | k | (shape) | 0.018 | sigma | (scale) | 3.398 | mu | (location) | -93.474 |
| 2457 | generalized extreme value | k | (shape) | -0.110 | sigma | (scale) | 3.226 | mu | (location) | -93.403 |
| 2462 | generalized extreme value | k | (shape) | -0.241 | sigma | (scale) | 3.229 | mu | (location) | -93.138 |
| 2467 | generalized extreme value | k | (shape) | -0.078 | sigma | (scale) | 3.405 | mu | (location) | -93.458 |
| 2472 | generalized extreme value | k | (shape) | -0.256 | sigma | (scale) | 3.264 | mu | (location) | -93.321 |

The values shown in Table 7 are the main parameters of the best PDF for the scanned frequencies. Frequencies are shown in the first left column. The second column indicates which is the best fitting PDF, and the remaining columns represents the derived main values of the associated PDF, as in Equations (17) and (19).

6.3.4.5 Home and office environments

The measurements in the home (Figures 39 and 40) and office environments (Figures 41 and 42) have been carried out for **one week** with the same device and setting of the ones described in the previous clause. The office environment, as well as the home, is a typical modern city office, with several internal Wi-Fi access points and surrounded by other offices and houses. The city has also a free Wi-Fi access network for public use and its signal is received also in the office. The home environment has similar characterization apart from the public Wi-Fi, which is not present there.

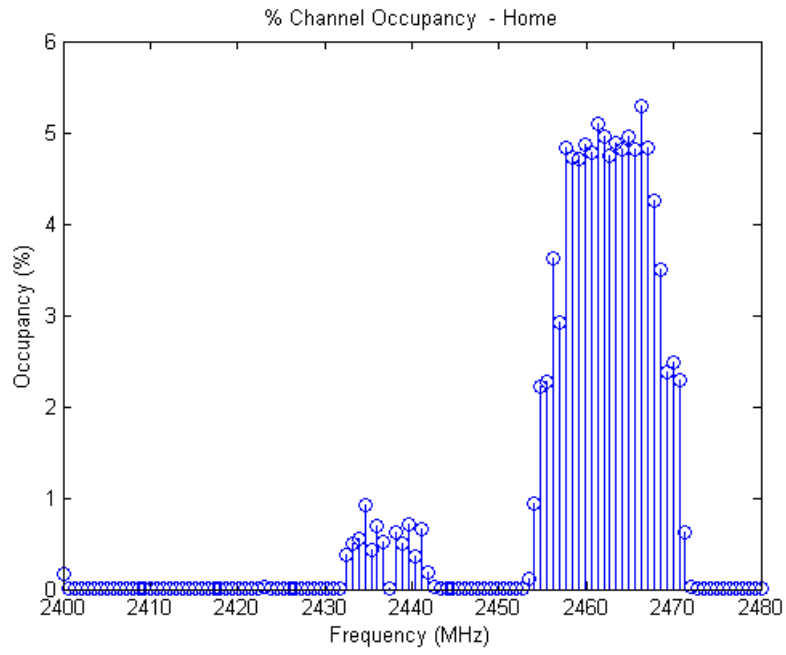


Figure 39: Occupancy @ HOME

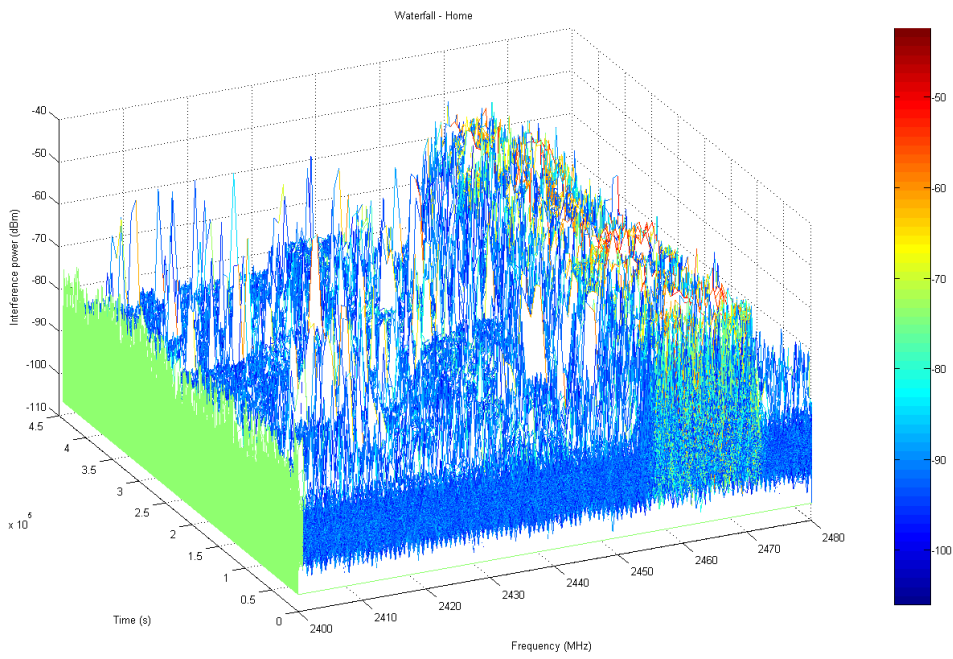


Figure 40: Waterfall @ HOME

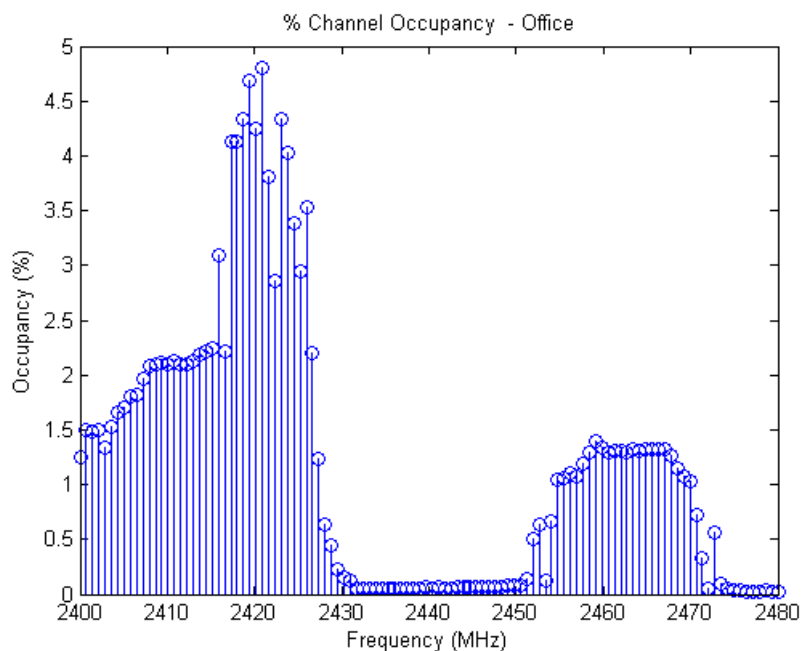


Figure 41: Occupancy @ OFFICE

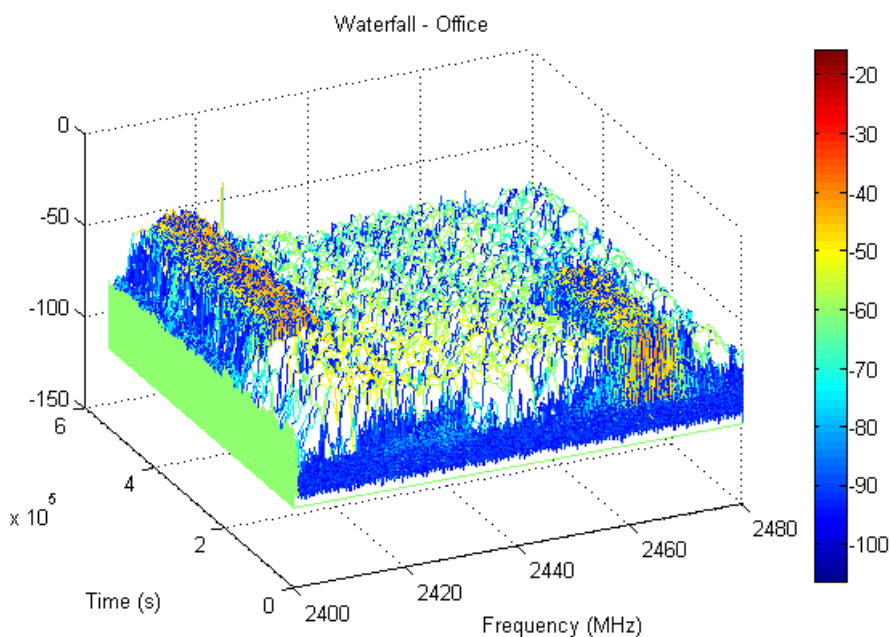


Figure 42: Waterfall @ OFFICE

Analysing the results, there is a correlation between the occupancy and the estimated distribution of the channel. In fact:

- for frequencies that are poorly utilized, the best fitting PDF of the interference samples over time is a normal or a generalized extreme value distribution;
- for frequencies with high percentage of occupancy, the best fitting PDF of the interference samples is a t location-scale distribution.

6.3.4.6 Extract the mathematical model

6.3.4.6.0 Introduction

The above experiments and parameters extraction can be used to characterize the aggregate interference.

6.3.4.6.1 First results of CNIT-UNIFI

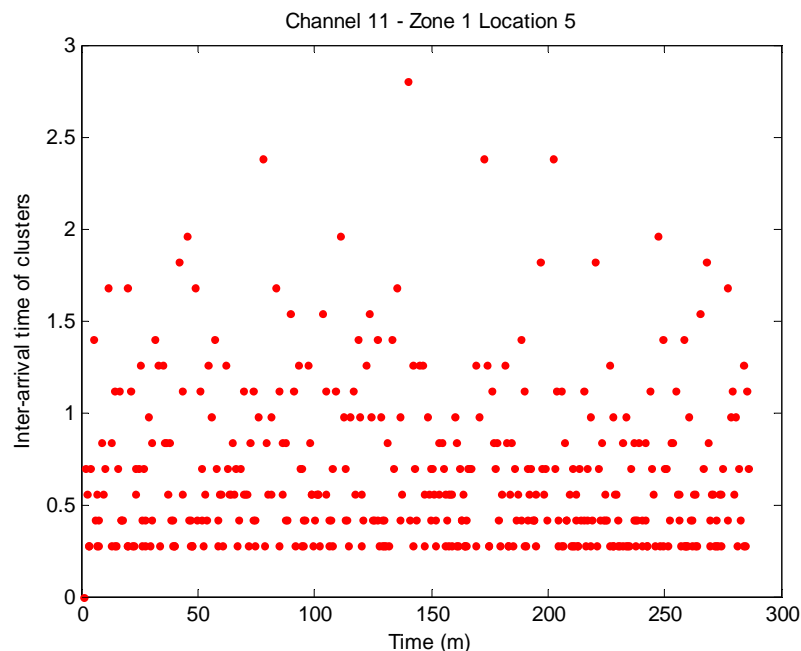
$T_c = 1,25$ ms

Centre Frequency: 2,462 GHz (Channel 11)

Zone 1 - Location 5

Inter-arrival time of interference clusters

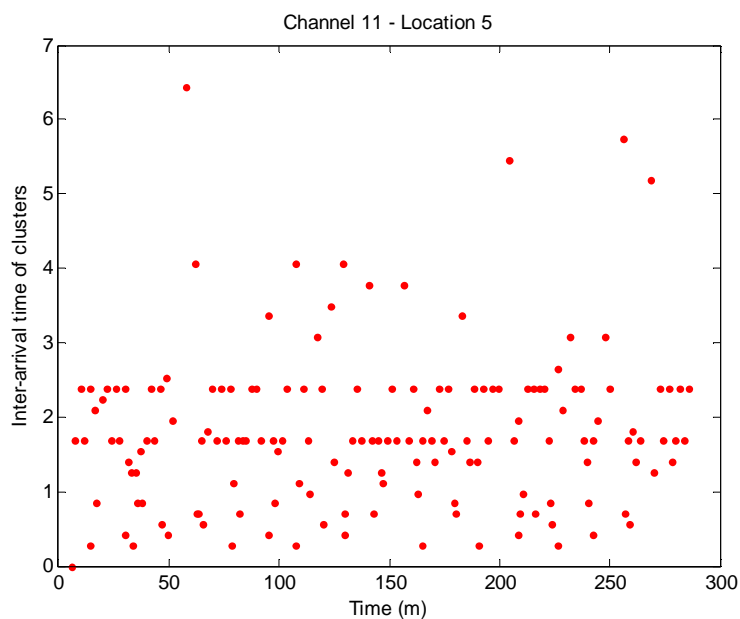
Figure 43 show how the inter-arrival time between the interfering clusters is distributed over time. Figures 43 and 44 report in the x-axis the time measured in minutes, while in the y-axis the unit is microseconds.



NOTE: Inter-arrival time of interference clusters. The threshold is set at -90 dBm.

Figure 43: Inter-arrival time of interference clusters

- DistName: 'generalized extreme value'
 - NLogL: 1,2199e+03
 - BIC: 2,4588e+03
 - AIC: 2,4459e+03
 - AICc: 2,4459e+03
- ParamNames: {'k' 'sigma' 'mu'}
- ParamDescription: {'shape' 'scale' 'location'}
- Params: [0,5052 1,3957 1,9574]



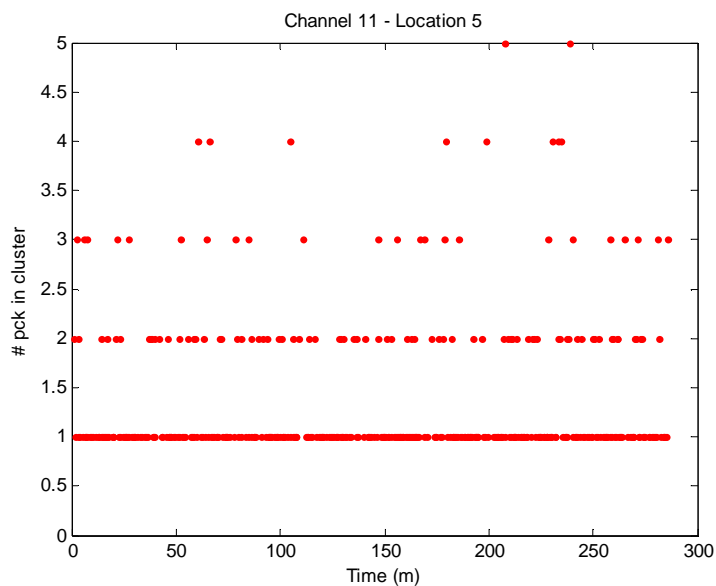
NOTE: Inter-arrival time of interference clusters. The threshold is set at -80 dBm.

Figure 44: Inter-arrival time of interference clusters

- DistName: 'generalized extreme value'
 - NLogL: 525,6960
 - BIC: 1,0666e+03
 - AIC: 1,0574e+03
 - AICc: 1,0575e+03
- ParamNames: {'k' 'sigma' 'mu'}
- ParamDescription: {'shape' 'scale' 'location'}
- Params: [-0,0066 5,9304 9,3913]

Dimension of clusters

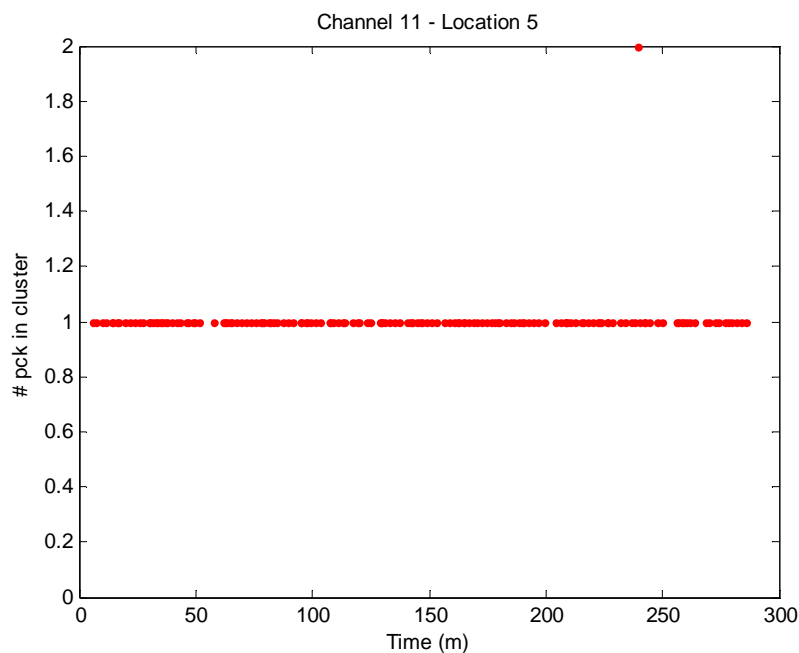
The following graphs show how the dimension of the interfering clusters is distributed over time. Figures 45 and 46 report in the x-axis the time measured in minutes, while in the y-axis the unit is number of samples per cluster.



NOTE: Inter-arrival time of interference clusters. The threshold is set at -90 dBm.

Figure 45: Dimension of interfering clusters

- DistName: 'generalized pareto'
 - NLogL: -1,1562e+04
 - BIC: -2,3106e+04
 - AIC: -2,3119e+04
 - AICc: -2,3119e+04
- ParamNames: {'k' 'sigma' 'theta'}
- ParamDescription: {'shape' 'scale' 'threshold'}
- Params: [11,5876 3,1761e-15 1,0000]



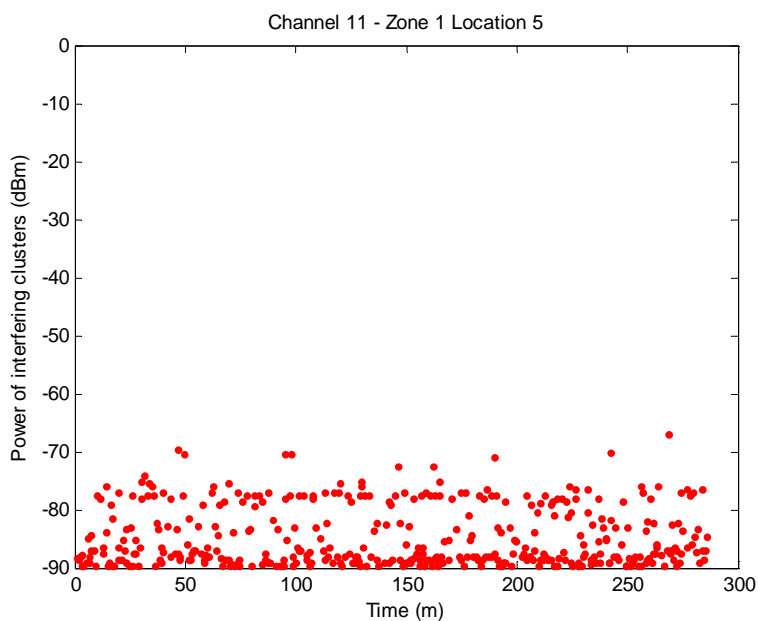
NOTE: Inter-arrival time of interference clusters. The threshold is set at -80 dBm.

Figure 46: Dimension of interfering clusters

- DistName: 'generalized extreme value'
 - NLogL: -1,1002e+05
 - BIC: -2,2002e+05
 - AIC: -2,2003e+05
 - AICc: -2,2003e+05
- ParamNames: {'k' 'sigma' 'mu'}
- ParamDescription: {'shape' 'scale' 'location'}
- Params: [28,9517 1,6105e-307 1]

Power of clusters

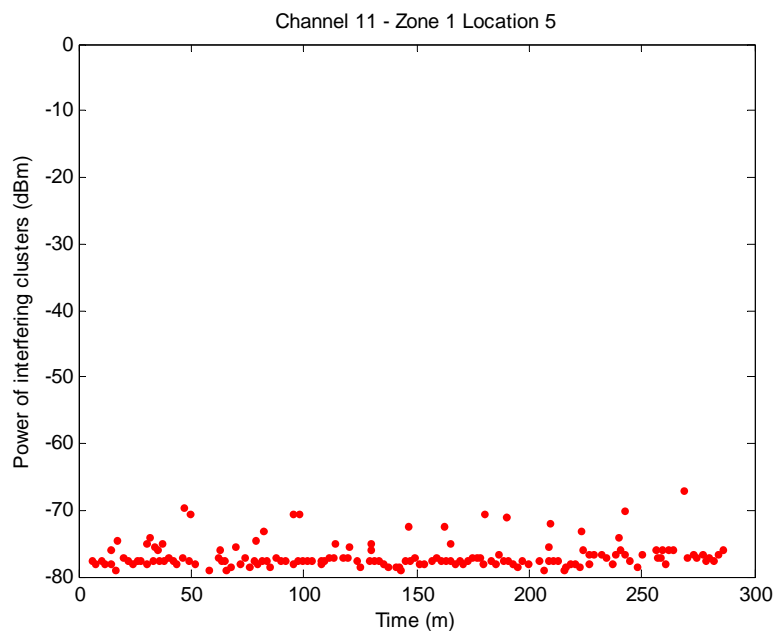
Figures 47 and 48 show how the amplitude of the interfering clusters is distributed over time. The figures report in the x-axis the time measured in minutes, while in the y-axis the unit is dBm.



NOTE: Inter-arrival time of interference clusters. The threshold is set at -90 dBm.

Figure 47: Power of the interference clusters

- DistName: 'generalized extreme value'
 - NLogL: 1,4321e+03
 - BIC: 2,8832e+03
 - AIC: 2,8702e+03
 - AICc: 2,8703e+03
- ParamNames: {'k' 'sigma' 'mu'}
- ParamDescription: {'shape' 'scale' 'location'}
- Params: [1,2060 1,4499 -88,6043]



NOTE: Inter-arrival time of interference clusters. The threshold is set at -80 dBm.

Figure 48: Power of interference clusters

- DistName: 'generalized extreme value'
 - NLogL: 274,2105
 - BIC: 563,5897
 - AIC: 554,4209
 - AICc: 554,5778
- ParamNames: {'k' 'sigma' 'mu'}
- ParamDescription: {'shape' 'scale' 'location'}
- Params: [0,2444 1,0261 -77,6274]

Zone 1 - Room 31

Inter-arrival time of clusters

Figures 49 and 50 show how the inter-arrival time between the interfering clusters is distributed over time. The figures report in the x-axis the time is measured as number of samples, while in the y-axis the unit is samples.

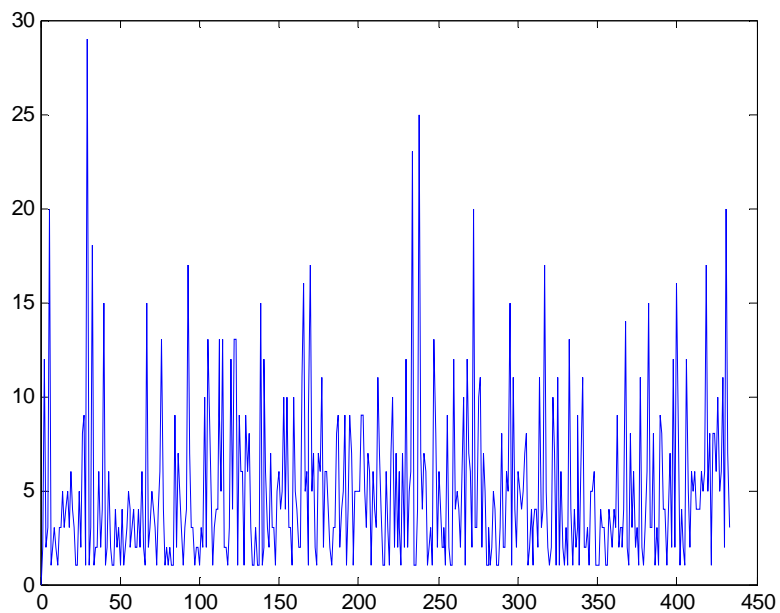


Figure 49: Inter-arrival discrete time of the interference clusters

- DistName: 'generalized extreme value'
 - NLogL: 1,0920e+03
 - BIC: 2,2022e+03
 - AIC: 2,1900e+03
 - AICc: 2,1900e+03
- ParamNames: {'k' 'sigma' 'mu'}
- ParamDescription: {'shape' 'scale' 'location'}
- Params: [0,4614 1,9890 2,5822]

Dimension of clusters

Figures 50 and 51 show how the dimension of the interfering clusters is distributed over time. The figures report in the x-axis the time is measured as number of samples, while in the y-axis the unit is samples.

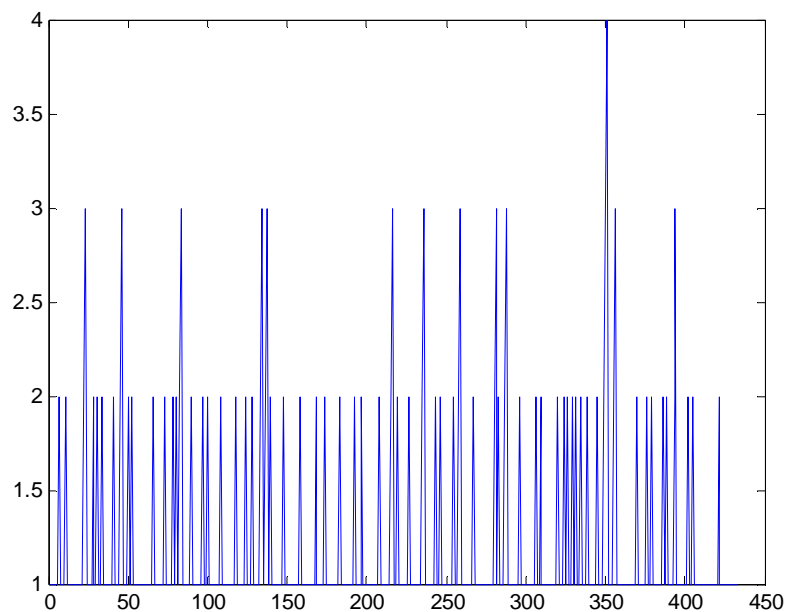


Figure 50: Interference cluster (discrete) dimension

- DistName: 'generalized pareto'
 - NLogL: -1,0466e+04
 - BIC: -2,0913e+04
 - AIC: -2,0926e+04
 - AICc: -2,0926e+04
- ParamNames: {'k' 'sigma' 'theta'}
- ParamDescription: {'shape' 'scale' 'threshold'}
- Params: [8,3355 2,8089e-15 1,0000]

Mean power of clusters

Figure 51 shows how the power of the interfering clusters is distributed over time. The figures report in the x-axis the time is measured as number of samples, while in the y-axis the unit is dBm.

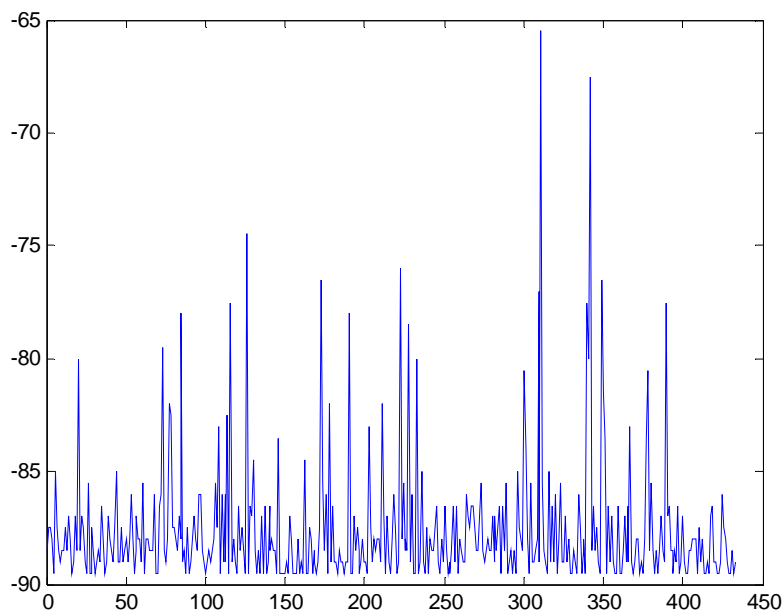


Figure 51: Mean power of the interference clusters

- DistName: 'generalized extreme value':
 - NLogL: 739,8401
 - BIC: 1,4979e+03
 - AIC: 1,4857e+03
 - AICc: 1,4857e+03
- ParamNames: {'k' 'sigma' 'mu'}
- ParamDescription: {'shape' 'scale' 'location'}
- Params: [0,7747 0,7522 -88,9698]

6.4 Statistical model of the interference

6.4.0 Introduction

The statistical model of the interference in the ISM band has been developed using only data from the two measurement campaigns (December 2013 and June 2014) carried out at Oulu University Hospital, since the measurements in Florence's hospital did not have sufficient amount of samples per sweep.

In particular, two channels have been evaluated: the best and the worst one. Channel #6 (2 437 MHz) of December 2013 measurements is the best one and Channel #1 (2 412 MHz) of June 2014 measurements is the worst one.

The statistical model of the interference starts modelling three characteristics of the interference: clusters dimension, interarrival time and cluster amplitude.

6.4.1 Cluster dimension

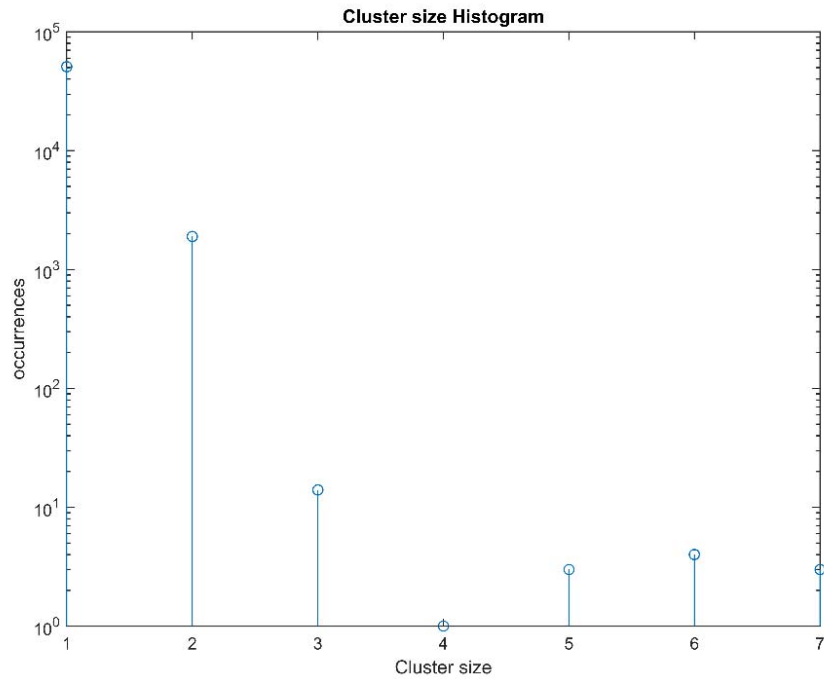


Figure 51a: Channel 6 (December 2013) - Cluster dimension

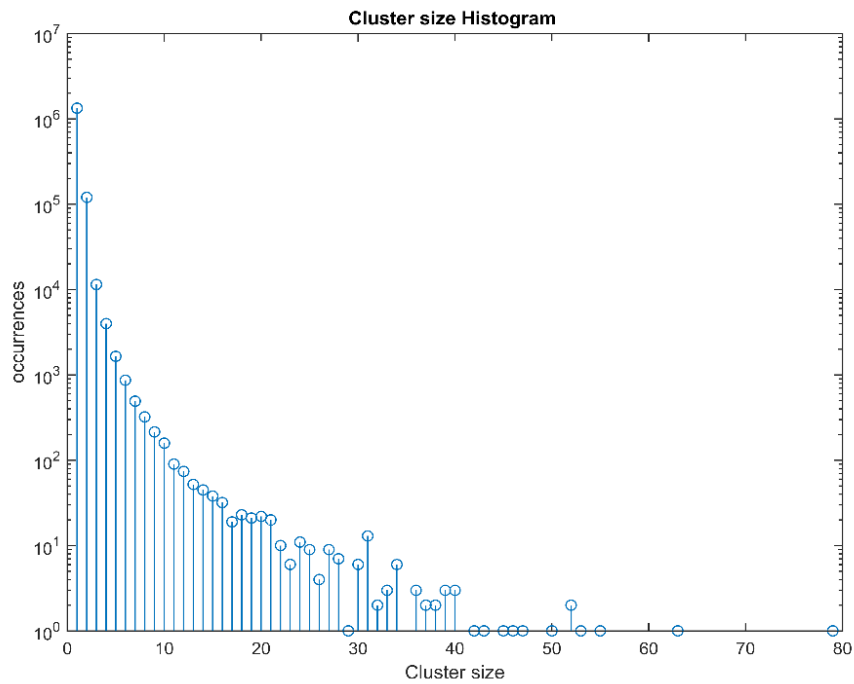


Figure 52: Channel 1 (June 2014) - Cluster dimension

Maximum dimension of cluster in December 2013 is only 7, while in June 2014 is 80 consecutive samples as shown in Figures 51a and 52, respectively.

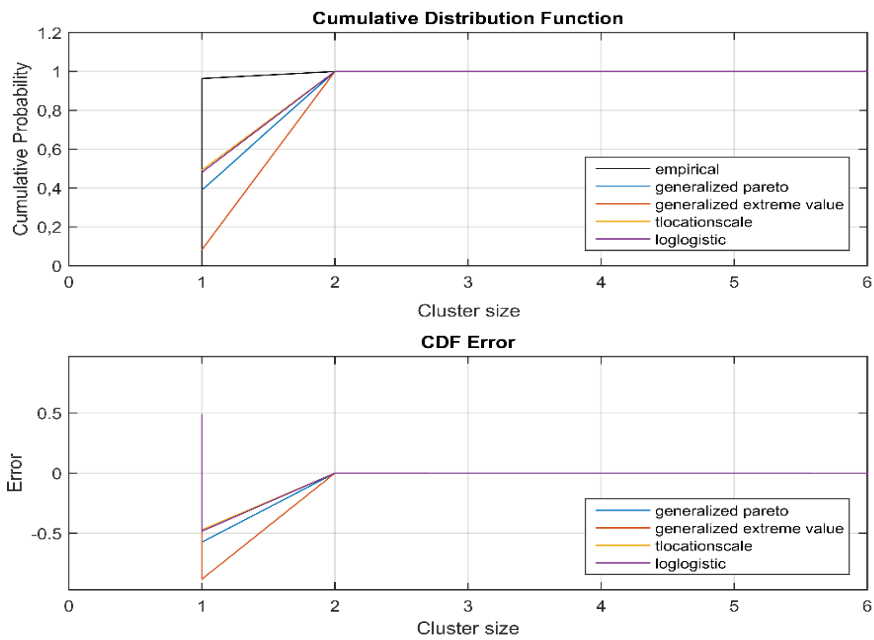


Figure 53: Cluster dimension CDF - Ch #6

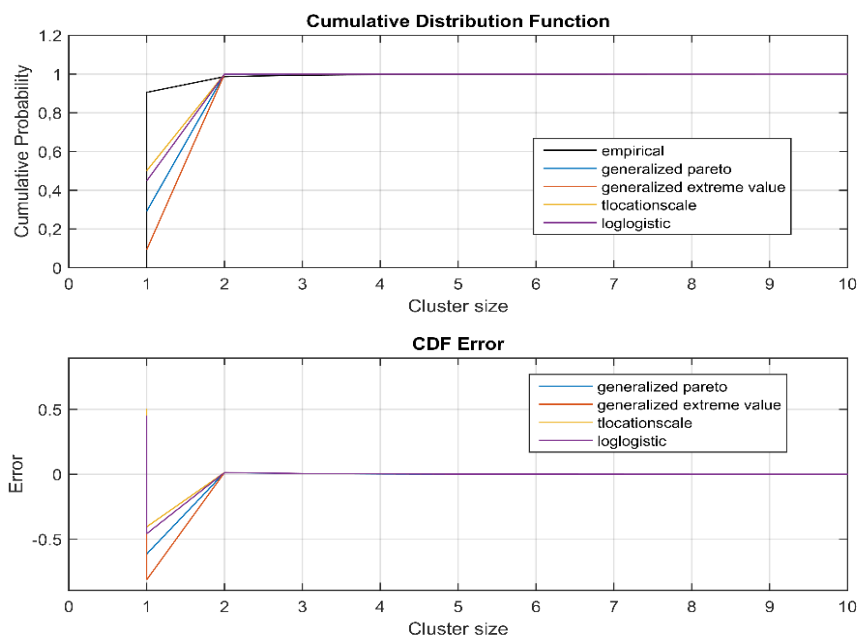


Figure 54: Cluster dimension CDF - Ch #1

Best fitting distribution for cluster dimension is Pareto for both Channel # (worst)1 and #6 (best). The error between the different CDFs to the original data set are presented in Figures 53 and 54 for Channels #6 and #1, respectively.

6.4.2 Inter-arrival time

In channel #6 (December 2013) the interarrival time is much larger, i.e. interference clusters occur sporadically. This means intermittent interference in the band (2 437 MHz). The results are shown in Figure 53.

In channel #1 (June 2014) the interarrival time is very low, i.e. interference clusters occur very frequently. This means almost continuous interference in the band (2 412 MHz). The results are shown in Figure 54.

Corresponding CDF curves are shown on Figures 55 and 56 for Channel #6 and Channel #1, respectively.

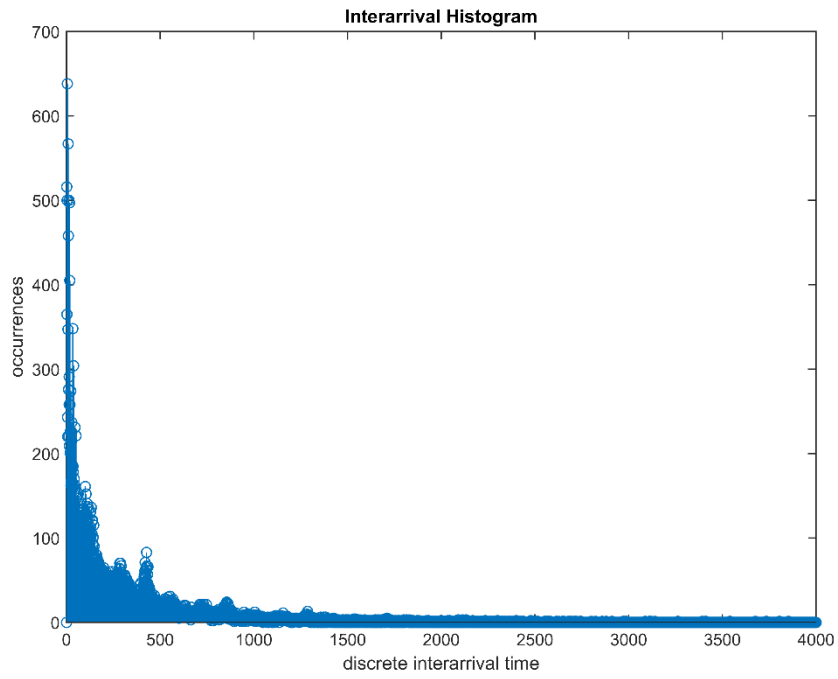


Figure 55: Inter-arrival time, Channel 6 (December 2013)

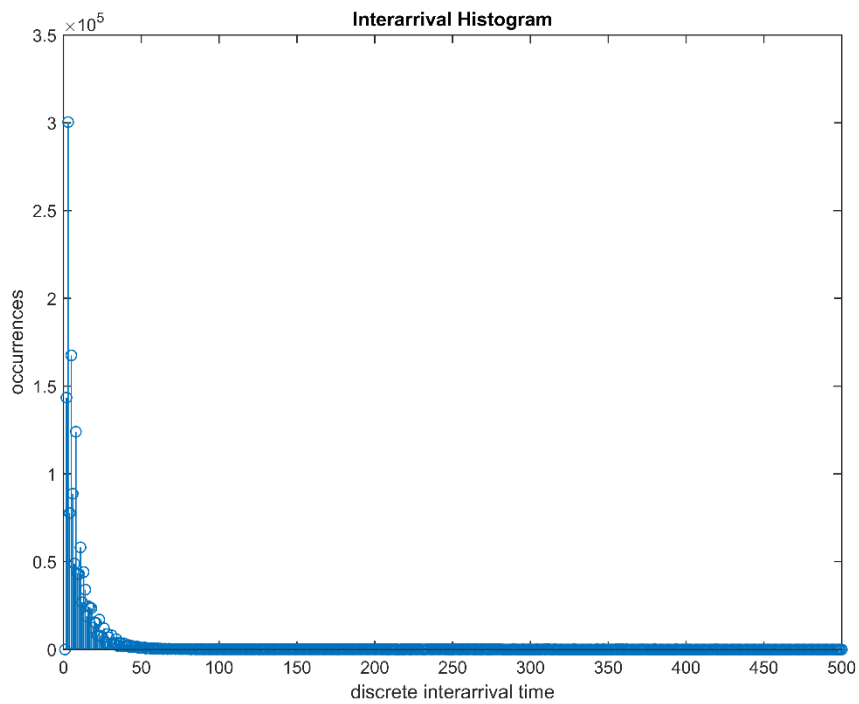


Figure 56: Inter-arrival time, Channel 1 (June 2014)

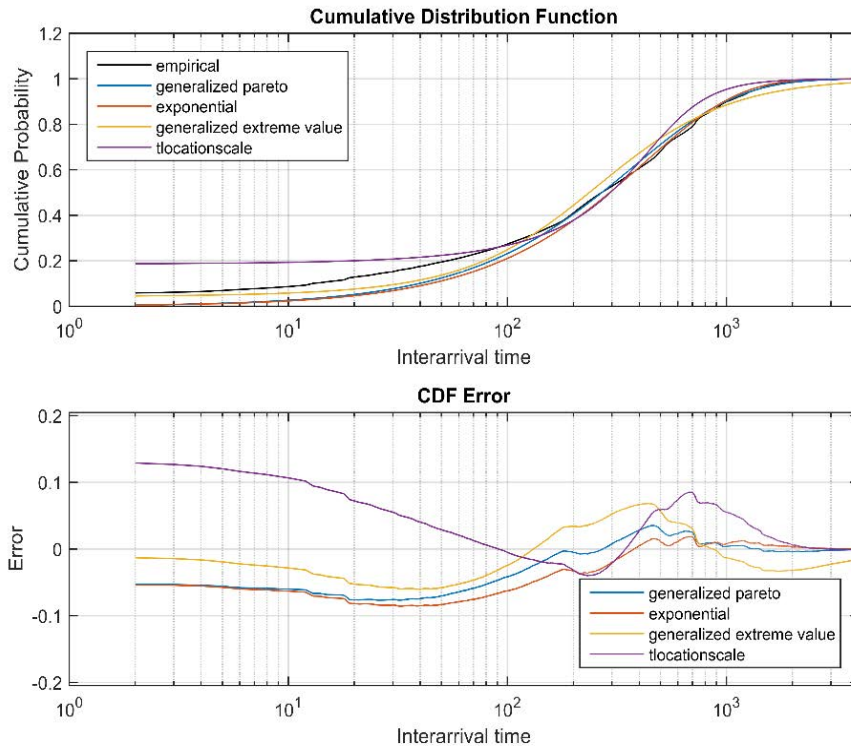


Figure 57: Inter-arrival time CDF - Ch #6

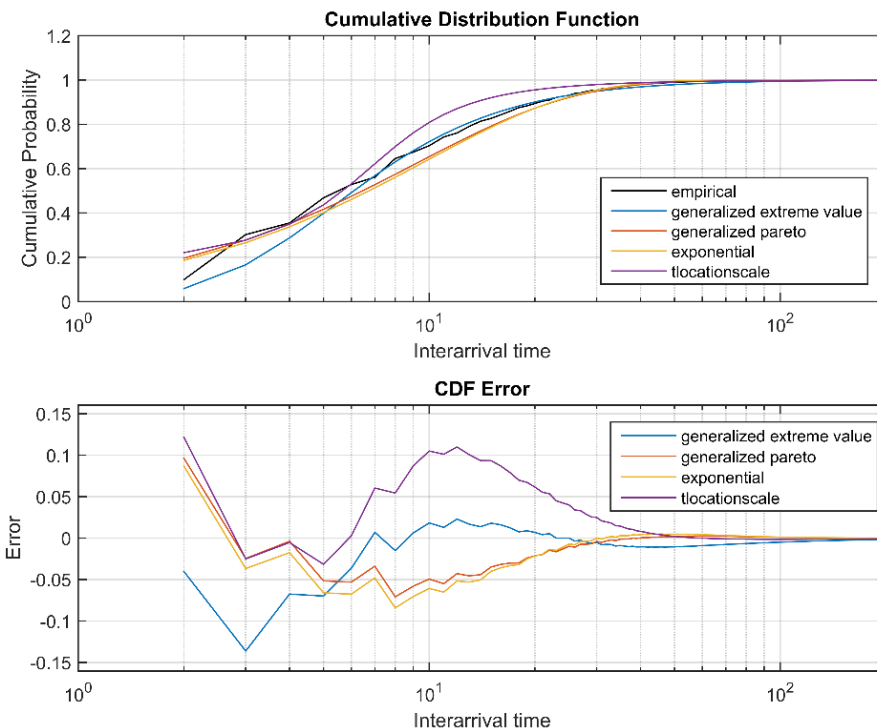


Figure 58: Inter-arrival time - Ch #1

Best fitting distribution for inter-arrival time of clusters is Pareto for both Channel #1 (worst) and Channel #6 (best).

6.4.3 Interfering cluster amplitude

In Channel #6 (December 2013) the amplitude of the clusters ranged between -87 and -85 dBm (Figure 59), while in Channel #1 (June '14) ranged between -84 and -62 dBm (Figure 60). The best fitting CDF for the cluster amplitude is the GEV for both the Channel #6 (best) and Channel #1 (worst) as shown in Figures 61 and 62, respectively.

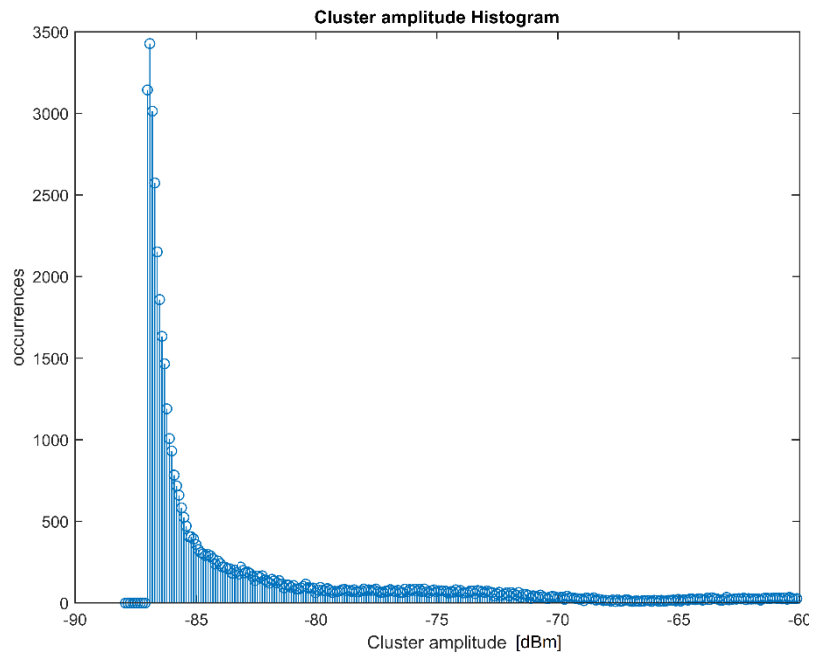


Figure 59: Cluster amplitude, Channel 6 (Dec.'13)

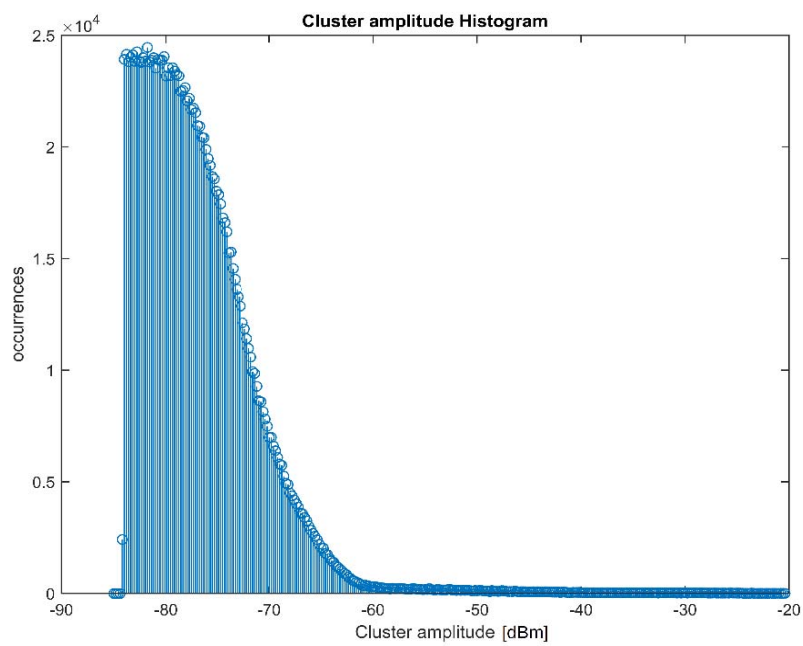


Figure 60: Cluster amplitude, Channel 1 (June 2014)

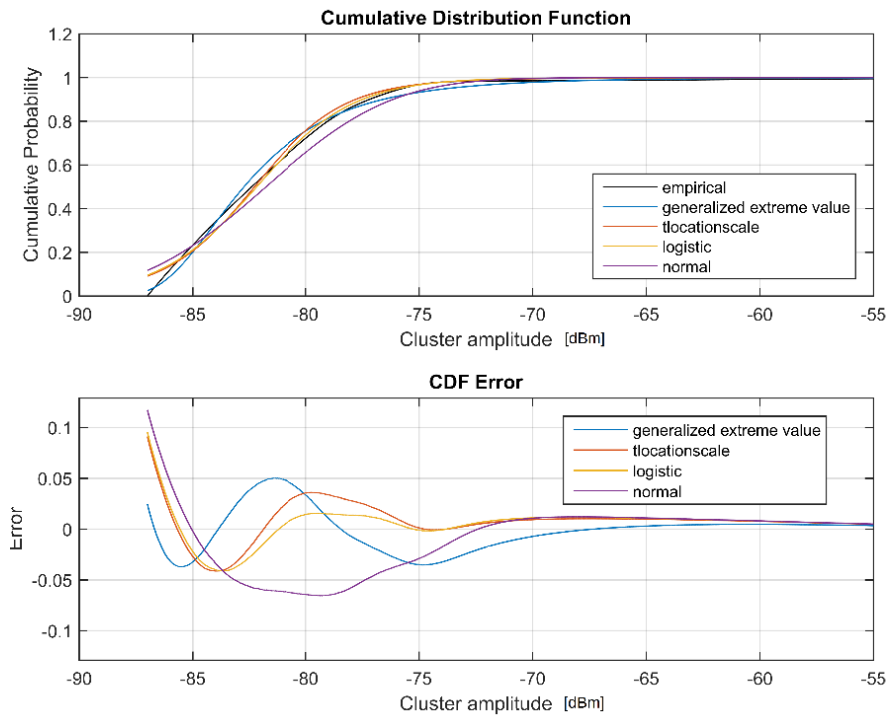


Figure 61: Cluster amplitude - Ch #6

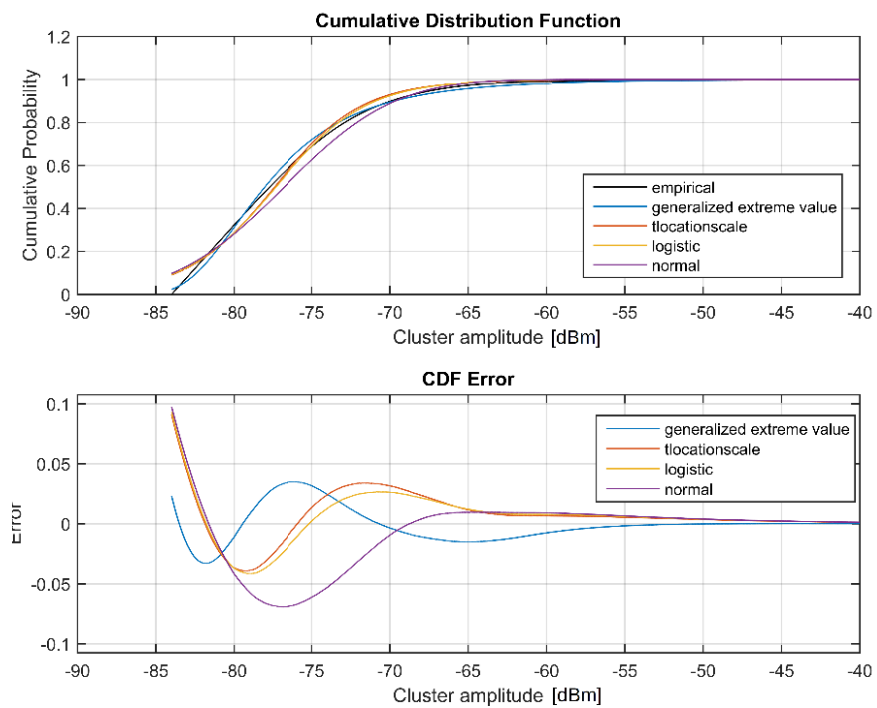


Figure 62: Cluster amplitude - Ch #1

6.4.4 Conclusions

The three parameters (cluster dimension, interarrival time and cluster amplitude) can be used to build a Matlab function that simulates the best case (Ch #6) and worst case (Ch #1) of interference in ISM band. The block can be used to simulate the realistic interference caused at the studied environments, thus allowing an evaluation of the performance of a WBAN system the real use case scenario. The statistical parameters of the interference clusters have been used to build a Matlab simulator. The simulator creates a cluster-based interference vector which follows the statistics of the selected scenario: low, moderate or high interference.

6.5 Extracting the mathematical model of the interference

The statistical parameters of the interference clusters have been used to build a Matlab simulator. The simulator creates a cluster-based interference vector which follows the statistics of the selected scenario: low or high interference.

In this clause a cluster-based stochastic model of the aggregate interference is derived. In particular, two channels have been evaluated: the best and the worst one among all the measurement campaigns. Channel 6 (2 437 MHz) of Measurement Campaign (MC) no. 1 is the best one (Low Interference, LI) and Channel 1 (2 412 MHz) of MC no. 2 is the worst one (High Interference, HI).

The statistical model of the interference starts modelling three characteristics of the interference: clusters dimension, interarrival time of the clusters and cluster amplitude. A cluster is defined as a group of consecutive samples that overcome the threshold of the noise level.

Figures 63 and 64 show the occurrences of the dimension of the clusters over one week for the channel 6 (low interference) and channel 1 (high interference), respectively. Maximum dimension of cluster in channel 1 is 80 consecutive samples, while in channel 6 is only 7.

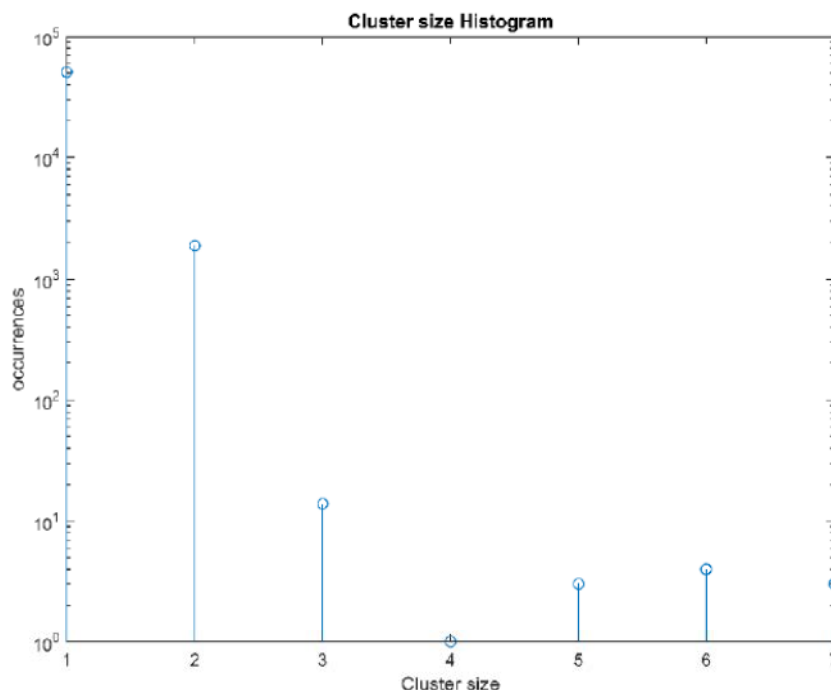
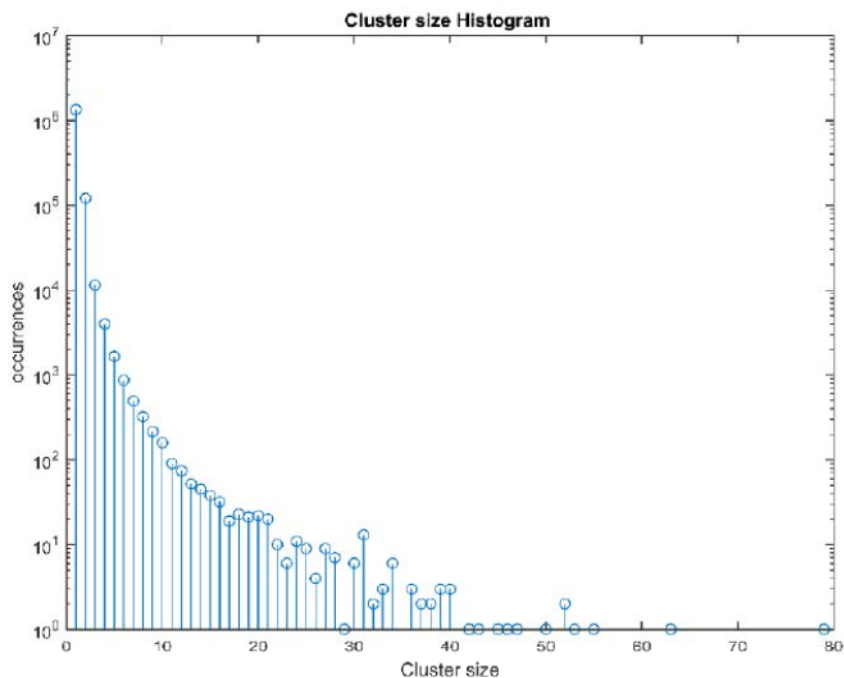


Figure 63: Occurrences of the dimension of the clusters; Channel 6 (Low Interference)



**Figure 64: Occurrences of the dimension of the clusters;
Channel 1 (High Interference)**

Best fitting distribution for the dimension of the cluster is Pareto for both Channel 1 and 6, as depicted in Figures 65 and 66. Generalized Pareto distribution is:

$$f(x|k, \sigma, \theta) = \frac{1}{\sigma} \left(1 + k \left(\frac{x - \theta}{\sigma} \right) \right)^{-1-1/k} \quad (22)$$

where k is the shape parameter, σ is the scale parameter and θ is the threshold parameter. Channel 6 (LI) shows $k = 4,8$, $\sigma = 2,5e-15$ and $\theta = 1$, while Channel 1 (HI) shows $k = 2,43$, $\sigma = 2,34e-15$ and $\theta = 1$. The most frequent cluster size in Channel 6 (LI) is 1 sample.

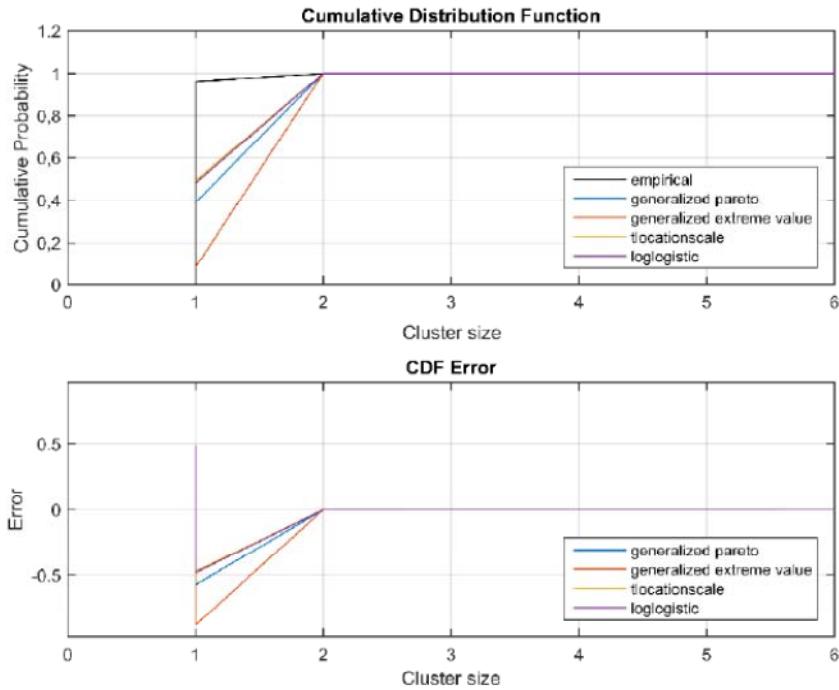


Figure 65: Best fitting CDF and CDF error of the dimension of the clusters; Channel 6 (Low Interference)

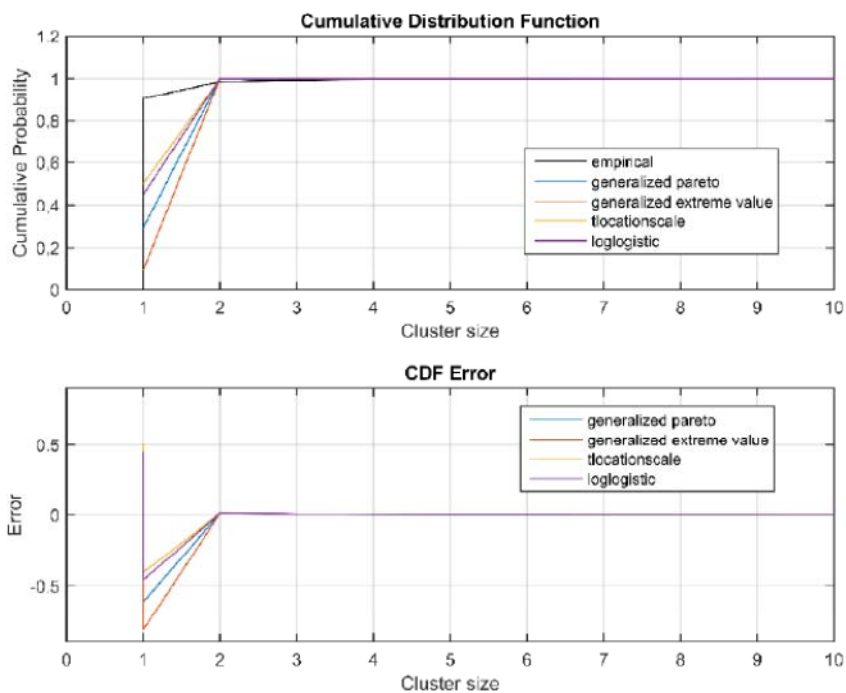
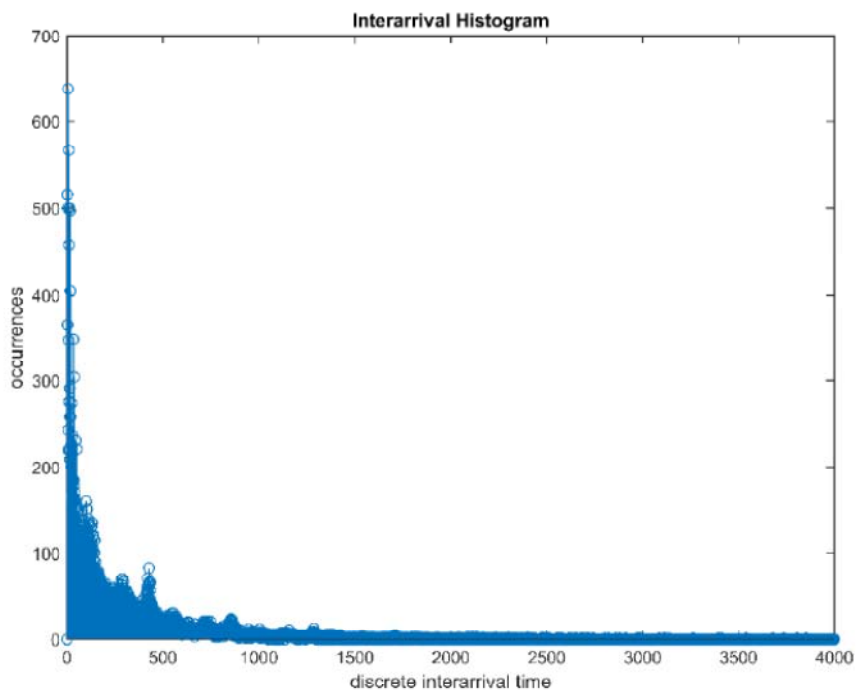
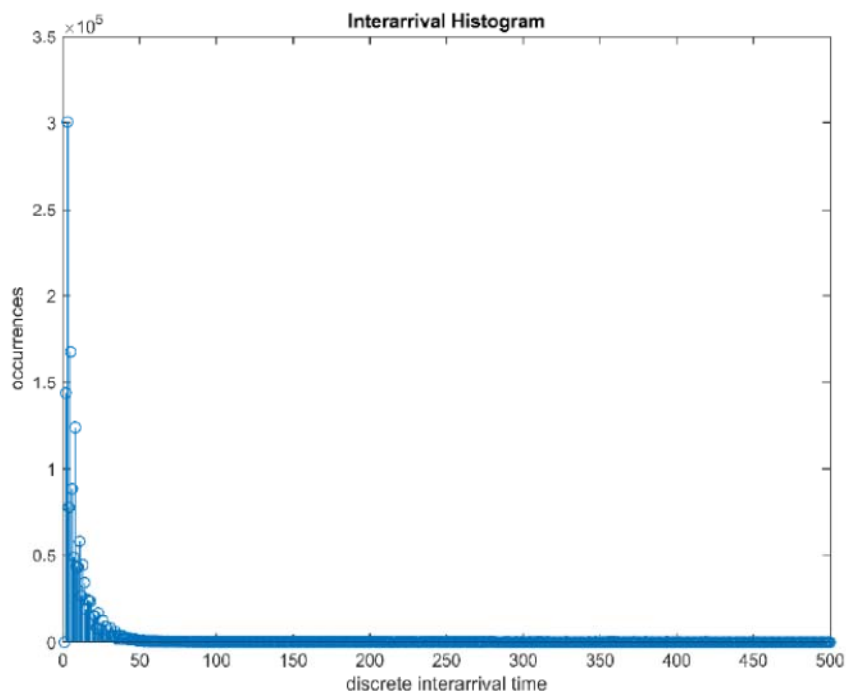


Figure 66: Best fitting CDF and CDF error of the dimension of the clusters; Channel 1 (High Interference)

Figures 67 and 68 show the occurrences of the inter-arrival time of the clusters over one week for the channel 6 (low interference) and channel 1 (high interference), respectively. In channel 1 (HI) the interarrival time is very low, i.e. interference clusters occur very frequently. This means almost continuous interference in the band (2 412 MHz). In channel 6 (LI) the interarrival time is much larger, i.e. interference clusters occur sporadically. This means intermittent interference in the band (2 437 MHz). The empirical CDF (black line in Figure 23), related to interarrival time vector of the HI case, reaches a value equal to 0:7 when an interarrival time is equal to 10 and a value equal to 0:9 when an interarrival time is equal to 20. This means that interarrival times greater than 20 are improbable. The CDF error is remarkable for every distribution considered, but only for the first value of the clusters size.



**Figure 67: Occurrences of the inter-arrival time of the clusters;
Channel 6 (Low Interference)**



**Figure 68: Occurrences of the inter-arrival time of the clusters;
Channel 1 (High Interference)**

This error is determined by the inability of the statistical distributions considered by the MATLAB function `allfitdist` to represent perfectly the particular shapes of the empirical cluster size CDF. It is possible that another statistical distribution, not considered by the function could represent in a better way the empirical cluster size CDF.

Best fitting distribution for the inter-arrival time of clusters is Pareto for Channel 6 (LI), as depicted in Figure 69. The parameters of the distribution in this case are: $k = 0,12$, $\sigma = 373,5$ and $\theta = -2,2e-15$. The CDF error, between the empirical CDF and the CDF of every distribution represented, is in the range $-0,1:0,15$. Best fitting distribution for the interarrival time of clusters is Generalized extreme value (GEV) for Channel 1 (HI), as depicted in Figure 70. The parameters of the distribution in this case are: $k = 0,55$, $\mu = 4,7$ and $\sigma = 3,42$. The error between the empirical CDF and any other CDF of fitting distributions is in the range $-0,14:0,12$.

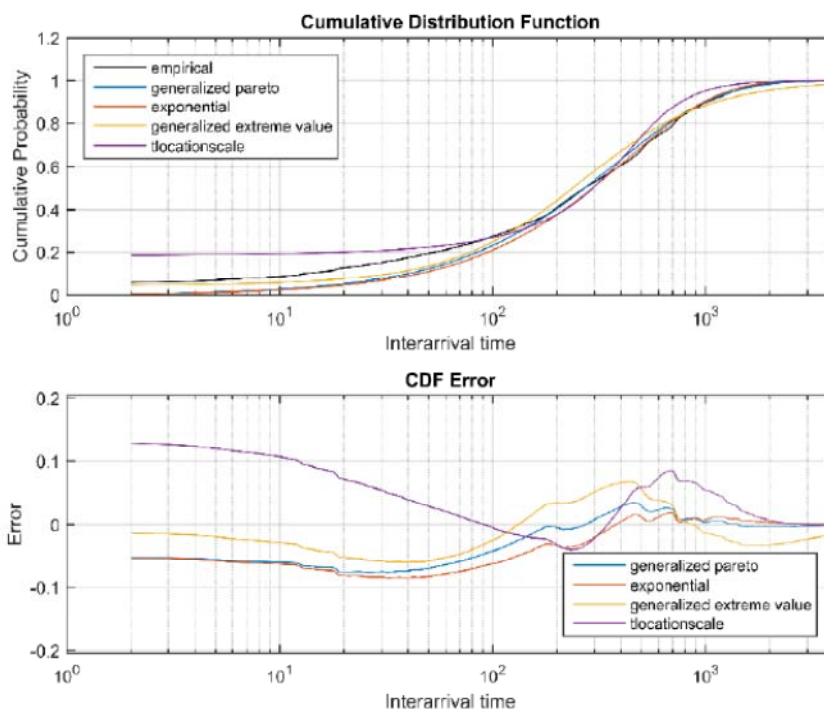


Figure 69: Best fitting CDF and CDF error of the inter-arrival time of the clusters; Channel 6 (Low Interference)

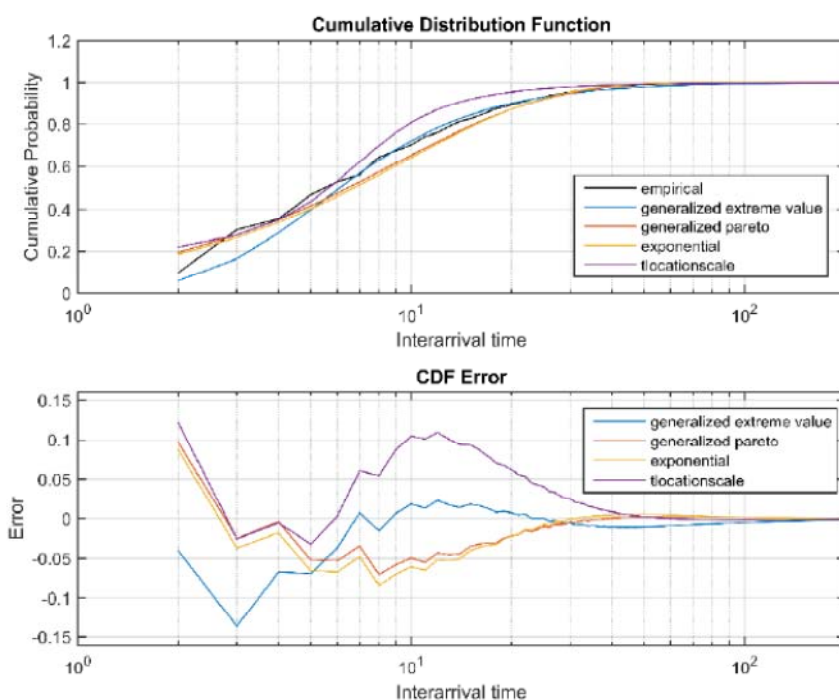
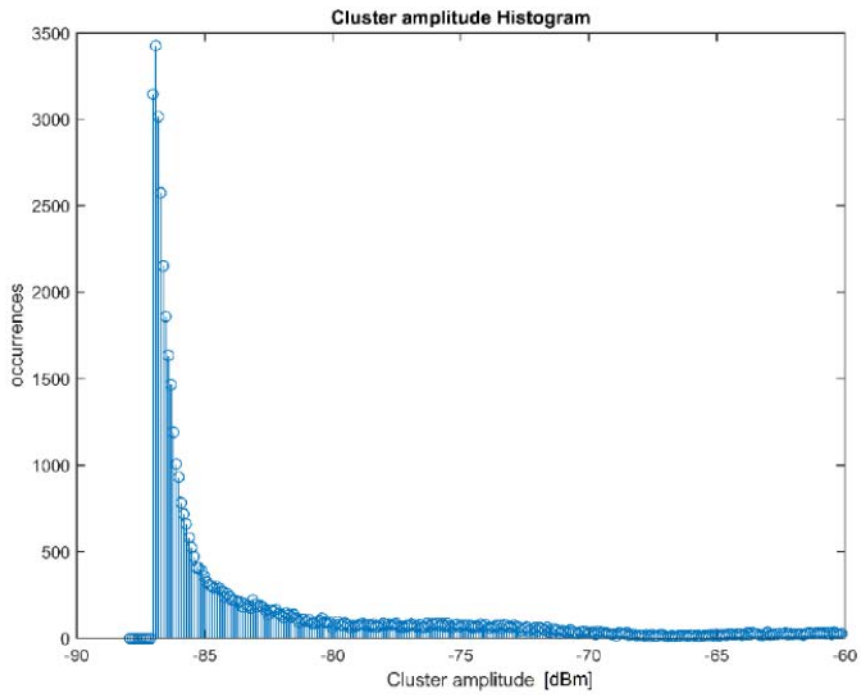
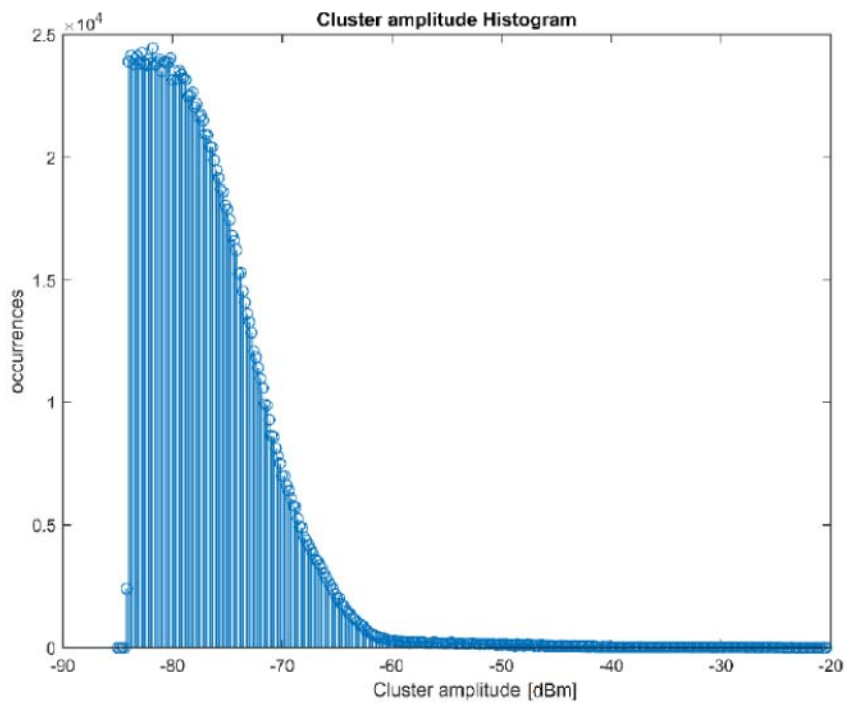


Figure 70: Best fitting CDF and CDF error of the inter-arrival time of the clusters; Channel 1 (High Interference)

Figures 71 and 72 show the occurrences of the amplitude of the clusters over one week for the channel 6 (low interference) and channel 1 (high interference), respectively. In Channel 6 (LI) the amplitude of the clusters ranged from -87 to -85 dBm, while in Channel 1 (HI) ranged from -84 to -62 dBm. The best fitting distribution for the amplitude of the clusters is the GEV for both the Channel 6 and Channel 1, as depicted in Figures 73 and 74. The GEV representing Channel 6 (LI) has the following parameters: $k = 0.14$, $\mu = -83.7$ and $\sigma = 2.7$. The CDF error is in the range $-0.06; 0.12$. The GEV representing Channel 1 (HI) has the following parameters: $k = 0.12$, $\mu = -79.4$ and $\sigma = 3.7$. The CDF error is in the range $-0.07; 0.1$, for every distribution represented.



**Figure 71: Occurrences of the amplitude of the clusters;
Channel 6 (Low Interference)**



**Figure 72: Occurrences of the amplitude of the clusters;
Channel 1 (High Interference)**

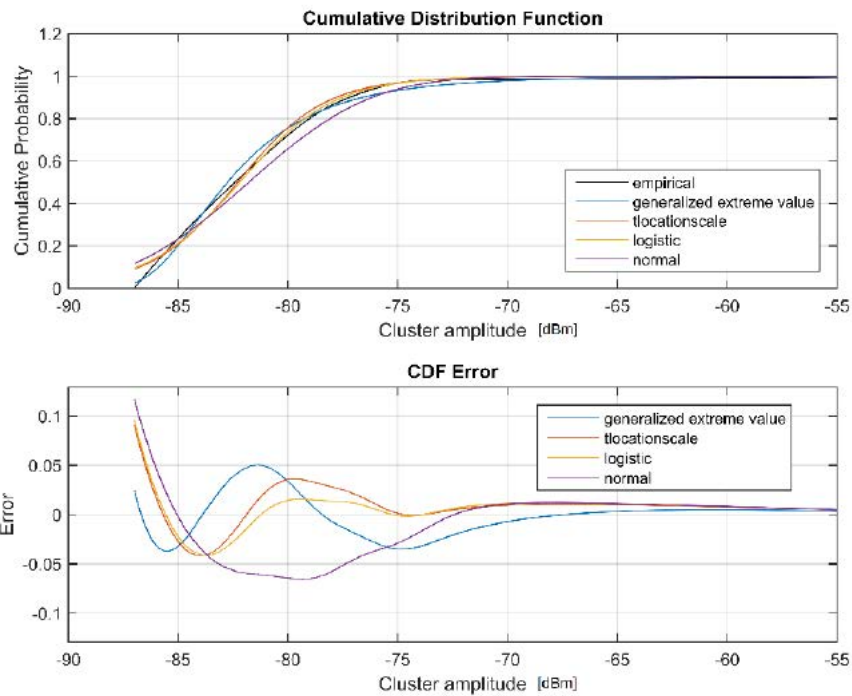


Figure 73: Best fitting CDF and CDF error of the amplitude of the clusters; Channel 6 (Low Interference)

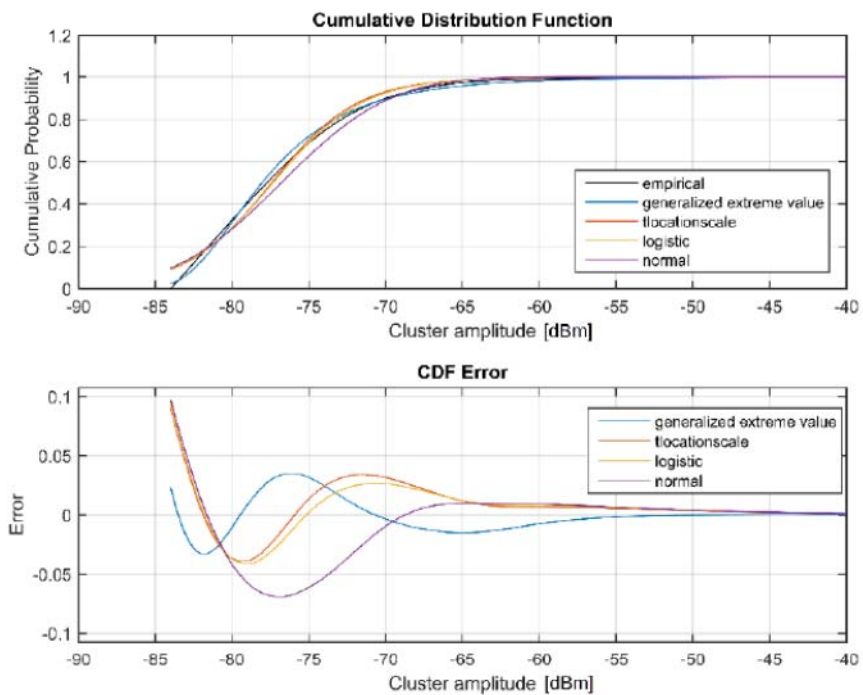


Figure 74: Best fitting CDF and CDF error of the amplitude of the clusters; Channel 1 (High Interference)

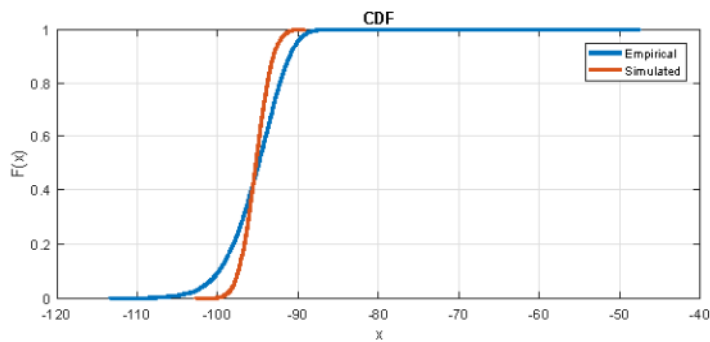
Cluster-Based Interference Simulator

The statistical parameters of the interference clusters have been used to build a Matlab simulator. The simulator creates a cluster-based interference vector which follows the statistics of the selected scenario: low, moderate or high interference.

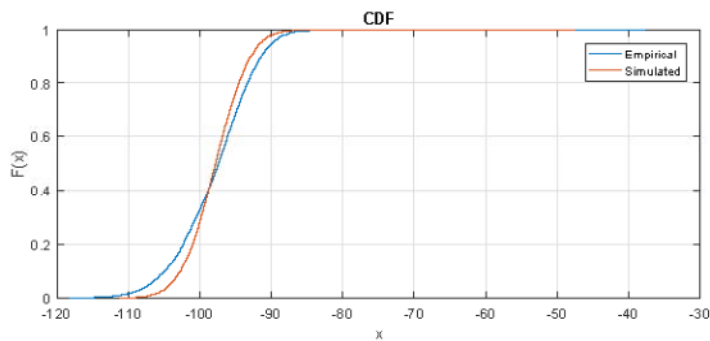
In order to measure the accuracy of the cluster-based statistical model of the interference, the two-sample Kolmogorov-Smirnov (KS) test is applied to the empirical data and the simulated data. The Kolmogorov-Smirnov test is a nonparametric hypothesis test that evaluates the difference between the cdfs of the distributions of the two sample data vectors over the range of x in each data set. The two-sided test uses the maximum absolute difference between the cdfs of the distributions of the two data vectors. The test statistic is:

$$D = \max_x (CDF_1(x) - CDF_2(x)) \quad (23)$$

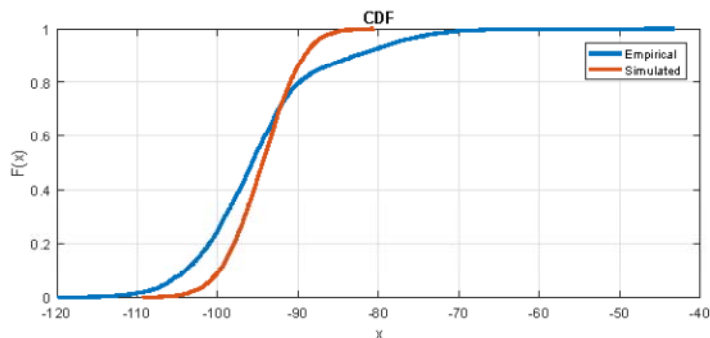
where $CDF_1(x)$ is the proportion of x_1 values less than or equal to x and $CDF_2(x)$ is the proportion of x_2 values less than or equal to x . Figure 75 shows the CDFs of the empirical and simulated data for the low, moderate and high interference scenarios. The KS test always rejects the null hypothesis with a significance level of 5 %.



(a) Low interference scenario.

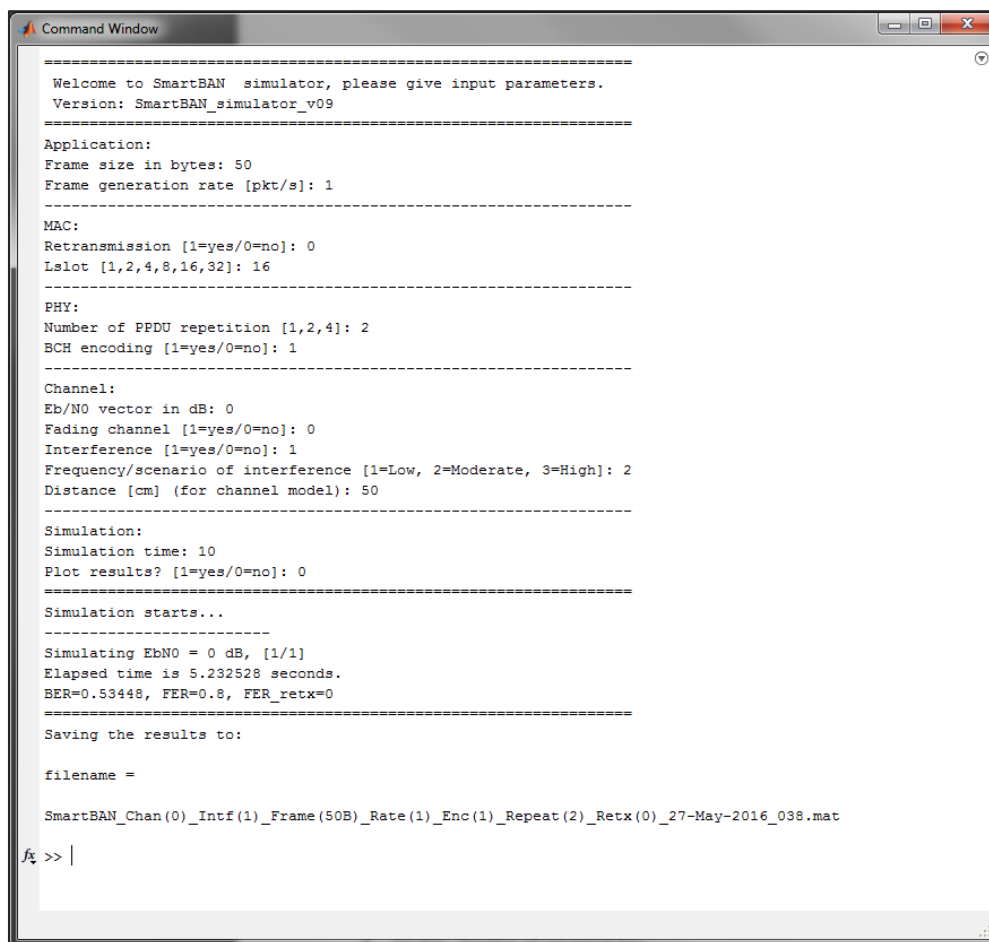


(b) Moderate interference scenario.



(c) High interference scenario.

Figure 75: CDFs of the empirical and the simulated data



```

=====
Welcome to SmartBAN simulator, please give input parameters.
Version: SmartBAN_simulator_v09
=====
Application:
Frame size in bytes: 50
Frame generation rate [pkt/s]: 1
=====
MAC:
Retransmission [1=yes/0=no]: 0
Lslot [1,2,4,8,16,32]: 16
=====
PHY:
Number of PPDU repetition [1,2,4]: 2
BCH encoding [1=yes/0=no]: 1
=====
Channel:
Eb/N0 vector in dB: 0
Fading channel [1=yes/0=no]: 0
Interference [1=yes/0=no]: 1
Frequency/scenario of interference [1=Low, 2=Moderate, 3=High]: 2
Distance [cm] (for channel model): 50
=====
Simulation:
Simulation time: 10
Plot results? [1=yes/0=no]: 0
=====
Simulation starts...
-----
Simulating EbN0 = 0 dB, [1/1]
Elapsed time is 5.232528 seconds.
BER=0.53448, FER=0.8, FER_retx=0
=====
Saving the results to:

filename =

SmartBAN_Chan(0)_Intf(1)_Frame(50B)_Rate(1)_Enc(1)_Repeat(2)_Retx(0)_27-May-2016_038.mat
fx >> |

```

Figure 76: User interface of the simulator

When simulation is finished the results are saved to `\Results` -folder to the file `SmartBAN_Chan(0)_Intf(1)_Frame(50B)_Rate(1)_Enc(1)_Repeat(2)_Retx(0)_27-May-2016_038.mat`. The filename is updated automatically based on the parameters used and time of simulation to make it easier to distinguish different result files.

The file contains `outputs` -structure including:

- *BERvec*: Bit error rate vector, one value for each E_b/N_0 value, computed from MPDUs
- *FERvec*: Frame error rate vector, one value for each E_b/N_0 value, computed from MPDUs
- *FERretxvec*: Frame error rate vector for retransmission scheme, one value for each E_b/N_0 value, computed from MPDUs
- *SimBits*: Number of simulated bits, computed from MPDUs
- *SimFrames*: Number of simulated frames, computed from MPDUs
- *EbN0vec*: E_b/N_0 vector
- *params*: Simulation parameters
- *model*: Simulator model
- *SimTime*: Simulation time (duration)
- *SimDate*: Date of simulation
- *uniqueID*: Unique identification number for a file

The results can be plotted by selecting 'yes' before starting simulations or typing:

```
>> Plot_Results('filename')
```

This will save a figure as a JPG file.

The simulator can also be opened in Simulink by double-clicking the filename or typing:

```
>> open_system('model_name')
```

The simulator parameters can be changed by double-clicking the *Simulation parameters* -block (Figure 78). If this simulation approach is used, transmitted frames, errors, retransmission, etc. can be monitored, but the results should be saved manually.

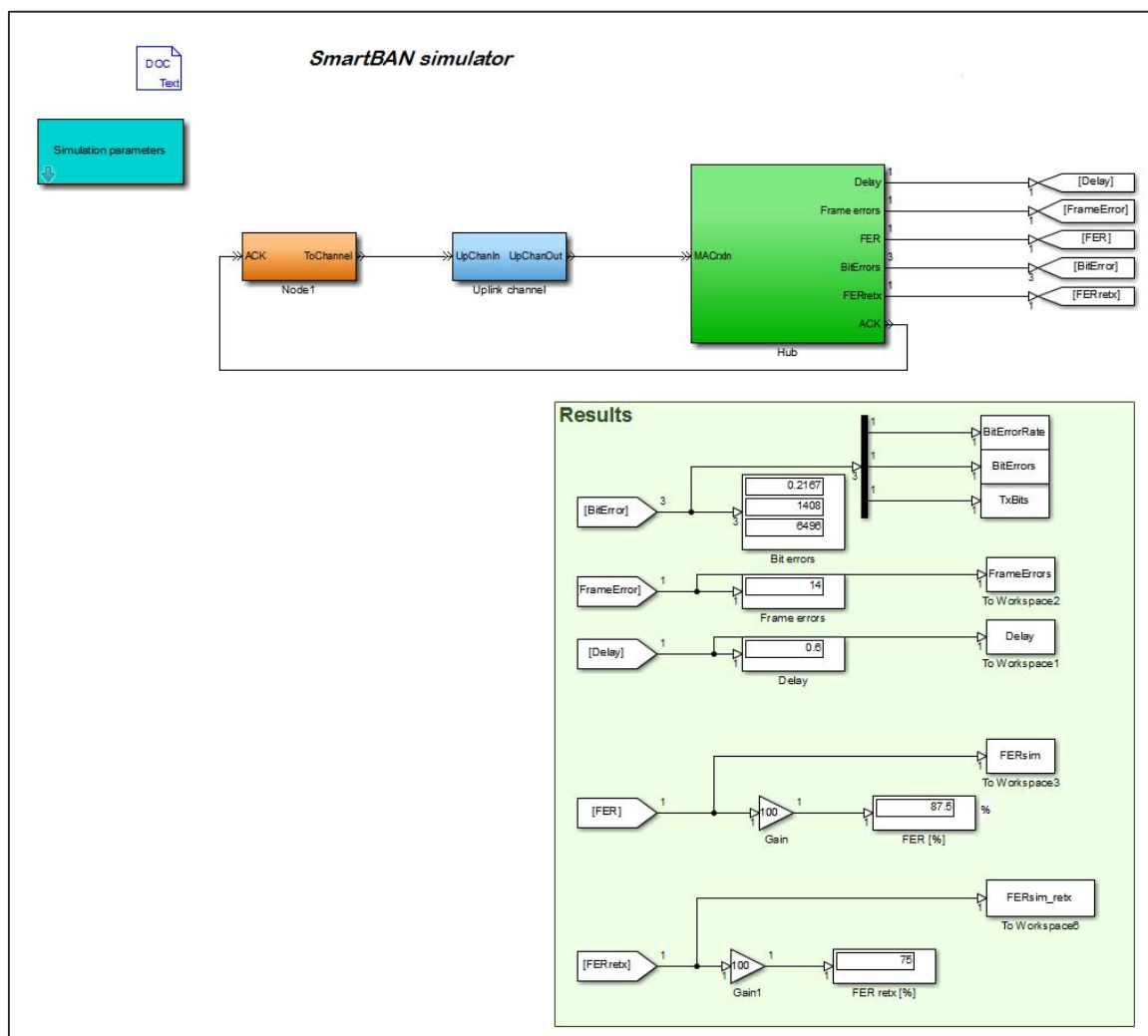


Figure 77: Simulink model of the simulator

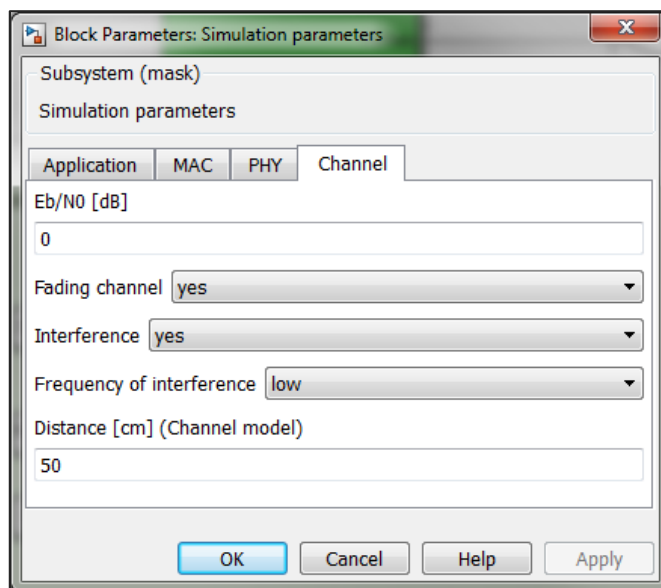


Figure 78: Graphical user interface of the simulation parameters

7.2 Simulator model

7.2.0 Introduction

The simulator model is introduced in details in this clause.

7.2.1 Node

The simulation model for node is shown in Figure 79.

Random bits form a MPDU having a size defined by the given frame size. The size of the frame is limited by a slot time T_S , which is equal to $T_{\min} * L_{\text{slot}}$ as defined in [i.1.1] and the PPDU repetition. Next, the 'dummy' bits, i.e. zeros are appended as parity bits and header. Each frame has given a unique sequence number and a node number. The frame generation rate defines how often the frame is generated. The distribution of frame generation interval can be also adjusted. These features were designed keeping in mind further development of the simulator where multiple nodes, and hence, medium access is implemented.

The *Admission control* -block is for admitting a new frame to proceed where permission is given by the transmitter logic.

The lower part of the transmitter structure is for retransmission procedure. All frames are replicated and saved to a buffer. Based on *FrameError* in the received acknowledgement frame, the frame is discarded, i.e. the port switch p has the value of 2. The frame is retransmitted only once, therefore the port switch q is set to 1. T_x and $Retx$ are the gate release triggers deciding if a new frame or old frame proceeds.

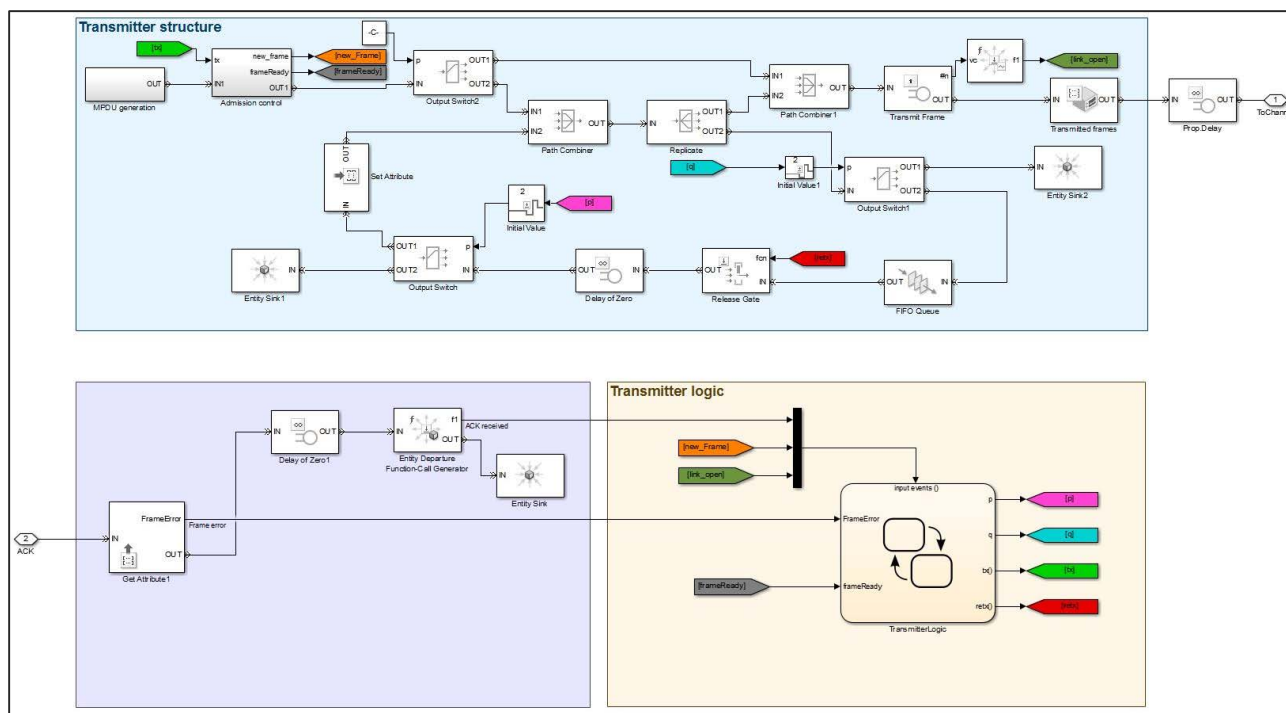


Figure 79: Node model

7.3 Hub

7.3.0 Introduction

The hub contains full PHY layer transceiver chain including the noise and fading channel. This approach solves issues using SimEvents and Communication System blocks together. Hub model is shown in Figure 80.

Based on the correctness of the received frame, *ReceiverLogic* sends the acknowledgement frame with *FrameError* indicating the frame error. *Results* - block computes the performance metrics, which are:

- Total number of transmitted bits
- Total number of bit errors
- Bit error rate: Ratio between total number of bit errors and total number of transmitted bits
- Frame error rate: Ratio between total number of frame errors and total number of transmitted frames
- Frame error rate with retransmission: Ratio between total number of errors of generated frames and total number of generated frames

7.4 PHY layer

7.4.0 Introduction

The physical layer model, shown in Figure 81, follows the technical specification of SmartBAN PHY [i.1]. For definitions of applied Matlab functions, objects and blocks, see Matlab Help [i.12].

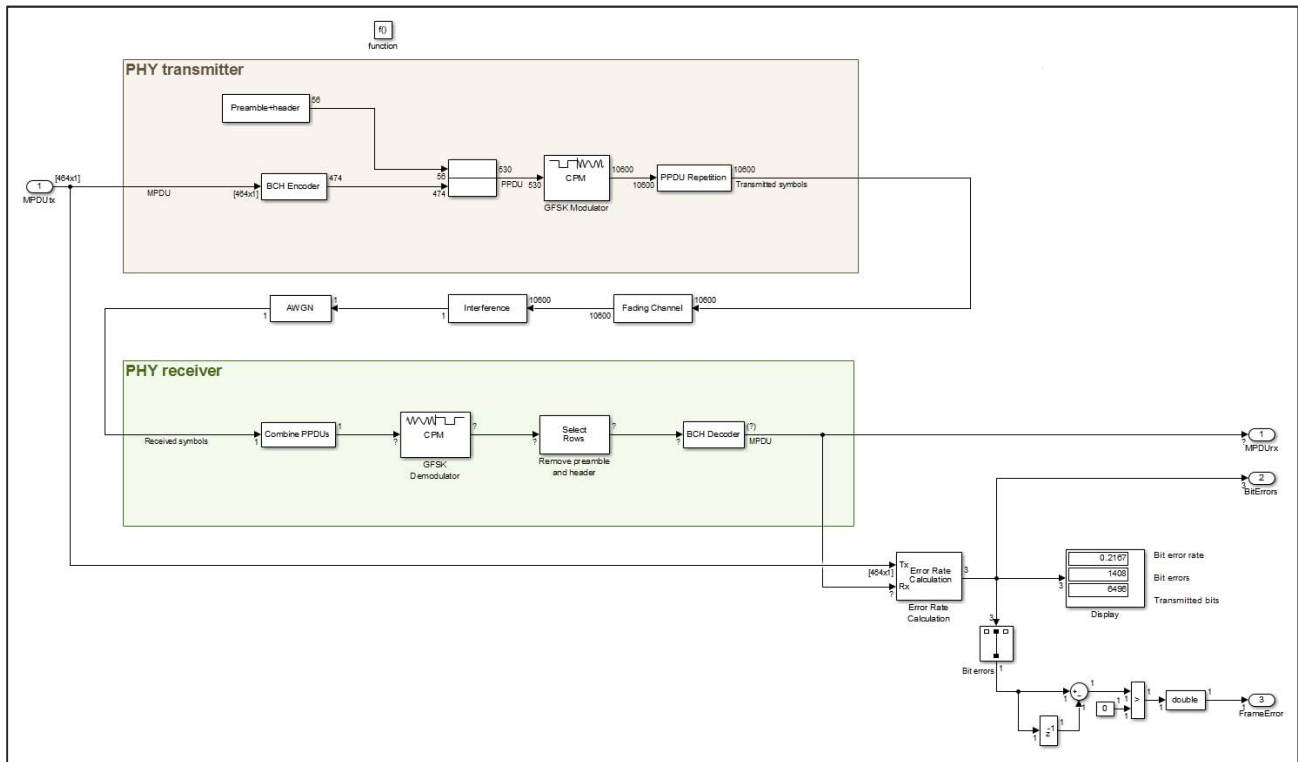


Figure 81: PHY layer model

7.4.1 PHY transmitter

The generation of a transmitted PPDU is as follows:

- *BCH Encoder*: MPDU is encoded as defined in clause 7.3.2 of [i.1]. Due to the delay of the GFSK demodulator, additional zeros are appended which are removed before decoding process.
- *Preamble+header*: PSDU is formed by appending random bits as PLCP header and preamble.
- *GFSK Modulator*: The modulator generates symbols according to clause 7.2 of [i.1]. It uses 20 samples per symbol, pulse length of 1, modulation index (h) of 0,5 and bandwidth-time product (BT) of 0,5.
- *PPDU Repetition*: PPDU is repeated by 1, 2 or 4 times as given in clause 7.3.1 of [i.1].

7.4.2 Channel, interference and noise

7.4.2.0 Introduction

The transmitted signal goes through a fading channel, if it is selected. The channel is assumed as constant for each PPDU. After that, interference and noise are added to the signal. The applied channel model is the IEEE 802.15.6 [i.17] body surface to body surface CM3 (Scenario S4 & S5) for 2,4 GHz [i.13], where flat small-scale fading is represented by a Ricean distribution with K factor:

$$K_{\text{dB}} = K_0 - m_K PL_{\text{dB}} + \sigma_K n_K, \quad (24)$$

where:

- $K_0 = 30,6$ dB;
- $m_K = 0,43$ dB/cm;
- $\sigma_K = 3,4$ dB.

Pathloss (PL_{dB}) is given by

$$PL_{dB} = -10\log_{10}(P_0e^{-m_0d} + P_1) + \sigma_P n_P \text{ [dB]}, \quad (25)$$

where:

- $P_0 = -25,8$ dB;
- $m_0 = 2,0$ dB/cm;
- $P_1 = -71,3$ dB;
- $\sigma_P = 3,6$ dB;
- $d =$ distance.
- Calculated pathloss of the IEEE 802.15.6 [i.17] CM for $d = 45$ cm is shown in Figure 82.

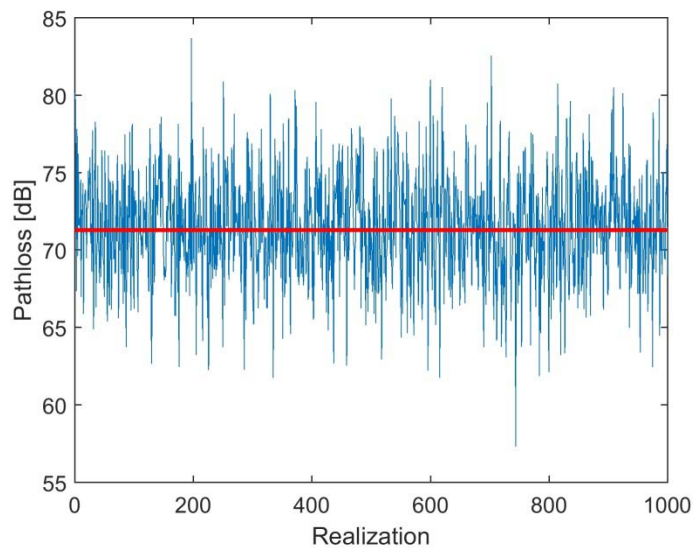


Figure 82: Pathloss of the IEEE 802.15.6 [i.17] CM for $d = 45$ cm

7.4.2.1 Interference

The generated interference vector is added with the signal in this block. The frequency or scenario is either low, moderate or high as selected at the beginning of the simulation. These models are discussed in clause 6 in detail. Figure 70 illustrates one interference realization for each interference scenario. 12 000 samples correspond to one transmitted PPDU with 50 octets frame body size.

The interference matrix having 100 realization used in simulation is generated in the `initMask.m` function. For high interference frequency, a pregenerated interference matrix saved into `IntfMatrix_HIGH_100real.mat` is used. The MAC frame size for high interference frequency is only to 50 octets. The use of pregenerated interference matrices in the simulations is justified by high memory allocation and processing time of interference generation, especially when using high interference frequency.

An interference level is adjusted so that pathloss given in equation 23 and the signal transmission power of -10 dBm, as defined in [i.17], are met.

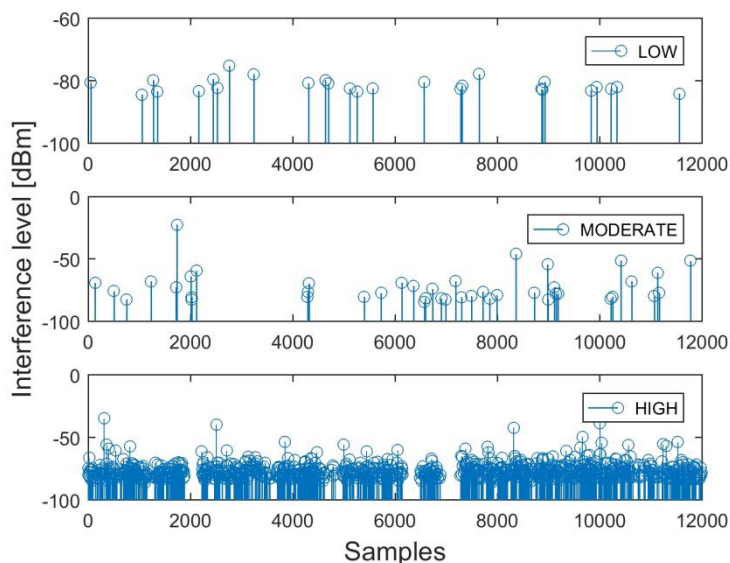


Figure 83: Interference realizations

7.4.3 PHY receiver

The signal is received as follows:

- 1) *Combine PPDU*s: Received PPDU's are combined by using the Equal Gain Combining (EGC) method, where perfect channel phase estimation is assumed.
- 2) *GFSK Demodulator*: The demodulator is an optimum one where a correlator is followed by a maximum-likelihood sequence detector (MLSD). The Viterbi algorithm is used to perform MLSD. The demodulator has the traceback depth parameter D influencing to the output delay, which is the number of zero symbols that precede the first meaningful demodulated value in the output. The "five-time-constraint-length" rule is used to estimate the optimal traceback depth [i.1]. It corresponds to $5 \times \log_2(\text{numStates})$, where:

$$\text{numStates} = \begin{cases} p \cdot M^{(L-1)}, & \text{for even } m \\ 2p \cdot M^{(L-1)}, & \text{for odd } m, \end{cases} \quad (26)$$

where: m is the numerator of modulation index;
 p is the denominator of the modulation index;
 M is the M-ary number;
 L is the pulse length.

- 3) *Remove Preamble and Header*: The block removes the preamble and PLCP header.
- 4) *BCH Decoder*: The block decodes the input signal.
- 5) *Error Rate Calculation*: It calculates the transmitted bits, bit errors and bit error rate. The frame error rate is also calculated.

7.5 MAC - Frame retransmission

A user can select if a frame retransmission is enabled or not. If a frame is corrupted, i.e. having $\text{FrameError}=1$, then the frame is retransmitted once. *ReceiverLogic* --chart sends an ACK-frame including indication of frame error introduced in Fig. 71. The chart has the following inputs and outputs:

- p : indicates a port of a switch to be selected. '1' is for discard, '2' for retransmission and '3' for reception.
- send_ack : a generated event for ACK frame.

- *FrameError*: indicates if a frame is corrupted or not.
- *FrameRetransmitted*: parameter indicating if a frame is retransmitted or not.

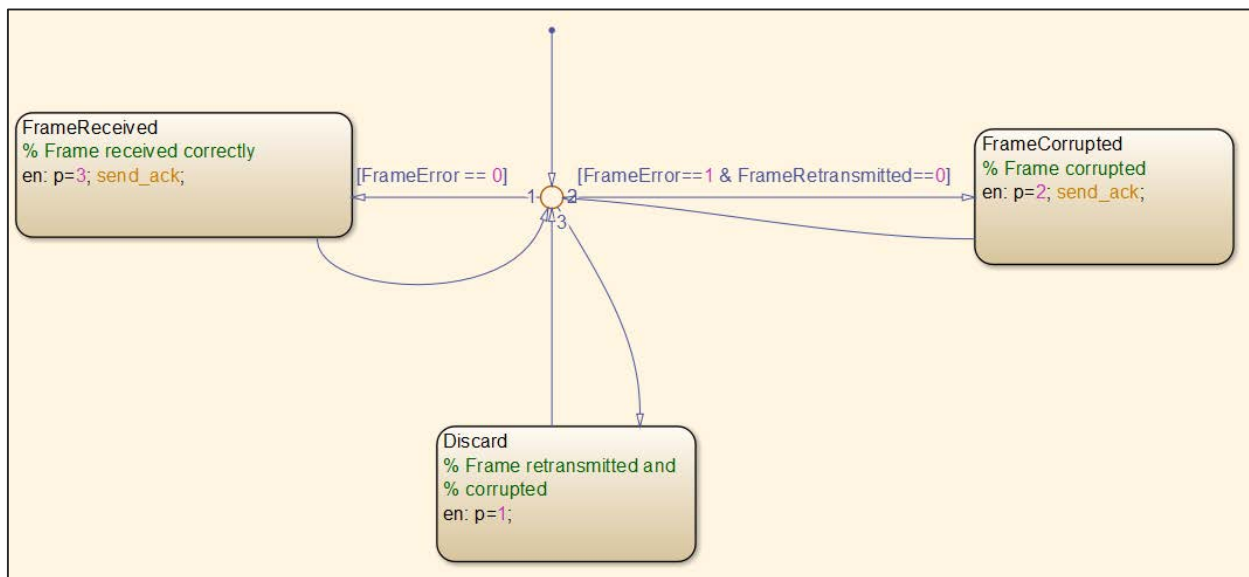


Figure 84: Receiver logic

TransmitterLogic -chart, shown in Figure 85, decides if a new frame transmission or retransmission takes place. Decision logic is as follows:

- At the beginning of a simulation, there are a frame generated. *Transmitting* -state is selected and entry (en) values are given; the frame is replicated ($q = 2$) and saved to a buffer and *tx* is sent. When the frame has been transmitted transition guards are checked in this order:
 - 1) ACK frame is received (*new_ack*) and there is no error ($FrameError = 0$). If it is true, discard an acknowledged frame by setting $p = 2$, $q = 2$ and send *retx* and proceed to a connective junction.
 - 2) ACK frame is received and there is error ($FrameError = 1$), move to *Retransmitting* -state if retransmission is enabled ($Retx = 1$). When entering to the state, release a buffered frame ($p = 1$, *retx*) and do not buffer it again ($q = 1$).
 - 3) Otherwise, move directly to the connective junction.
- Connective junction:
 - 1) Proceed to *Idle* -state if there is no frame to transmit ($FrameReady = 0$).
 - 2) Return to *Transmitting* -state if a frame is ready.
- Idle state:
 - 1) ACK frame is received (*new_ack*) and there is no error ($FrameError = 0$). If it is true, discard an acknowledged frame by setting $p = 2$, $q = 2$ and send *retx* and proceed to a connective junction.
 - 2) ACK frame is received and there is error ($FrameError = 1$), move to *Retransmitting* -state if retransmission is enabled ($Retx = 1$). If it is true, discard an acknowledged frame by setting $p = 2$, $q = 2$ and send *retx* and proceed to a connective junction.
 - 3) A new frame is generated, *new_frame* occurs.

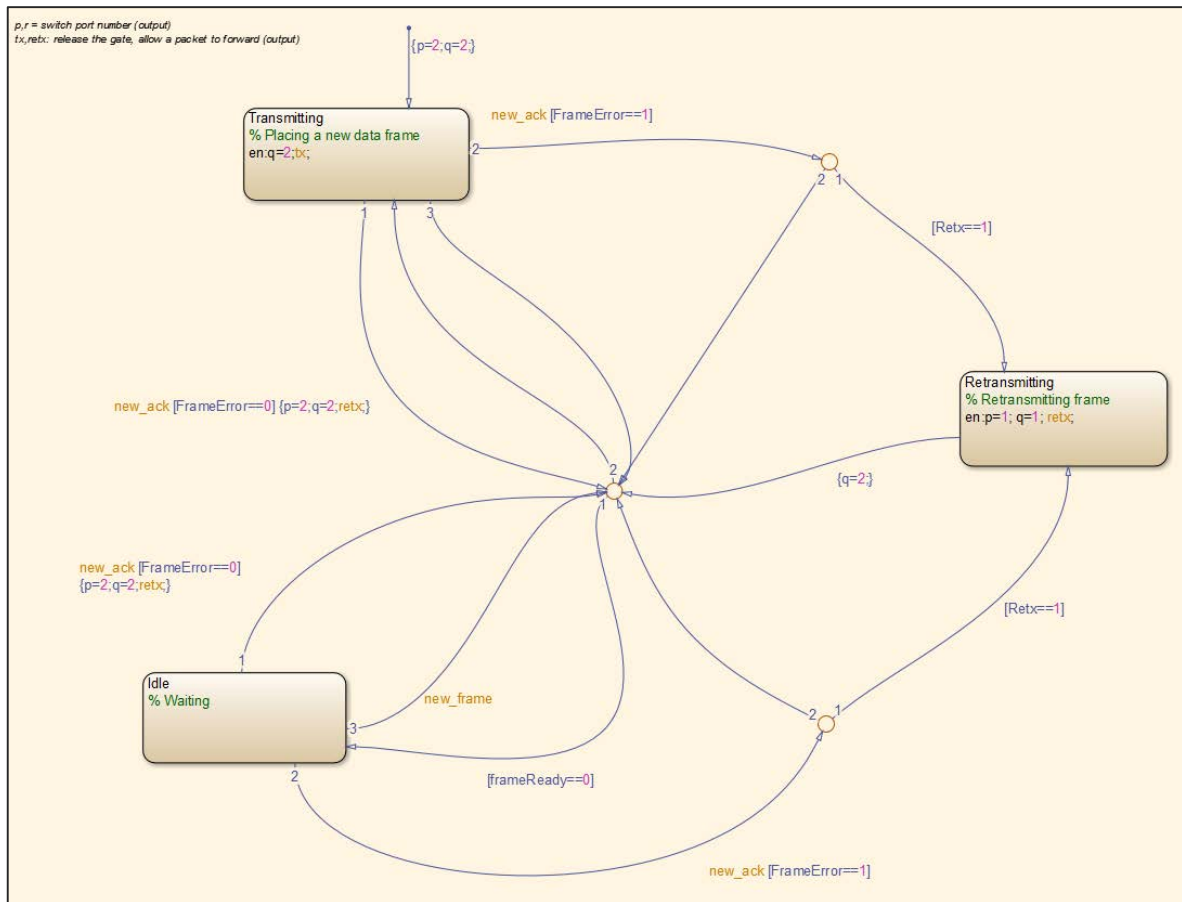


Figure 85: Transmitter logic

Figure 86 illustrates behaviour of frame transmission. For each generated frame is given an unique sequence number (Seq.Num). As it can be seen, some of the frames are transmitted twice, i.e. being corrupted and generating ACK frame with a frame error.

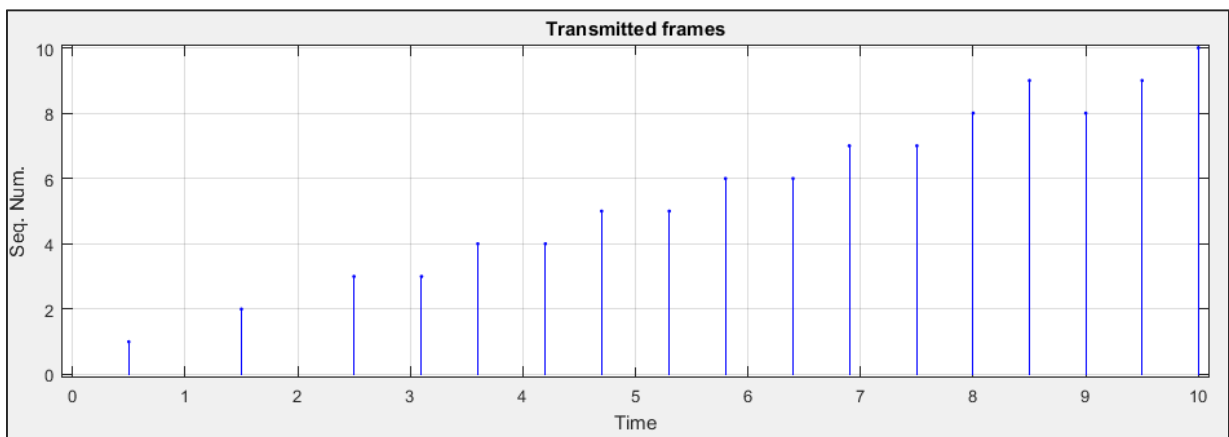


Figure 86: Transmitted frames

7.6 Verification results

For binary Gaussian frequency shift keying (GFSK) with modulation index $h=1/2$, the bit error probability P_b at high E_b/N_0 is closely approximated by [i.14] and [i.15].

$$P_b = Q\left(\sqrt{2 \cdot \frac{\epsilon_b}{N_0}}\right) \quad (27)$$

Figure 74 shows the results of the verification simulations. The following conclusion can be drawn: the simulation result (Uncoded, $PPDU_{rep} = 1$) follows the theoretical bit error probability given above. $PPDU_{rep}$ indicates the number of PPDU repetitions.

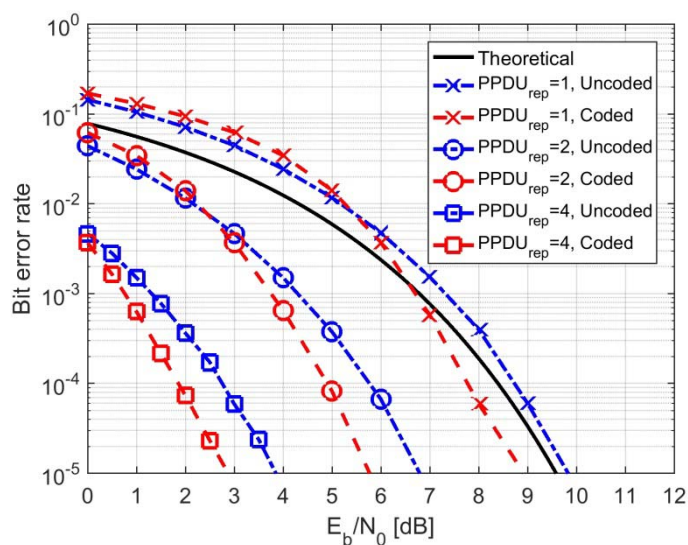


Figure 87: Verification results

8 Simulation results

8.0 Introduction

Simulation results using the simulator described earlier are given in this clause. Clause 8.1 gives the simulation parameters, clause 8.2. includes the results in AWGN channel, clause 8.3. fading channel results and clause 8.4 results with the interference.

8.1 Simulation parameters

Table 7a summarizes the used simulation parameters. Parameters related to the SmartBAN transceiver are directly from the technical specifications, channel parameters are introduced in clause 7.3.2 and interference is discussed in clause 6.

Table 7a: Simulation parameters

| Parameter | Value(s) | Unit | Explanation |
|---------------------------|---------------------|---------|---|
| noRepeatPPDU | 1,2,4 | - | PPDU repetition |
| Retx | no, yes | - | Retransmission |
| frameSize | 50, 250, 500, 1 000 | octets | MAC frame body [octets] |
| EbN0 | - | dB | E_b/N_0 vector |
| packetGenRate | 100 | pps | Packet generation rate |
| NoSamplesPerSymbolGFSK | 20 | samples | The number of output samples for each bit |
| PulseLengthGFSK | 1 | symbols | The length of the frequency pulse shape |
| TraceBackDepth | 10 | - | The number of trellis branches used to construct each traceback path |
| distance | 45 | cm | Distance for the channel model |
| Lslot | 32 | - | Defines the size of T_s , and therefore, limits the size of the MAC frame body. |
| enableChannel | no, yes | - | Enable channel. |
| enableBCH | no, yes | - | Enable encoding, $n = 127$, $k = 113$. |
| enableInterference | no, yes | - | Enable interference. |
| freqInterference | low, moderate, high | - | Frequency/ scenario of interference |
| NoInterferenceRealization | 100 | - | Number of interference realizations |
| simuTime | 2 000 | s | Simulation time |
| NoSimulatedFrames | 40 000 | frames | Number of frames to be simulated per E_b/N_0 value |

8.2 AWGN channel

The simulation results in the AWGN channel is applied to define the requirement for the receiver sensitivity as in Clause 8.9.1 of the IEEE 802.15.6 standard [i.17]. As defined in the standard, it is assumed that PSDU is 255 octets, noise figure is 13 dB and the implementation losses is 6 dB. The total loss is defined as:

$$S_{\text{dBm}} = -174 \text{ dBm} + NF_{\text{dB}} + \frac{E_b}{N_0} + 10 \cdot \log_{10}(R) + I_{\text{dB}}. \quad (28)$$

where:

NF_{dB} is the noise figure in dB;

E_b/N_0 is threshold value for FER < 10 % in dB;

R is the data rate;

I_{dB} is the implementation losses in dB.

Figures 88 and 89 represent the simulation results in the AWGN channel for BER and FER, respectively, and Table 8 gives the receiver sensitivity numbers according to the simulation results and equation 26.

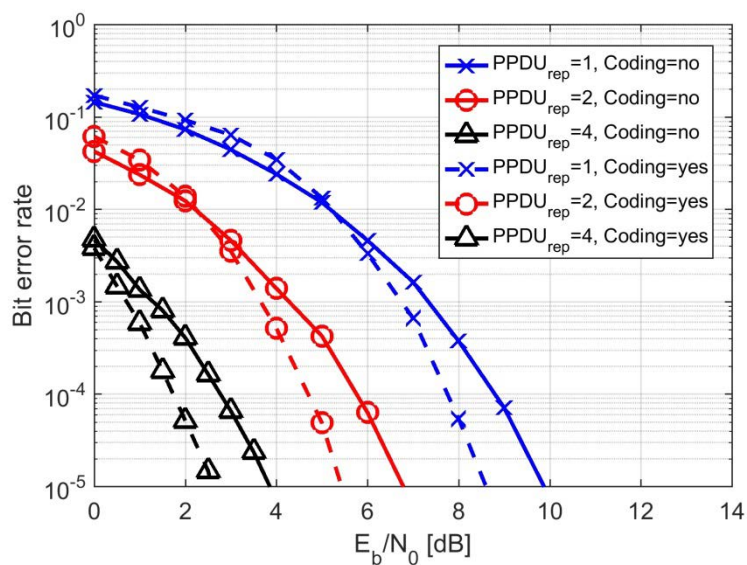


Figure 88: AWGN, BER

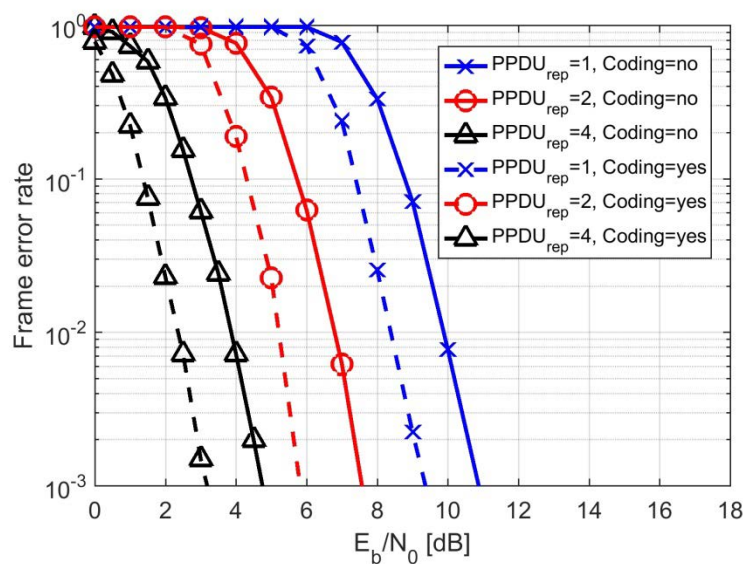


Figure 89: AWGN, FER

Table 8: Receiver sensitivity numbers

| Symbol rate (Msymbols/s) | Code rate | Repetition | Information rate (Mbps) | E_b/N_0 , FER =10% | Maximum input level at sensitivity (dBm) |
|--------------------------|-----------|------------|-------------------------|----------------------|--|
| 1,0 | 1 | 1 | 1,0 | 8,8 | -86,2 |
| 1,0 | 1 | 2 | 0,5 | 5,8 | -92,2 |
| 1,0 | 1 | 4 | 0,25 | 2,8 | -98,2 |
| 1,0 | 113/127 | 1 | 0,89 | 7,4 | -88,1 |
| 1,0 | 113/127 | 2 | 0,44 | 4,3 | -94,3 |
| 1,0 | 113/127 | 4 | 0,22 | 1,4 | -100,2 |

8.3 Fading channel

The simulation results using encoding in the fading channel are presented in Figures 77 to 81. Figure 77 gives the results for BER using 1-, 2- and 4-time PDU repetition ($PPDU_{rep}$). Next figures illustrate FER for 50-, 250-, 500- and 1 000-octets MAC frame body without and with retransmission (Retx). The 4-time PDU repetition cannot be applied for 1 000-octets frame body due to the limitation of the packet length given in clause 8.1 of [i.1]. Table 9 gives the E_b/N_0 values for the FER level of 1 % and 10 %.

Table 9: E_b/N_0 values for FER=[1, 10]%

| FER | | 10 % | | 1 % | |
|----------------|--------------|----------|---------|----------|---------|
| Retransmission | | w/o Retx | w/ Retx | w/o Retx | w/ Retx |
| Frame size | $PPDU_{rep}$ | | | | |
| 50 | 1 | 16 | 9,4 | 26,3 | 15,3 |
| | 2 | 8,8 | 5,0 | 13,9 | 8,6 |
| | 4 | 3,8 | 1,5 | 7,3 | 3,7 |
| 250 | 1 | 17,7 | 9,8 | 27,8 | 16,2 |
| | 2 | 9,1 | 5,4 | 15,0 | 8,7 |
| | 4 | 4,2 | 2,4 | 7,2 | 4,1 |
| 500 | 1 | 17,7 | 10,2 | 28,2 | 16,4 |
| | 2 | 9,5 | 6,4 | 15,1 | 9,4 |
| | 4 | 5,3 | 2,6 | 7,6 | 5,3 |
| 1 000 | 1 | 17,8 | 10,4 | 28,3 | 16,9 |
| | 2 | 9,6 | 6,4 | 15,9 | 9,6 |

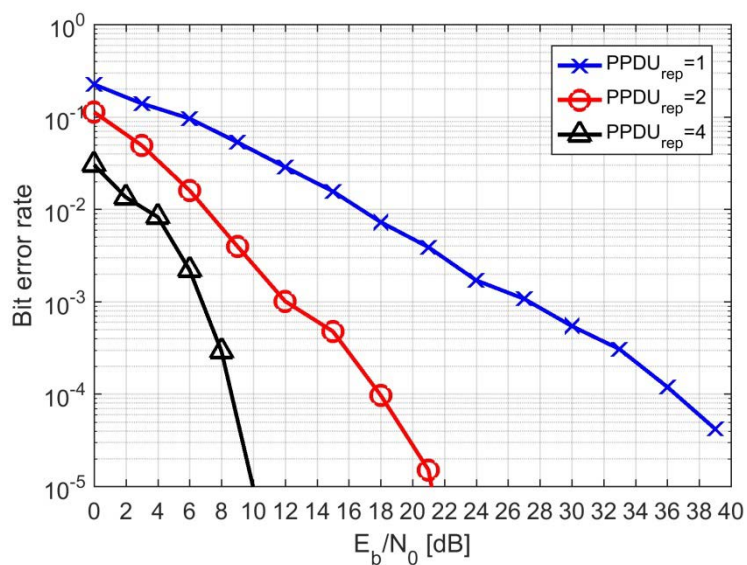


Figure 90: Fading channel, BER

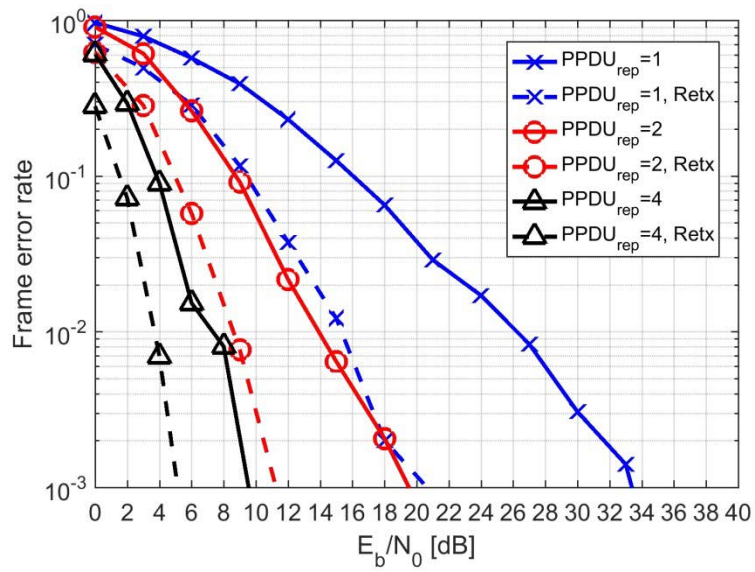


Figure 91: Fading channel, FER, frame size = 50 octets

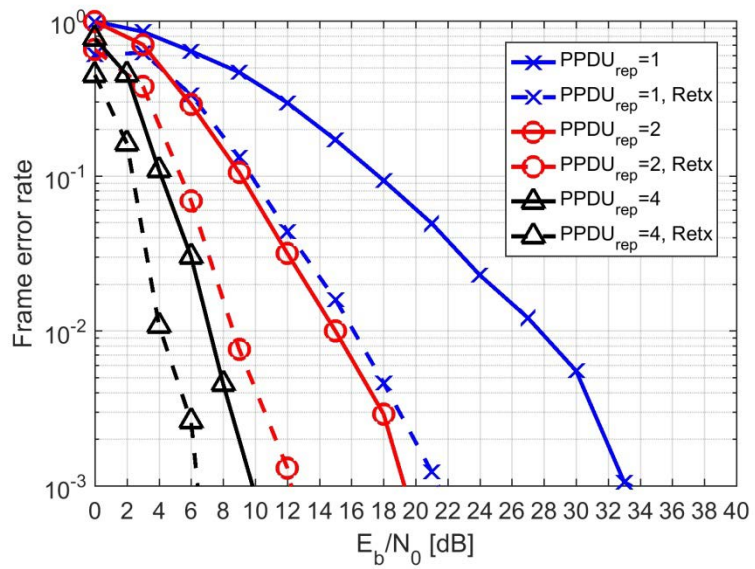


Figure 92: Fading channel, FER, frame size = 250 octets

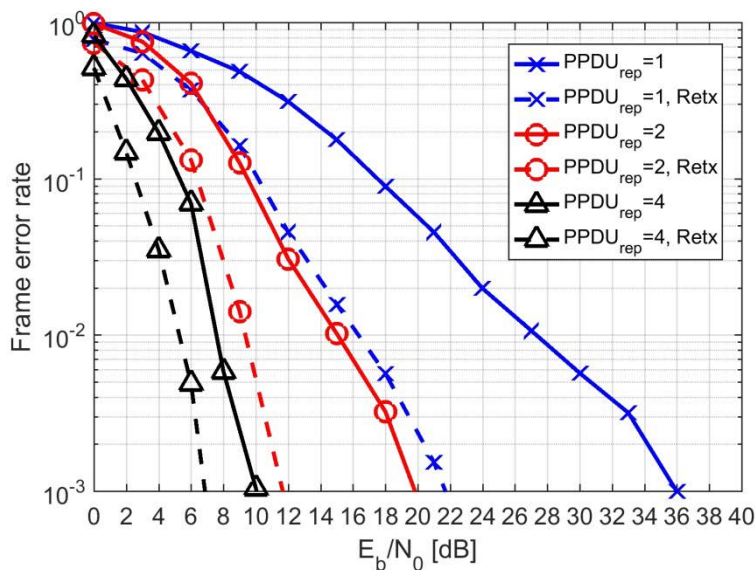


Figure 93: Fading channel, FER, frame size = 500 octets

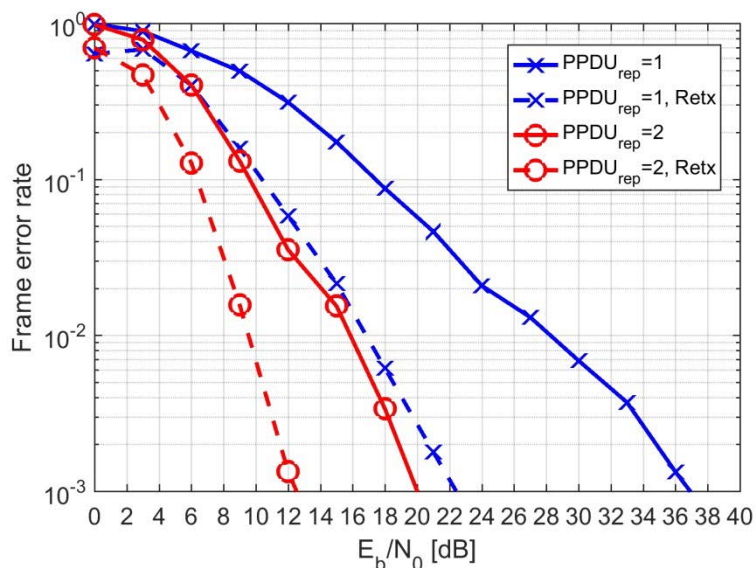


Figure 94: Fading channel, FER, frame size = 1000 octets

8.4 Fading channel and interference

Figures 82 and 83 present the simulation results using the fading channel and interference. The frame body size of 50 octets were applied. An interference scenario is either low, moderate or high. As results show, the interference has minimal impact on the system performance when the interference scenario is low. Other interference scenarios cause a great distortion to a received signal.

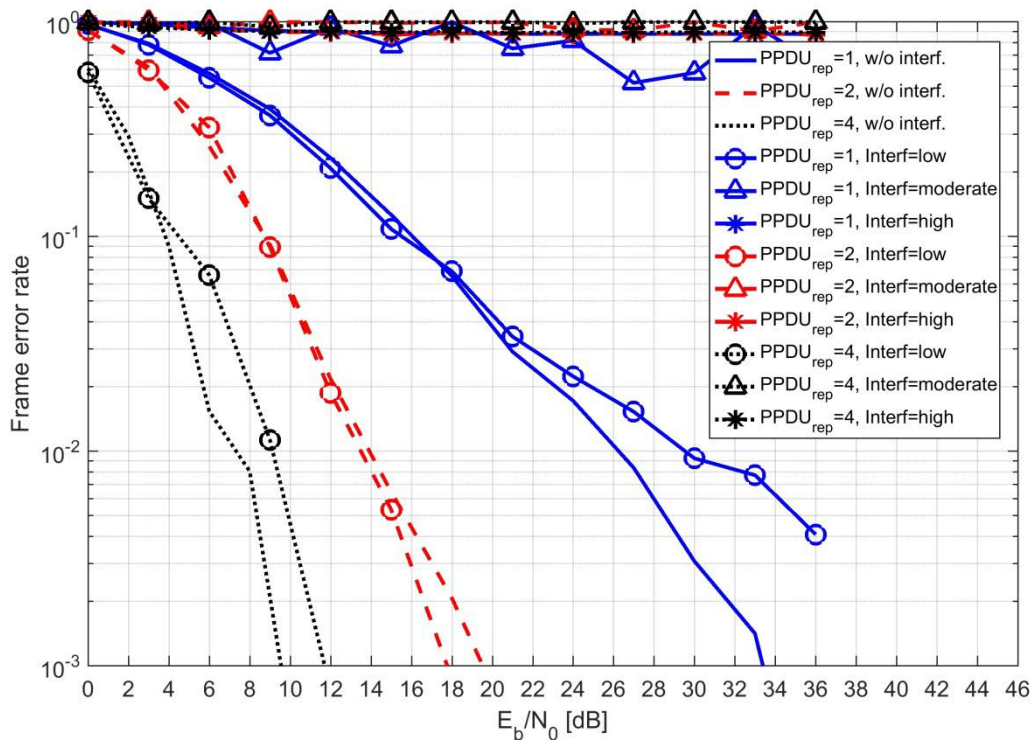


Figure 95: Fading channel and interference, FER, frame size = 50 octets

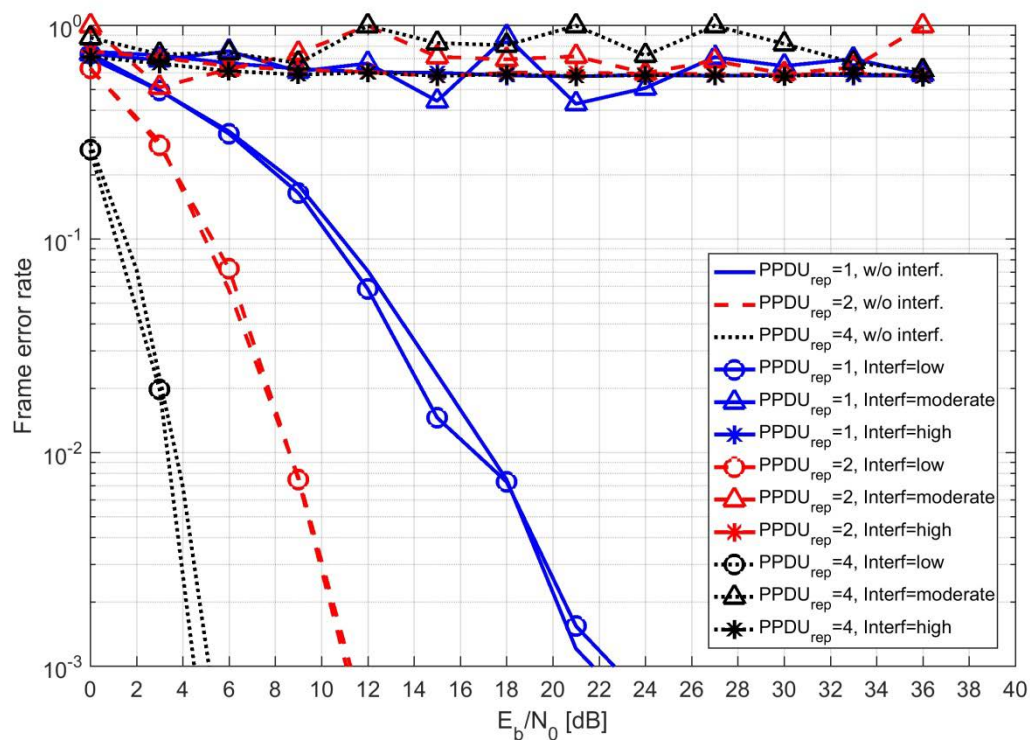


Figure 96: Fading channel and interference, FER with retransmission, frame size = 50 octets

8.5 Discussion

This clause presented the simulation results of the SmartBAN PHY with and without transmission of a PPDU. The SmartBAN receiver was implemented by using optimal solutions. The coherent demodulator applied a correlator followed by the Viterbi implementation of MLSD. In diversity combining of PPDU, an EGC combinator assuming the perfect channel phase estimation was implemented. These choices give a basis for further receiver design.

The simulator gives a possibility to implement channel access logic and study channel access delay of a SmartBAN system at some level. It requires copies of nodes and a stateflow chart modelling the logic for channel access. Since the simulator is modular, it is straightforward to study other receiver structures. Future work could also include studies using other channel models than the IEEE 802.15.6 [i.17] model.

The system performance in a interfered fading channel needs more detailed studies. Now, the simulations were completed by using the transmitted power of -10 dBm and the IEEE 802.15.6 [i.17] channel model. The average pathloss for 45 cm is -71,3 dB. When comparing the received signal power to the interference levels as illustrated in Figure 70, it is obvious that when an intensity of the interference rises, the system performance falls.

Annex A: Spatial Sample Clustering Algorithm

Spatial Sample Clustering Algorithm is presented here. For more details and exact method to use the algorithm, please refer to [i.8].

Part 1 Data Declaration (SSC)

Input Data:

- 1: $S(n)$ \leftarrow sample space where n represents the samples.
- 2: RB_{40} \leftarrow Relative bandwidth for IEEE 802.11n
- 3: RB_{20} \leftarrow Relative bandwidth for IEEE 802.11b/g
- 4: RB_{NB} \leftarrow Relative bandwidth for NB Systems
- 5: RB_{Set} \leftarrow Array of relative bandwidths for all systems
- 6: MG_{WB} \leftarrow Max. Gap limit for wideband systems
- 7: MG_{NB} \leftarrow Max. Gap limit for narrowband systems
- 8: MG_{Set} \leftarrow Array of gap limits for all systems
- 9: N \leftarrow Noise threshold for the current sweep given by Med-FCME
- 10: $BinWidth$ \leftarrow Width of one individual sample in whole sample space
- 11: f_{cSet40} \leftarrow A set of legitimate center frequencies (in MHz) of IEEE 802.11n
- 12: f_{cSet20} \leftarrow A set of legitimate center frequencies of (in MHz) IEEE 802.11b/g

Variables:

- 13: EI \leftarrow End index, i.e., index of the last sample
 - 14: ECI \leftarrow 0, Edge check index, i.e., Index of the sample under observation
 - 15: SB_{II} \leftarrow 0, Index of initial signal boundary
 - 16: SB_{FI} \leftarrow 0, Index of final signal boundary
 - 17: $Pivot_{Index}$ \leftarrow 0, Index of the pivot sample
 - 18: $Sig_{Counter}$ \leftarrow 0, Signal counter for this sweep
 - 19: $Gap_{Counter}$ \leftarrow 0, A counter for keeping track of samples below noise level
 - 20: BW_{Est} \leftarrow 0, Estimated bandwidth in MHz
 - 21: FC_{Est} \leftarrow 0, Estimated center frequency in MHz
 - 22: $Cluster(n)$ \leftarrow An array of size n to hold sample cluster, potentially a signal
 - 23: $map < k, v >$ \leftarrow A key-value pair map where values v are estimated center frequencies and the keys k are system names
 - 24: $Map < K, map < k, v >>$ \leftarrow A map containing $map < k, v >$ as value and keys are sequential integers starting from 1
 - 25: ▷ Actual algorithm starts from Part 2.
-

Part 2 Wideband Signal Search

Initiate Wideband Signal Search

```

26: while  $ECI < EI$  do
27:   if  $S(ECI) > N$  then
28:      $SB_{II} := ECI$ 
/*Call the LOOPER function*/
29:     LOOPER ( $S(n), SB_{II}, MG_{WB}$ )
/*Looper returns*/
30:      $BW_{Est} \leftarrow$  Estimated bandwidth
31:      $ECI \leftarrow$  Current edge index
32:      $Pivot_{Index} \leftarrow$  Current pivot element
/*Continue and Validate cluster as legitimate Signal*/
33:     Set  $SB_{FI} = ECI$ 
34:     switch  $BW_{Est}$  do
35:       case  $BW_{Est} \geq RB_{40}$ 
/*Mark an IEEE 802.11n signal*/
36:         Increment  $Sig_{Counter}$ 
37:          $FC_{Est} = \operatorname{argmin}|Pivot_{Index} - fc_{Set40}|$ 
38:         Add  $FC_{Est}$  to  $map < k, v >$ 
39:         Set  $K := Sig_{Counter}$ 
40:         and  $V := map < k, v >$ 
41:         Add  $K, V$  to  $Map < K, V >$ 
42:         Mark  $S(n)$  from  $SB_{II}$  to  $SB_{FI}$  as NaN
43:       case  $BW_{Est} \geq RB_{20} \ \&\& \ BW_{Est} < RB_{40}$ 
/*Mark an IEEE 802.11b/g signal*/
44:         Increment  $Sig_{Counter}$ 
45:          $FC_{Est} = \operatorname{argmin}|Pivot_{Index} - fc_{Set20}|$ 
46:         Add  $FC_{Est}$  to  $map < k, v >$ 
47:         Set  $K := Sig_{Counter}$ 
48:         and  $V := map < k, v >$ 
49:         Add  $K, V$  to  $Map < K, V >$ 
50:         Mark  $S(n)$  from  $SB_{II}$  to  $SB_{FI}$  as NaN
51:       case None of the above
52:         Cluster invalid, false alarm
53:     else
54:       Increment  $ECI$ 
55:     end if
56:   end while
57:
58: Reset all counters except  $Sig_{Counter}$ 
59:   ▷ Send the modified  $S(n)$  in which, wideband signal cluster/clusters (if any) are marked
   NaN, for Narrowband search.

```

Part 3 Narrowband Signal Search

Initiate Narrowband Signal Search

```

60: while  $ECI < EI$  do
61:   if  $S(ECI) > N$  then
62:      $SB_{II} := ECI$ 
/*Call the LOOPER function*/
63:     LOOPER ( $S(n), SB_{II}, MG_{NB}$ )
/*Looper returns*/
64:      $BW_{Est} \leftarrow$  Estimated bandwidth
65:      $ECI \leftarrow$  Current edge index
66:      $Pivot_{Index} \leftarrow$  Current pivot element
/*Continue and Validate cluster as legitimate Signal*/
67:     if  $BW_{Est} \geq RB_{NB}$  then
68:       Increment  $Sig_{Counter}$ 
69:        $FC_{Est} = Pivot_{Index}$ 
70:       Add  $FC_{Est}$  to  $map < k, v >$ 
71:       Set  $K := Sig_{Counter}$ 
72:       and  $V := map < k, v >$ 
73:       Add  $K, V$  to  $Map < K, V >$ 
74:     end if
75:   else
76:     Increment  $ECI$ 
77:   end if
78: end while
79:

```

▷ Return the $Map < K, V >$ to the main Script.

Part 4 LOOPER Function

```

80: function LOOPER( $S(n), SB_{II}, MaxGap$ )
81:    $Sample_{Counter} = 0$ 
82:   while  $Gap_{Counter} \leq MaxGap \parallel ECI \neq EI$  do
83:     for ( $j = SB_{II} ; j \leq ECI ; j++$ ) do
84:       if  $S(j) > N$  then
85:         Increment  $Sample_{Counter}$ 
86:         Add  $S(j)$  to  $Cluster(j)$ 
87:         Mark  $Pivot_{Index} = argmax|Cluster|$ 
88:         Set  $Gap_{Counter}=0$ 
89:       else if  $S(j) < N$  then
90:         Increment  $Gap_{Counter}$ 
91:       end if
92:       if  $Gap_{Counter} == MaxGap$  then
/*Edge check index becomes the current sample index*/
93:         Set  $ECI = j$ 
/*Bandwidth estimate of the cluster in MHz*/
94:          $BW_{Est} = \frac{Sample_{Counter} \times BinWidth}{10e6}$ 
95:         Break
96:       end if
97:     end for
98:   end while
99:   return  $BW_{Est}, ECI, Pivot_{Index}$ 
100: end function

```

History

| Document history | | |
|-------------------------|---------------|-------------|
| V1.1.1 | December 2016 | Publication |
| | | |
| | | |
| | | |
| | | |